Development of a Phantom Tissue for Blood Perfusion Measurement and Noninvasive Blood Perfusion Estimation in Living Tissue

Ashvinikumar V. Mudaliar

Dissertation submitted to the Faculty of
Virginia Polytechnic Institute and State University
in partial fulfillment of the requirements for the degree of

Doctor of Philosophy
in
Mechanical Engineering

Dr. Thomas E. Diller, Sc.D., Chair
Dr. Elaine P. Scott, Ph.D. Co-chair
Dr. Otto I. Lanz, DVM, Diplomate ACVS
Dr. Danesh Tafti, Ph.D.
Dr. Brian Vick, Ph.D.

January 23rd, 2007
Blacksburg, Virginia

Keywords: Phantom Tissue, Blood Perfusion, Contact Resistance, Heat flux, Parameter Estimation

Development of a Phantom Tissue for Blood Perfusion Measurement and Noninvasive Blood Perfusion Estimation in Living Tissue

Ashvinikumar V. Mudaliar
Virginia Polytechnic Institute and State University, 2007
Supervisors: Dr. Thomas E. Diller and Dr. Elaine P. Scott

Abstract

A convenient method for testing and calibrating surface perfusion sensors has been developed. A phantom tissue model is used to mimic the non-directional blood flow of tissue perfusion. A computational fluid dynamics (CFD) model was constructed in Fluent® to design the phantom tissue and validate the experimental results. The phantom perfusion system was used with a perfusion sensor based on the clearance of thermal energy. A heat flux gage measures the heat flux response of tissue when a thermal event (convective cooling) is applied. The blood perfusion and contact resistance are estimated by a parameter estimation code. From the experimental and analytical results, it was concluded that the probe displayed good measurement repeatability and sensitivity. The experimental perfusion measurements in the tissue were in good agreement with those of the CFD models and demonstrated the value of phantom tissue system.

This simple, cost effective, and noninvasive convective blood perfusion system was then tested in animal models. The perfusion system was evaluated for repeatability and sensitivity using isolated rat liver and exposed rat kidney tests. Perfusion in the isolated liver tests was varied by controlling the flow of the perfusate into the liver, and the perfusion in the exposed kidney tests was varied by temporarily occluding blood flow through the renal artery and vein. The perfusion estimated by the convective perfusion probe was in good agreement with that of the metered flow of perfusate into the liver model. The liver tests indicated that the probe can be used to detect small changes in perfusion (0.005 ml/ml/s). The probe qualitatively tracked the changes in the perfusion in kidney model due to occlusion of the renal artery and vein.

Author's Declaration

I hereby declare that I am the sole author of this dissertation.
I authorize the Virginia Tech to lend this thesis to other institutions or individuals for the purpose of scholarly research.

Ashvinikumar Mudaliar
Signature

I further authorize the Virginia Tech to reproduce this thesis by photocopying or by other means, in total or in part, at the request of other institutions or individuals for the purpose of scholarly research.

Ashvinikumar Mudaliar
Signature

Preface

This dissertation is organized in a manuscript format that includes two individual research papers that document the main focus of the work. The first chapter briefs about the introduction and the objectives of the research carried out. A literature review of the past work and latest developments in blood perfusion measuring techniques are presented in chapter 2. The first paper (chapter 3) describes the design of the phantom tissue and its validation. The second paper (chapter 4) documents the testing of the convective perfusion probe on the animal model (*in vivo* and *ex vivo*). Overall conclusion and the future recommendations are described in chapter 5. A series of appendices then follows which provide additional information on the bioheat transfer model, the parameter estimation, finite difference model, the phantom tissue test stand development and computational fluid dynamics model development (CFD), all of which were used in the process of pursuing this research.

Acknowledgements

I'd like to thank first and foremost my advisors; Dr. Thomas Diller and Dr. Elaine Scott for there support both financially and mentally during my research work. During my stay at heat transfer lab I have got advice, help and encouragement from many people whom I would like to thank. I'm extremely grateful for the guidance of Dr. Diller and for his mentoring, encouragement and consistently helping me to get over several obstacles that I've come across during my research I'm also very thankful to Dr. Elaine Scott for inputs and suggestions from time to time to improve the parameter estimation model.

I would also like to thank to my committee members Dr. Otto Lanz, Dr. Danesh Tafti and Dr. Brian Vick for reviewing my work and providing valuable suggestions. Special thanks to Dr. Otto Lanz for helping us in conducting rat test at veterinary school and making us laugh all the time during the tests. I would also like to acknowledge Dr. Charles Lee from UNC Charlotte for letting us to conduct *ex vivo* tests at his facility. Special thanks to Dr. Al Wicks for helping in resolving the noise issue in the DAQ.

I would like to thank my parents and my family members for their support and encouragement, without which it wouldn't be possible for me accomplish the task. I was privileged to work in heat transfer lab and would like to thank my old lab mates Peng, Scott, Marie, Dion, Sandra, and Caroline. I would also like to thank my present lab mates Tricia, Brent and Leah for helping me in conducting experiments in the lab as well as in the veterinary school and of course for all the fun in 100V.

I would like to thank my best friends Aroon, Vikram, Nitin, Pradeep and Anirban and Satyaprakash. Thank you very much for being with me during my ups and downs and thanks for all your help. I would like to thank specially Nitin and Vikram for providing me accommodation in their apartment during my last phase of PhD. I would also like to thank Rahul and Sunita for their words of encouragement and support all the time. I have also enjoyed the company of Akhilesh, Ritesh, Parthiban, Shrenik who have hung out with me at Tech.

Finally I would like to acknowledge ME staff (Cathy, Kathy, Lisa and Melissa) and SBES staff (Linda and Tess) for their help all the time. Thanks to Ben and Jamie for fixing all the computer problems and for the interesting conversation. And thank you God for keeping me safe and healthy.

Dedication

To my Family, Mentors and Friends

Attribution

Paper 1: A Phantom Tissue System for the Calibration of a Perfusion System

Co-authors

Brent E. Ellis (MS)[1, 2], Patricia L. Ricketts (BS)[1, 2], Otto I. Lanz (DVM)[1, 3], Elaine P. Scott (PhD)[1,2], Thomas E. Diller (ScD)[1, 2]

Brent and Patricia helped me in conducting experiments and running the parameter estimation code. Dr. Diller, Dr. Scott and Dr. Lanz provided technical advice and guidance for conducting the experiments and troubleshooting the problems that arose during the experiments.

Paper 2: Non – Invasive Blood Perfusion Measurements of an Isolated Rat Liver and an Anesthetized Rat Kidney

Co-authors

Brent E. Ellis (MS)[1, 2], Patricia L. Ricketts (BS)[1, 2], Otto I. Lanz (DVM)[1, 3], Elaine P. Scott (PhD)[1, 2], Thomas E. Diller (ScD)[1, 2], Charles Y. Lee (PhD) [4]

Brent and Patricia helped me in conducting experiments and running the parameter estimation code for the animal tests conducted. Dr. Lee provided his lab facility at UNC Charlotte to conduct ex *vivo* tests and guidance for conducting the liver test. Dr. Lanz helped in conducting the *in vivo* test on the rat kidney at Small Animal Clinics at Virginia Tech. Dr. Diller and Dr. Scott provided technical advice and guidance for conducting the experiments and troubleshooting the problems that arose during the experiments.

[1] Virginia Tech – Wake Forest University of Biomedical Engineering and Sciences
[2] Department of Mechanical Engineering, Virginia Tech
[3] Department of Small Animal Clinical Sciences, Virginia Tech
[4] Department of Mechanical Engineering Science, UNC Charlotte

Table of Contents

List of Figures

List of Tables

Nomenclature

Nomenclature Used in Finite Difference Equations

α	Thermal Diffusivity	Δr	Radial Distance Between Two Cells
T	Temperature (^{o}C)	Δz	Axial Distance Between Two Cells
t	Time (sec)		
k	Thermal Conductivity (W/m-K)	q''	Heat Flux (W/m^2)
ω	Blood Perfusion (mL/mL/s)	h	Heat Transfer Coefficient (W/m^2-K)
R_c	Contact Resistance (m^2-K/W)	j	Node Index in Radial Direction
r	Radial Direction	i	Node Index in Axial Direction
z	Axial Direction	P	Time Index

Subscripts

t	Tissue	$t1$	First Row of Cells in Tissue
s	Heat flux Gage	nt	Last Row of Cells in Tissue
1	First Row of Cells in Gage	mt	Last Column of the Cells in Tissue
sn	Last Row of Cells in Gage	∞	Free Stream (Ambient)
ms	Last Column of Cells in Gage	a	Arterial

Nomenclature Used in Parameter Estimation

S	Objective Function	β	Estimated parameter Vector
$\vec{q}$"	Vector of Heat Flux Values	b	Approximation of β
(W/m^2)		$\vec{X}$	Sensitivity Coefficient Vector
$\vec{T}$	Vector of Temperature Values (^{o}C)	Δb	Change in Parameter Estimate
σ	Variance		

Subscripts

m	Measured	q	Heat Flux
c	Calculated	T	Temperature
i	Index		

Superscripts

k	Iteration Number
T	Transpose

Chapter 1
Introduction

Advances in medical diagnostic equipment have improved the ability of medical professionals to detect and treat various forms of illness and disease. Through this ongoing research and the continual improvement of patient care, the lives of many people are enhanced. Much of this progress has been localized in the development of pharmaceuticals, biomedical implants, imaging techniques, information transfer ability, remote diagnostic procedures and even robotic surgical assistance. The research outlined in this work focuses on a lesser well publicized, however important, advance in medical equipment that is expected to fill some holes left by current technology, as well as open up new avenues of exploration.

Tissue blood flow, often called perfusion, can be defined as the rate at which the quantity of blood in a given mass or volume of tissue is replenished at the level of the capillary network. Blood perfusion represents the local flow through the capillary network and extracellular space of tissue. This flow is so convoluted as to be considered non-directional at the macroscopic level. Blood flow and blood perfusion are related, however local perfusion abnormalities may exist even in the presence of normal blood flow. Perfusion is a primary factor in the local transport of oxygen, nutrients, waste products, heat, and drugs. It is necessary for normal tissue physiology and is part of the thermoregulatory system of the body. It does not include the bulk flow of blood through major blood vessels, such as arteries and veins.

As such, measurement of blood perfusion is a valuable medical diagnostic. For example, blood perfusion measurements can determine the success or failure of skin grafts and any related healing. The ability to measure perfusion has been sought for many years, as this fundamental parameter holds the key to an improved understanding of both normal and pathologic physiology, as well as the diagnosis and management of numerous medical situations including shock and tissue viability subsequent to traumatic injury, transplantation and non-surgical treatments of cancer. Some of the more specific fields of interest are the healing of burns and skin grafts, cerebral perfusion in head trauma patients, and the detection of tumors. In each instance, researchers look for blood perfusion that differs from normal levels to determine areas of tissue damage, regions of elevated healing response, or inconsistencies in expected function. In addition, there are many clinical diagnostic applications that would be improved or made possible by a reliable quantitative method to measure blood perfusion.

While the overall importance of blood flow to human health has led to many techniques being proposed and/or pursued to quantify perfusion, many of these do not lend themselves to routine clinical application. Such techniques include: radioactive tracer washout techniques; positron emission tomography (PET); magnetic resonance imaging (MRI); radioactive microspheres; and laser-Doppler flowmetry (LDF); thermal diffusion probes; pulse oximetry and Hydrogen clearance technique. Although these methods have been used to measure blood perfusion, most of them have been not able to achieve absolute measurement while being non-invasive in nature. Most of these methods are expensive and therefore have limited usage, making it impractical for clinical application.

This research is part of ongoing development of a noninvasive blood perfusion probe at Virginia Tech. The underlying physics is that by applying a thermal event (convection) to the skin surface, the tissue's heat flux response can be evaluated in order to obtain an estimate of the local blood perfusion. The probe measures both temperature and heat flux data from the surface of the skin through a differential thermopile sensor manufactured by Vatell Corporation. The blood perfusion can be estimated by parameter estimation.

1.1 Motivation and Significance

Based on these previous studies, an ideal perfusion measurement system should be safe, cost effective, operable in a variety of clinical environments (including surgery), noninvasive, and easy to use. Further, the system should be able to provide measurements which are absolute, repeatable, accurate, and obtainable in a timely manner. No existing method provides all of these characteristics. For example, MRI provides accurate and repeatable measurements, but requires bulky, costly equipment unsuitable for use in a surgical environment. The Laser Doppler Flowmetry gives the measurement in relative units.

The thermal perfusion system has the potential to address most, if not all, of these important characteristics. Since the probe operates by cooling rather than heating, it is inherently safe for any patient application. The computer based system has a simple probe design and does not require any additional fundamentally expensive equipment for operation; therefore, it is expected to be very cost effective. The probe design is inherently noninvasive. As a hand held or potentially taped on device, the units should be easily operable. Due to use of a model based estimation procedure, the system is fundamentally absolute in its design.

Being able to monitor and quantify the local perfusion very quickly or over extended time periods could be useful in measuring both changes in normal physiologic activity such as athletic training or exercise, as well as the presence, degree, extent, and changes in pathologic conditions as previously

described. A noninvasive probe to assess local circulatory function would have many current medical uses and could become a major new tool for research and clinical use. It is anticipated that the proposed system will be developed into a clinical device to diagnose circulation problems and monitor the healing progress of tissue along with other applications. (A U.S market of $20 million per year is conservatively estimated.).

1.2 Objectives

The overall goal of this research effort is to develop and characterize the sensitivity and repeatability of an easy to use, non-invasive, absolute thermal blood perfusion measurement system for use in a variety of clinical applications. It has been shown to distinguish between the values of blood perfusion for varying physiologic conditions through testing on canine thoracic and pelvic limbs. Physiologic variability in humans and animals makes it impossible to establish an exact value for blood perfusion. Also, this physiologic variability makes it difficult to obtain repeatable results, as the blood perfusion is dependent on many factors, such as the probe location, the subject's health, and the contact resistance between the sensor and the tissue.

The main goal of the ongoing research was to design and develop a controlled perfused phantom tissue test stand to validate the blood perfusion measurements measured by Virginia Tech bioprobe. The other secondary goals were to validate the experimental results of the phantom tissue with CFD model using Fluent and develop a robust parameter estimation routine to express the outcome of the bioprobe in terms of blood perfusion and contact resistance. *In-vivo* and *ex-vivo* tests were performed on rat's liver and kidney, to further validate the quantitative and qualitative performance of the bioprobe by considering physiological variability in living tissue. However, all these goals merely supported the phantom tissue desire to prove the bioprobe concept.

Following are the tasks that were executed to achieve the goals described above.

1. A compact controlled perfusion phantom tissue test stand was developed for assessing the measurement, repeatability and sensitivity of the probe. An empirical relationship was established between the in flow rate and the estimated local perfusion.
2. A CFD model was constructed using commercial software (Fluent) to validate the experimental results from the controlled perfusion phantom test stand.
3. Improved data acquisition techniques were established for the existing DAQ card to obtain high sampling and low noise in the collected data.

4. The newly developed smaller size probe of size 1cm. × 1 cm was validated.
5. Experimental protocol was established by testing on the epidermal surface of anesthetized rats.
6. Laser Doppler Flowmetry was carried out to have direct comparison with the bio-probe developed at Virginia Tech.
7. *In-vivo* and *ex-vivo* tests were conducted to validate the performance of the bioprobe under different physiological conditions.

Chapter 2

Literature Review

The significance of this research and its goals can be made most evident through comparison with other work in the field. Of prime importance are the methods of measurement employed by a variety of other blood perfusion measurement devices, the success and advancements guiding today's research, as well as the limitations displayed by current technology. Several key areas of scientific literature give insight to the fundamentals behind the process used in this research. Understanding this literature lends support to the methods used in the current research and gives a basis for comparison of the research to the existing technologies.

2.1 Methods of measuring blood perfusion

The methods discussed in this section include Laser Doppler Flowmetry (LDF), Magnetic Resonance Imaging (MRI), Doppler Ultrasound (DU), Positron Emission Technology (PET), and other thermal and chemical marking methods. Some of the limitations discussed are ease of operation, repeatability and sensitivity of the measurement, continuous acquisition of the measurement, portability and operational cost.

2.2 Laser Doppler Flowmetry (LDF)

Laser Doppler flowmetry is an established technique for the real-time measurement of red blood cells (or erythrocyte) motion in tissue. Perfusion is sometimes also referred to as microvascular blood flow or red blood cell flux. Laser Doppler signals from the tissue are recorded in BPU (Blood Perfusion Units) which is a relative units scale calibrated using a carefully controlled motility standard comprising a suspension of latex spheres undergoing Brownian motion. Laser Doppler Flowmetry (LDF) works by illuminating the tissue under observation with low power laser light from a probe containing optical fiber light guides. Laser light from one fiber is scattered within the tissue and some is scattered back to the probe. Another optical fiber collects the backscattered light from the tissue and returns it to the monitor.

Most of the light is scattered by tissue that is not moving but a small percentage of the returned light is scattered by moving red blood cells. The light returned to the monitor undergoes signal processing whereby the emitted and returned signals are compared to extract the Doppler shift related to the velocity of red blood cells. The perfusion measurement is derived from the product of the mean

velocity and the concentration of the red blood cells within the volume of the tissue being measured (Svedman *et al*., 1998).

The method of LDF was first introduced by Riva et al. in 1972. Michael D. Stern was the first one to suggest the use of LDF for measuring tissue perfusion (Stern *et al.*, 1977). LDF is considered to be the standard technique for instantaneously and continuously performing real time perfusion measurements (Vajkoczky *et al.*, 2000). This is due to the fact that light is capable of measuring the relatively low speeds at which the red blood cells travel through the capillaries. Exploiting this Doppler shift allows for the measurement of perfusion, utilizing short wave length or extremely high frequencies of visible infra red light (Shepherd, 1990). Laser Doppler Imaging (LDI) is based on Laser Doppler Flowmetry. LDI follows the same basic principles of LDF, except that it eliminates the need of the probe to be affixed to the skin (Svedman *et al*., 1998). The LDI method consists of a laser light source, a scanner, a photo detector, and a processing unit. The image of the tissue is achieved by sequentially moving the laser beam step by step over the tissue. LDF involves single point measurement, highly susceptible to movement and pressure, which is not necessarily representative of perfusion. The signal is averaged while LDI scans over an area of skin in a non-contact mode, thereby removing small movement artifacts and inconsistencies.

There are, however, many difficulties associated with LDF technology. By its nature, LDF makes velocity measurements in only one direction. If the direction of the flow is not in line with the measurement direction, something that is impractical to determine, then absolute and quantifiable measurements cannot be made. Another problem is that LDF is highly sensitive to the optical properties of the tissue being measured. These properties vary from person to person as well as directionally within the same tissue. For these reasons, LDF is used to make relative measurements of changes in blood flow in the tissue it is measuring. Other issues such as high sensitivity to movement, a high operational cost, lack of portability and susceptibility to interference with other equipment make the method less than ideal.

There is ongoing research attempting to improve the usability of LDF systems. Forrester et al. made measurement of tissue properties in conjunction with LDF measurement that could make it possible to accurately compare LDF output from two different test subjects (Forrester *et al.*, 2000). A high resolution laser speckle perfusion imaging system (LSI) was developed that allows measuring the degree of perfusion. The resulting signals from the back scattered light due to Doppler shift is used to calculate the degree of perfusion, which is expressed in arbitrary units. The value of LSI is not completely defined, but it was proposed to improve the quality of diagnostic information and treatment

plan for providing an alternative optical perfusion imaging technique. A method for determining penetration depth of the system was proposed and explored by Liebert *et al*. in 1998, using a multi-channel laser probe.

2.3 Doppler Ultrasound (DU)

Numerous technical improvements have been made in past years in the field of contrast ultrasonography. The development of more stable contrast particles has greatly improved the tissue delineation, as well as Doppler measurements. Past studies devoted to the qualitative analysis of myocardial perfusion have been reported using stable contrast particles (Porter *et al.*, 1996). Doppler imaging (PDI) has demonstrated significant improvement in the sensitivity of contrast ultrasonography in small vessels, myocardium and liver studies (Porter *et al.*, 1996, Burns *et al.*, 1994, Marayuma *et al.*, 1998). The best known applications of the Doppler principle in biology and medicine are a series of different techniques for assessing the blood flow from the Doppler shift that sound waves experience when they travel through the blood flowing in a relatively large blood vessel. One of the main advantages that Doppler ultrasound techniques such as pulse echo scanners offer, beside their noninvasiveness, is their ability to produce images of the heart and major blood vessels. However, it is impractical to use Doppler ultrasound methods to measure blood flow in what is most important, the microcirculation, within the tissues nourished by invisibly small blood vessels, as they are designed to present mean, maximum or eventually the spectrum of the blood flow velocities in a vessel, rather than inflow of blood to the selected body tissue.

2.4 Positron Emission Technology (PET) and Micro-Computer Tomography (MicroCT)

PET scans can be used to make measurements of blood perfusion, but require the introduction of a radioactive tracer into the blood supply. While a CT scan provides anatomical detail (size and location of the tumor, mass, etc.), a PET scan provides metabolic detail (cellular activity of the tumor, mass, etc.). CT scanners send x-rays through the body, which are then measured by detectors in the CT scanner. A computer algorithm then processes those measurements to produce pictures of the body's internal structures. PET images begin with an injection of a solution of glucose (sugar) that has been "tagged" with a radioactive chemical isotope (generally fluorine 18, or FDG). Metabolically active organs or tumors consume sugar at high rates, and as the tagged sugar starts to decay, it emits positrons. These positrons then collide with electrons, giving off gamma rays, and a computer converts the gamma rays into images. A radioactive tracer, usually N-ammonia or O labeled water, is placed on a glucose

molecule and injected into the blood stream (Schelbert, 2000). The blood distributes the sugar throughout the body. Perfusion is determined by a two step process. First, time activity curves are extracted from a dynamic scan (Nuutilia and Kalliokoski, 2000). Then, perfusion is determined based on an arterial input function (Boellaard *et al*., 2004).

Single-photon Emission Tomography (SPECT) is closely related to positron emission tomography. SPECT differs in that it uses radioactive substances with longer decay times and these substances emit single gamma rays rather than double gamma rays. However, it works in the exact same way. The emitted rays are recorded during a dynamic scan, and then perfusion is calculated based on the change in the activity curve (Petersson *et al.*, 2004). The costs for SPECT are significantly lower than for PET, increasing it's availability for clinical purposes. SPECT has proven to have a much higher resolution than MRI in detecting perfusion (Kinuya *et al.* 2004). However, SPECT has a lower spatial perfusion resolution compared to positron emission tomography, producing less detailed images (Gregory and Thirion, 2005). One current problem with this method is the image noise caused by movement, especially heart movement (Slomka et al., 2005). Advances in the quantification of SPECT imaging are currently being made to improve the reproducibility of clinical trials (Gregory and Thirion, 2005).

Micro-Computer Tomography (MicroCT) is another scanning method that has been proposed for measuring perfusion. This method was first introduced in the 1970's by Heymann *et al.* (1977) and revised by Prinzen and Bassingthwaighte (2000). This method works on the basic principle of injecting a tracer in the blood stream and then detecting the tracer and its movement. In this method silver coated microspheres are injected into the body. Then, a CT scanner takes a two dimensional image at several locations and a three dimensional model is developed. The microspheres are easily detected in this three dimensional model, and perfusion can be determined from the location of the microspheres (Marxen *et al*. 2006).

While accurate measurements can be made with PET, this method is time consuming, requires the injection of foreign substance into the body, and is incapable of making continuous measurements. PET is a quantitative tool that measures radioactive concentration (tissue or plasma) that can be easily converted to drug concentration, which can be used to infer tissue function *in vivo*: perfusion, glucose consumption, receptor densities etc. One problem with PET is that perfusion cannot currently be quantitatively evaluated. All of these scanning methods show promise, however they are not feasible for blood perfusion measurements during surgery and many other situations. The main problems with these methods are the cost, equipment size, and the processing time for perfusion estimates.

2.5 Magnetic Resonance Imaging (MRI)

In MRI perfusion is measured using either arterial spin labeling (ASL) or dynamic susceptibility contrast (DSC) based. DSC - MRI provides estimates of blood flow, blood volume and mean transit time. Commonly used DSC - MRI contrast agents are distributed into blood plasma and as such provide hemodynamic parameter related to blood flow, blood volume and mean transit time of the tracer. The DSC-MRI provides parametric maps of regional cerebral blood flow (rCBF), cerebral blood volume (rCBV) and mean transit time (MTT). The concept is based on the theory of intravascular tracers and requires monitoring of tracer concentration time curves, during the first passage, in an artery (for registration of the arterial input function (AIF)) and in tissue.

Arterial spin labeling (ASL) perfusion MRI is a noninvasive technique to directly measure blood flow by utilizing arterial blood as an endogenous tracer. The arterial spin labeling (ASL) technique determines spatially and temporally resolved perfusion in tissue (Liu *et al.*, 1999, Montet *et al*., 2003 and Vallee *et al.*, 2000). This technique was first developed for use in the brain by Wong *et al*. in 1997, and later adopted for use in muscle by Frank *et al*., in 1999. The technique of arterial spin labeling involves magnetically tagging the arterial blood proximal to an imaging slice, and then observing the changes that occur as blood flows through the volume of tissue. The local magnetic resonance signal that is detected is proportional to the amount of the arterial blood being delivered in a short time interval, and the value of the perfusion can be calculated (Wong *et al.*, 1997). During the past decade, methodologies for ASL perfusion imaging have evolved from feasibility studies into practical usage. However, the widespread application of ASL techniques has still been hampered by the relatively small fractional signal of the labeled blood, and transit related artifacts resulting from the proximity of the tracer decay rate (blood T1) to the arterial transit time.

The clinical applications of perfusion MRI has been limited by number of factors, including relatively poor spatial resolution, limited volume coverage and low signal to noise ratio (SNR). It is difficult to improve any of these aspects because both ASL and DSC methods require rapid image acquisition. Although the use of DSC and ASL to measure perfusion yields accurate, repeatable and absolute results of perfusion, this method is relatively expensive, and in general is inconvenient or impossible to use in critical settings, such as during surgery.

2.6 Thermal Methods

One of the thermal methods for invasively measuring blood perfusion is methods that use a Thermal Diffusion Probe (TDP). A TDP provides an absolute perfusion measurement through the insertion of a

self-heated thermistor bead into the tissue being measured (Eberhart *et al*., 1980, Valvano *et al*., 1984, Bowman, 1985, Patel *et al*., 1987, Vajkoczky *et al*., 2000). In this method, the thermistor bead is first used to sense the temperature of the tissue, before any heat is applied. The thermistor bead is then supplied with a controlled power sequence. Electrical energy is dissipated at the rate that will allow the bead to maintain a specified temperature difference above the equilibrium temperature of the bead and surrounding tissue. The electric power that is required to maintain this temperature is dependent on the heat transfer characteristics of the surrounding tissue, and thus, is a function of perfusion.

Several different heating protocols and modes have been used. These include temperature pulse-decay (Newman and Lele, 1985, Arkin *et al*., 1986, Kress and Roemer, 1987), temperature step function (Kress and Roemer, 1987), constant-power heat up (Kress and Roemer, 1987), two-phase, cyclical heating (Arnaud *et al*., 1994), sinusoidal heating (Liu and Xu, 1999), focused ultrasound (Anderson and Burnside, 1990), and Doppler ultrasound heating (Eriksson *et al*., 1991).

Although the results obtained from the methods using a TDP are absolute and quantifiable, can be made continuously, their invasive nature makes the procedure undesirable and inadequate for widespread clinical use. Also, the effects on the local tissue properties due to the partial or full insertion of a probe into the patient's tissue have not been fully explored. It should also be noted that although it has been stated that TDP measurement has never been verified with a phantom tissue.

There have been several attempts at creating instruments for measuring perfusion non-invasively, usually involving a heater and temperature sensor on the surface of the skin (Holti and Mitchell, 1979, Patel *et al*., 1987, Walsh and Bowman, 1984, Castallena *et al*., 1983, Woodcock, 1985, Anderson and Burnside, 1990, Rumberger, 1990, Peng *et al*., 2000). Patel et al. (1987) used an insulated thermistor probe. Walsh and Bowman (1984) expanded upon Patel's design by adding a second thermistor on top of the first to act as a heater guard. A thin film resistor placed on the surface skin for the purpose of providing heat and measuring the temperature was used by Castellana *et al*., (1983). Anderson and Burnside (1990) used focused ultrasound as the heating source for a thermistor placed on the tissue surface in order to measure the temperature response.

There has been limited success in measuring blood perfusion with these non-invasive thermal techniques. These limitations are due to the difficulty in measuring the actual heat flux going into the tissue, as the losses to the ambient are usually large. Also, the thermal contact resistance is an important property that affects the estimation of perfusion. The thermal contact resistance is difficult to determine for these non-invasive probes.

2.7 Clearance and Marker Methods

Another method that has been used for perfusion measurement is the hydrogen (or xenon) clearance technique (Machens *et al*., 1996; Woodcock, 1985). The basis of this technique is the theory of tracer clearance, which states that the product of arteriovenous concentration difference and blood flow is equal to the quantity of metabolically inert substance taken up or released by tissue during a specified time interval. It relies on the accuracy of the measurement of the tracer gas concentrations in the blood and tissue as a function of time. Although the values obtained for perfusion from this technique are absolute, their repeatability is questionable due to the dependence on the electrode placement. Also the electrodes are typically embedded, and as such this technique is invasive.

Radioactive microspheres are commonly used as markers for blood flow studies (Prinzen and Bassingthwaighte, 2000). The spheres are injected into the blood stream and become embedded in the tissue microcirculation on the first pass through. After tissue samples are harvested, the relative distribution of the blood flow is determined from the radiation emitted from each sample. The absolute perfusion through the tissue sample can be found if a sample of blood is also taken at a known flow rate from an artery downstream of the injection site. The tissue perfusion is then proportional to the ratio of the emitted radiation from the two samples multiplied by the rate of blood sample withdrawal (Heymann *et al.*, 1977). To eliminate the need to handle radioactive materials, the microspheres can be activated after collection by commercial labs (Reinhardt *et al.*, 2001). Because of the needed sacrifice of the tissue, this method is only useful for laboratory testing.

2.8 Other Methods

Pulse oximeters have been used for inferring blood perfusion as well, and are currently in wide use due to their convenient and inexpensive nature. Pulse oximeters are optical systems that measure the oxygen saturation of the blood within a localized area of the body. The basis behind this type of measurement is that changes in the hemoglobin saturation levels trigger changes in the amount of light absorption at specific wavelengths. These saturation level readings are indirectly indicators of the amount of blood perfusion present in that area. However, due to its optical nature, pulse oximeter readings can be influenced by factors other than the local blood perfusion, such as ambient light, interference from other electrical sources, or patient motion. Consequently, the perfusion measured is not accurate or absolute measurement. No direct correlation between O_2 saturation level and blood perfusion have been established yet.

The skin is the body's largest and most accessible organ and blood flow in the skin performs an essential role in the regulation of the metabolic, hemodynamic and thermal state of the individual. Nonetheless, the measurement of cutaneous microcirculatory blood perfusion has until quite recently proved a formidable task. By far the largest proportion of the body's dermal vasculature is involved in regulating body temperature and controlling systemic blood pressure. The degree of blood cell perfusion in this region of the microvascular tree, over both long and short time periods, can provide a reliable indicator of peripheral vascular disease or injury. Reduction or even complete occlusion of blood perfusion in the microcirculatory blood vessels can often be attributed to a variety of cutaneous vascularisation disorders.

There are many situations in routine clinical medicine where the measurement of blood perfusion in the cutaneous microcirculatory beds is required. Examples include Peripheral Vascular Diseases (where accurate assessment of reduced peripheral blood perfusion is necessary in order to decide upon the type of medical care) and reconstructive surgery (where it is important to be able to recognize the failure of a free flap transfer early on for the best chance of success in a subsequent operation). MRI, PET, Doppler Ultrasound and TDP cannot be used to measure skin perfusion; they are used to measure perfusion in deep tissues only to the best of our knowledge. To meet this specific requirement, there arises a need for a surface based sensor/probe that can measure skin perfusion absolutely. Currently in the market LDF is the only available surface based sensor that can measure skin perfusion. Absolute and quantifiable measurements cannot be made using LDF, also it is highly sensitive to the optical properties of the tissue being measured. The lack of ability to measure absolute blood perfusion noninvasively, lead to the design and development of the bioprobe at Virginia Tech. In order to achieve an absolute perfusion blood perfusion probe needs to be validated. Thus arises, the need for a phantom tissue that eliminates the physiologic and pathologic factors in living tissue so that the sensitivity and repeatability of the probe can be adequately assessed.

Chapter 3

Paper 1: A Phantom Tissue System for the Calibration of a Perfusion System

To be submitted to *Journal of Biomechanical Engineering*[*]

3.1 Abstract

A convenient method for testing and calibrating surface perfusion sensors has been developed. A phantom tissue model is used to simulate the non-directional blood flow of tissue perfusion. A computational fluid dynamics (CFD) model was constructed in Fluent® to design the phantom tissue and validate the experimental results. The phantom perfusion system was used with a perfusion sensor based on clearance of thermal energy. A heat flux gage measures the heat flux response of tissue when a thermal event (convective cooling) is applied. The blood perfusion and contact resistance are estimated by a parameter estimation code. From the experimental and analytical results it was concluded that the probe displayed good measurement repeatability and sensitivity. The experimental perfusion measurements in the tissue were in good agreement with those of the CFD models and demonstrated the value of the phantom tissue system.

[*] Co – authors: Brent E. Ellis, Patricia Ricketts, Dr. Elaine P. Scott, Dr. Thomas E. Diller,
Department of Mechanical Engineering, Virginia Tech
Dr. Otto I. Lanz, Department of Small Animal Clinical Sciences, Virginia Tech

3.2 Introduction

Blood perfusion is the local, non-directional blood flow per volume of tissue. It represents the local flow through the capillary network and intracellular space of tissue and is responsible for providing the oxygen and nutrients required by cells along with removing waste products.

Blood perfusion is so convoluted as to be considered non-directional at the macroscopic level. Conversely, fluid flow rate and velocity are directional. For example, the flow rate or velocity of a fluid through a straight pipe is constant in one direction. The corresponding perfusion, however, would not make sense because it would change with the length of the pipe. Perfusion must appear as if there is no entrance or exit in any direction.

Due to the vital role that blood perfusion plays in maintaining normal and physiologic conditions, it is very valuable to measure blood perfusion. Differences in local blood perfusion can be an indicator that the body is responding to an abnormal physiologic or pathologic state. These blood perfusion differences can be used to assess the progression of skin graft healing or the extent of burns. Low blood perfusion can also be an indicator of microcirculation problems in diabetes patients.

3.3 Background on Perfusion Measuring Techniques

Because of its importance, several methods have been developed for measuring blood perfusion. Noninvasive imaging techniques include Photon Emission Tomography (PET) [P1.1] and Magnetic Resonance Imaging (MRI) [P1.2]. Prinzen and Bassingthwaighte [P1.3] used Micro-Computer Tomography (MicroCT) to estimate blood perfusion. These systems have produced reliable perfusion estimates in deep tissues. They cannot be used in a surgical situation or for long term monitoring, however. They tend to be very large, costly, and require substantial processing time.

Laser Doppler systems use the scattering of light by the red blood cells just below the surface of tissue to measure the cell velocity [P1.4]. Although there is no reliable method to convert this measurement into perfusion, Laser Doppler Flowmetry (LDF) has recently been used for monitoring dialysis [P1.5], to assess the extent of burn wounds [P1.6], and transplant rejection [P1.7]. These systems are dependent on a number of factors other than perfusion, including the optical properties of the tissue, blood, and the optical fibers [P1.8]. Although there is no standard calibration system, calibration of Laser Doppler systems have been attempted using latex microspheres in Brownian motion in water [P1.9].

Other perfusion measurement systems work based on the clearance of a substance such as hydrogen [P1.10, P1.11]. The substance is injected into an artery and as the blood moves farther into the circulation system it diffuses to the surrounding tissue and the amount of tracer in the blood exponentially decays. Based on the arteriovenous concentration difference and the blood flow rate, perfusion can be determined.

The most common technique for invasively measuring blood perfusion uses a Thermal Diffusion Probe (TDP). This system works based on the clearance of thermal energy in the tissue [P1.12, P1.13]. A thermal diffusion probe uses a self-heated thermistor to measure absolute perfusion in real time by measuring the power required to keep the probe temperature higher than the tissue temperature [P1.14].

The convective perfusion probe used in the present research works on a principle similar to the thermal diffusion probe system. This probe induces a thermal event (convective cooling) on the surface of tissue and then measures the heat flux response of the tissue [P1.15]. An absolute perfusion value is calculated based on the transient thermal response.

Several of these perfusion measurement techniques have been validated using the microsphere technique [P1.3]. Microspheres are injected into the blood stream and become embedded in the tissue microcirculation. Then the tissue is harvested and the distribution of the blood flow is determined based on the amount of emitted radiation. Absolute perfusion is determined based on the amount of emitted radiation from a blood sample withdrawn at a known flow rate from an artery downstream of the tissue [P1.16]. Experiments proved there is a strong correlation between renal microsphere perfusion estimates and PET estimated perfusion [P1.17]. Monnet [P1.18] showed a correlation between the Laser Doppler Flowmetry measurements and a microsphere technique on dog stomach walls. Martin & Bowman [P1.19] were able to validate the thermal diffusion probe based on the microsphere technique.

A common problem with blood perfusion measurement systems is developing a reliable way to calibrate them without the presence of physiological and pathological variations and uncertainties. A more convenient system than the microsphere technique would be most useful. Although Robinson *et al.* [P1.20] were able to develop a phantom tissue system to test a thermal perfusion probe, the system was not used for calibration. There remains a need for a calibration system.

Therefore, the main objective of the current research is to develop a calibration phantom tissue system to mimic perfusion and the thermal effects of perfusion while eliminating physiological variations. A phantom tissue model was built using a porous media to model tissue. It was simulated

with commercial computational fluid dynamics software (Fluent) to help validate the experimental results. There are four main criteria to be fulfilled by the phantom tissue model: 1) simulation of non-directional perfusion, 2) properties similar to blood and tissue, 3) known perfusion values that are easily varied, and repeatability.

3.4 The Convective Perfusion Probe

The thermal response of tissue depends on the perfusion through the tissue. Therefore, the heat flux response of the tissue due to a thermal event is a function of the local blood perfusion. This is the basic principle behind both the thermal diffusion probe and the convective perfusion probe. The convective perfusion probe cools the tissue and then measures the thermal response of the tissue. The measured heat flux generates a temperature difference between the top of the convectively cooled sensor and the bottom surface of the sensor, which is warmed by the underlying tissue.

The current blood perfusion probe is a second generation design with a smaller housing and heat flux sensor than Cardinali *et al*. [P1.15]. The convective perfusion probe is shown in Figure 1. The probe housing dimensions are 12.7 mm × 12.7 mm × 10.2 mm. A Vatell heat flux gage (10 mm × 10 mm × 0.25 mm) is placed on the housing, which is connected to an air supply. The thermal event is created by convectively cooling the top surface of the sensor using an array of nine impinging jets in conjunction with the air supply. The air cools the heat flux sensor which produces a measurable heat flux response from the tissue. The shape of the resulting heat flux curve is dependent upon the effects of the blood perfusion in the tissue.

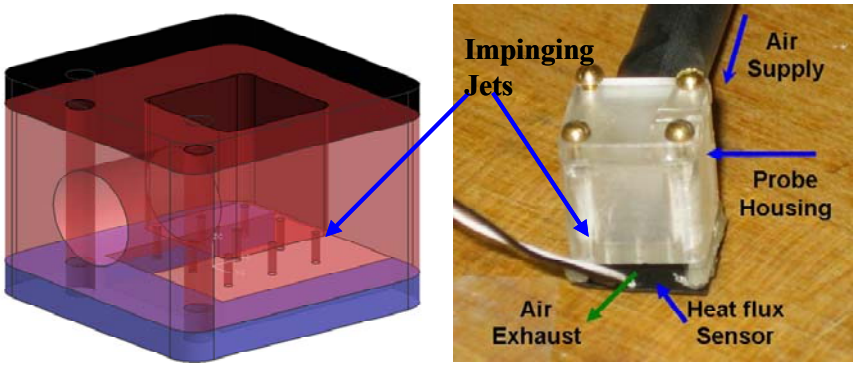

Figure 1: Convective perfusion probe (Left: 3D model of the housing, Right: Actual Probe with the sensor)

A Pentium 4 processor laptop was the base of the data acquisition system. National Instrument's LabView 7.1 in conjunction with a 16 bit, high performance multifunction National Instrument DAQ-Pad 6015 data acquisition system was used to record the voltage signals from the heat flux sensor and an inlet air temperature. These signals were amplified by an AMP-6 Vatell amplifier. The other temperature measurements were recorded by a Doric thermocouple reader.

3.5 Finite Difference Formulation and Parameter Estimation

The predicted heat flux response from the tissue is developed by solving a two-dimensional, finite difference model of the Pennes [P1.21] bioheat equation

$$(\rho C_p)_t \frac{\partial T_t}{\partial t} = k_t \nabla^2 T_t + (\rho C_p \omega)_b (T_a - T_v) \qquad (3.1)$$

where T is temperature, t is time, ρ is density, C_p is specific heat, k is thermal conductivity, and ω is blood perfusion. The subscripts t, b, v and a, corresponds to tissue, blood, venous and arterial respectively. The heat generated due to metabolic activity is assumed to be negligible. In the Pennes bioheat equation, the volume of tissue is assumed to be homogenous, and is supplied with arterial blood, which is at the body's core temperature. The blood flow is assumed to be uniform and the thermal properties of the tissue and the blood are also assumed to be constant. A two-dimensional finite-difference solution was used to solve equation (3.1). A cylindrical coordinate system was chosen for simplicity. Boundary conditions were determined from the experimental conditions discussed later.

An Alternating Directions Implicit (ADI) method [P1.22] was used to solve the discretized equations for the unknown temperature field.

The parameter estimation code compares the recorded heat flux data with corresponding predicted values from the bioheat transfer model in a least square sense to estimate for the value of the blood perfusion term in the Pennes bioheat equation. The parameter estimation routine flow chart is shown in Figure 2. The model is initially solved using guesses for the two unknown parameters, blood perfusion and contact resistance. This numerical solution is then compared to the data set gathered using the sensor. The code determines how closely correlated the estimated solution is to the experimental data via Gaussian minimization [P1.23] and then, if it is not satisfactorily accurate, it makes changes to the initial parameter and repeats the solution. This continues until the best match is achieved between the bioheat model and the recorded experimental data set. A typical convergence plot from parameter estimation routine for one of the test cases is shown in Figure 3.

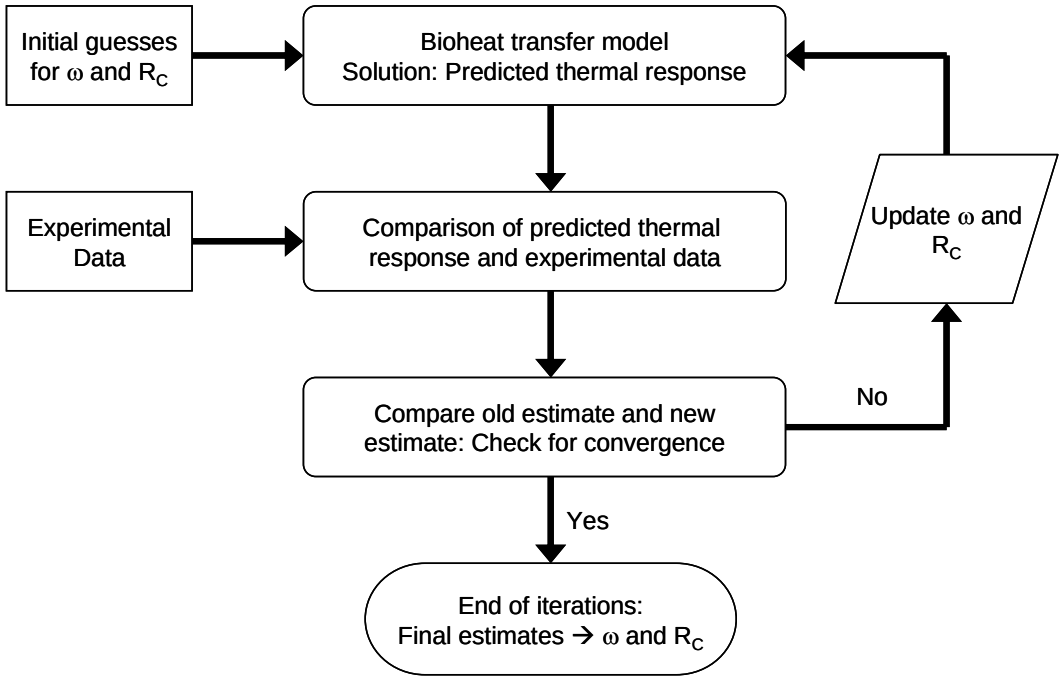

Figure 2: Model based estimation method used to estimate the unknown parameter, blood perfusion, ω, and contact resistance, Rc.

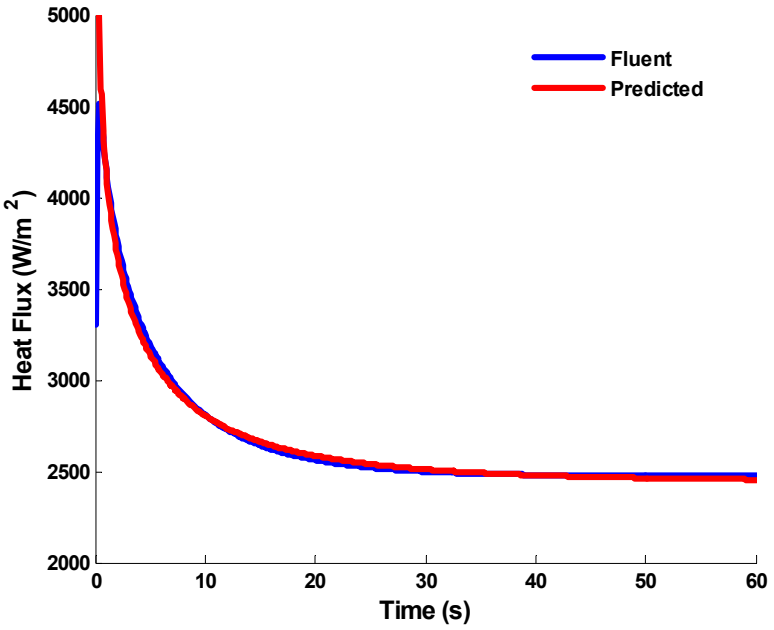

Figure 3: Typical heat flux convergence plot from parameter estimation routine

3.6 Phantom Tissue Test Stand Design

The phantom tissue design was initially modeled with commercial CFD software. The basic model of the phantom tissue was developed using Gambit 2.2.30® and was solved using Fluent® 6.2.16**.** Several configurations and specifications were tested and the final model was developed as illustrated in Figure 4. The flow near the top surface where the heat flux gage is placed is shown in Figure 5. This model has the perfusate (water) entering at the bottom through a flat plate. It was chosen over other configurations because it allows the water to be distributed through the porous matrix and gives multi-directional flow near the surface of the heat flux gage. Several porosities and porous media thicknesses were tested to determine the effects of these parameters on the model. The model showed that the width and length of porous matrix did not have any affect on the heat flux measured during the applied thermal event; however, the thickness did affect the heat flux response. The thickness and the porosity of the sponge used in experiments were measured to be 12.7 mm and 95% respectively. The porosity of the sponge was determined based on the wet and dry weight of the sponge.

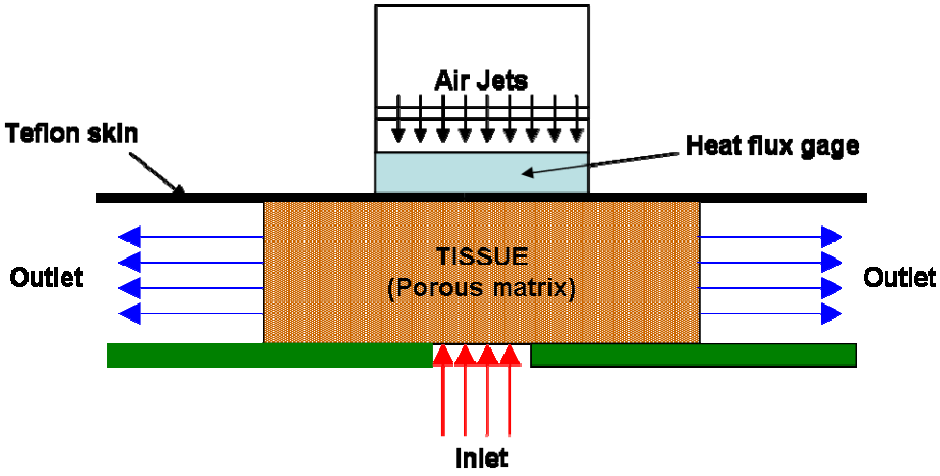

Figure 4: The basic concept for a controlled perfused phantom tissue

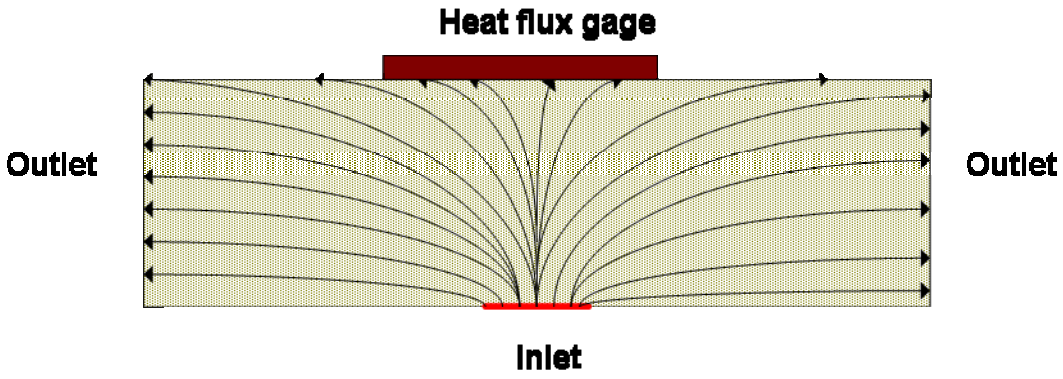

Figure 5: Non-directional flow near the surface of the heat flux gage in the phantom tissue

The complete design of the experimental setup can be seen in Figure 6. The porous media is enclosed in a tank that is completely filled with water. The system can be broken into two main parts: the water regulator system and the actual tissue simulator. The water regulator system includes a pump, a flow controller, and a heater. The tissue simulator system includes a skin simulator, a porous matrix, and a structural support system.

One of the objectives of the test stand is to supply perfusate into the tissue simulator at a controlled temperature and flow rate. For this reason, a plexiglass tank is used to enclose the phantom

tissue test stand. The bottom area of the tank stores water maintained at a constant temperature. The water bath is maintained at 37°C, i.e. core temperature of the human body, by a temperature controller in conjunction with a cartridge heater, Figure 6. The flow into the tissue is provided by a small centrifugal pump that pumps water from the water bath directly through a flowmeter, a Dwyer Instruments Inc. Visi-Float® model VFB-82-BV (0-30 cc/min flow range), into the tissue simulator. The test stand also has leveling feet to ensure the system is true.

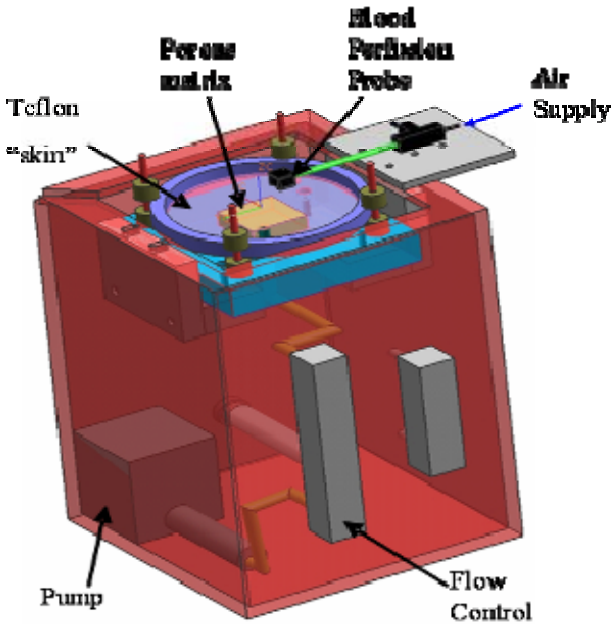

Figure 6: Schematic of phantom tissue test stand and probe

The tissue simulator is made of seven parts, shown in Figure 7. The system is mounted to the plexiglass tank by two plexiglass brackets. The inlet plate, which rests on the brackets, is a 127 mm x 127 mm piece of plexiglass with a tapped hole in the center for the water inlet. A tube of 6.35 mm diameter and 100 mm length is connected to the tapped hole to allow the flow to develop inside the tube before entering the test section. Also, this piece supports the entire tissue simulator section. Above the center hole of the inlet plate is the 40 mm x 40 mm x 12.7 mm porous matrix. On top of the porous matrix lies the simulated skin, Teflon. The Teflon sheet of 0.05 mm thickness is kept taut by a fabric hoop. The supports for the fabric hoop are adjustable to insure that the porous matrix is not

compressed. The blood perfusion probe is then attached to the Teflon using double-sided tape. The water flows through the inlet plate into the porous matrix, and exits through all sides of the porous matrix into the water bath.

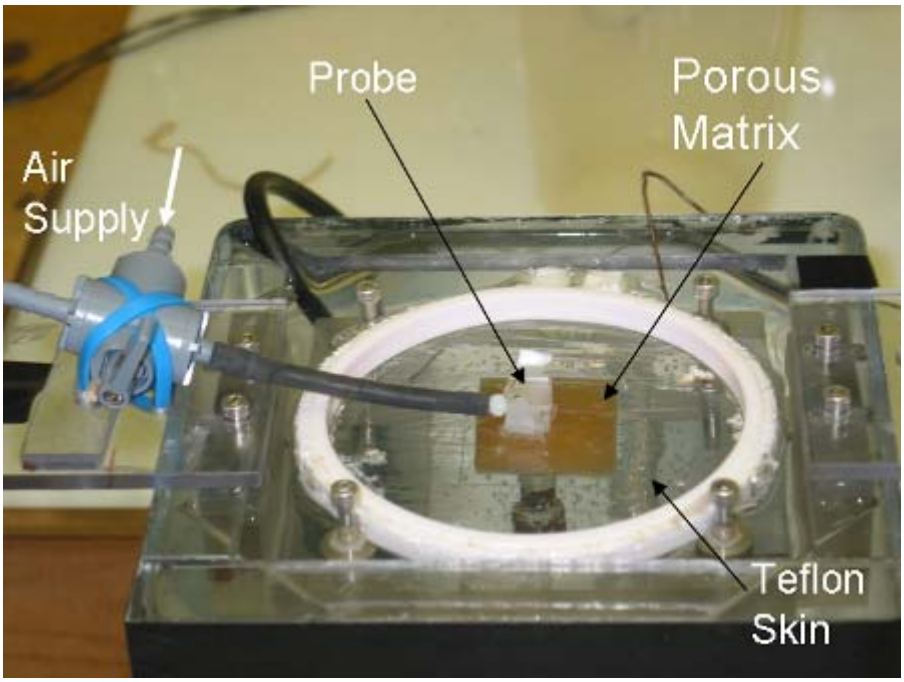

Figure 7: Photograph of the Experimental Test Section setup.

Thermocouples are used at a number of locations to document the temperature distribution throughout the system. Two thermocouples are placed at the top and bottom of the porous media, shown in Figure 8. The bottom thermocouple is used to measure the arterial temperature. Two more thermocouples measure the temperature of the air entering the housing and the temperature of the top of Teflon "skin". The thermocouples are labeled as follows in Figure 8: 1) air flow, 2) skin, 3) top of porous media, and 4) bottom (inlet) of porous media. The air temperature measurement is very important for the parameter estimation because it provides the convective boundary condition.

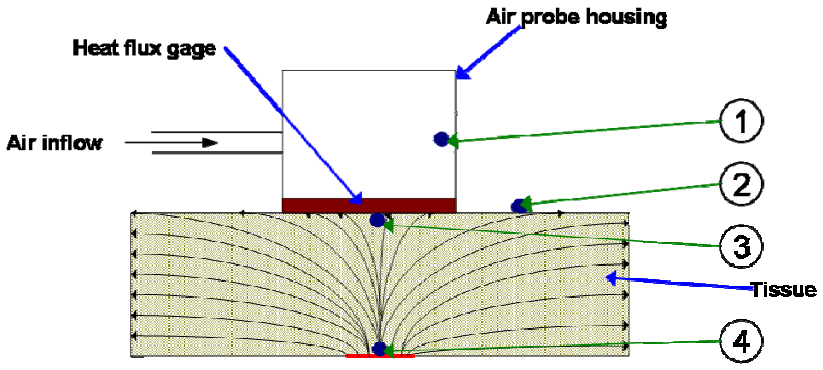

Figure 8: Schematic arrangement of the thermocouple in the test setup

3.7 Computational Model

The computational model with the boundary conditions marked is shown in Figure 9. Also shown are the temperature contours at the end of a thermal event (60s) for a typical flow of 15 cc/min. The thermal penetration in the tissue below the heat flux gage for this typical flow is approximately 1.25 mm and is independent of the thermal event time for times greater than 45s.

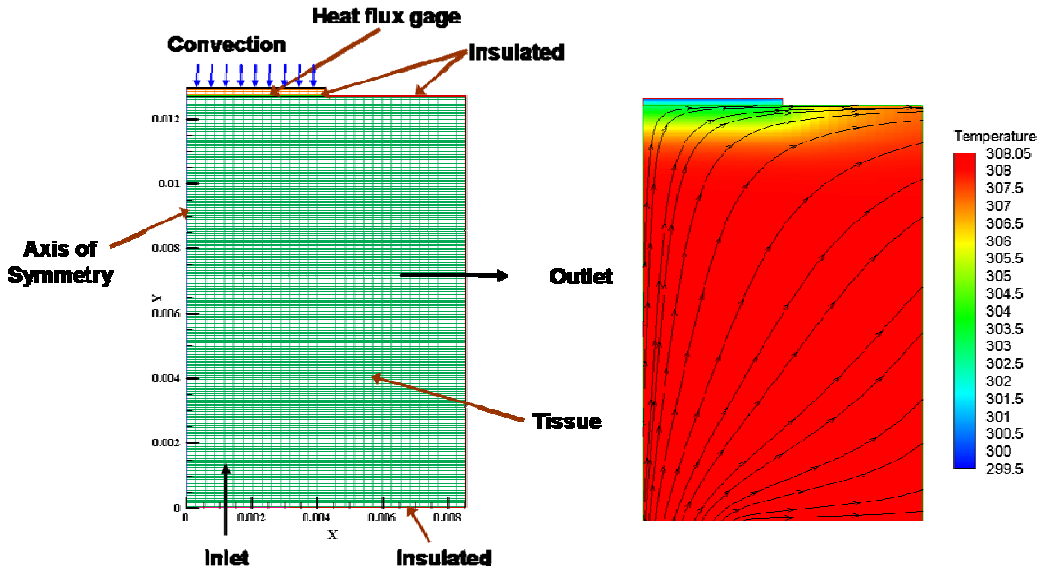

Figure 9: The Fluent axis symmetric model of the phantom tissue shown with boundary conditions, streamlines and temperature distribution.

The Reynolds number for the maximum flow rate of 30 cc/min is 100. Therefore, it takes only six diameters to get a fully developed flow at the inlet of the test section. Hence, a fully developed velocity profile was used in the Fluent model at the inlet. The actual heat flux gage is a thermopile; heat flux is measured as the differential voltage between the two faces of the gage. To incorporate the same into the model, the heat flux from the computational model is calculated as the conductive heat flux based on the area-weighted average temperature difference between the top and the bottom faces. The momentum and energy equations for Fluent were solved using a second-order upwind scheme and the unsteady formulation was carried out using the second-order implicit scheme.

Grid and time step independence tests were carried out before finalizing the computational model. Independence tests were carried out for steady-state conditions at 15 cc/min flow rate, with results shown in Table 1. There is negligible change in the heat flux for an increase of 21.6% in the number of cells, implying that the model is grid independent. The time step of 0.1s for both the parameter estimation program and CFD model was based on the sampling frequency of the DAQ used to acquire heat flux signals, which is 10 Hz. Time-step independence was tested with a time step of 0.05 s. The maximum difference in the resulting heat flux was less than 4% for both CFD and parameter estimation programs, thus demonstrating time-step independence.

Table 1: Grid independence test for 15 cc/min

No. of Cells	Heat flux (W/m^2)
7725	2472.77
9396	2473.00

3.8 Computational Results

To evaluate the best test, length Figure 10 shows the perfusion estimate as a function of thermal event duration for a typical flow of 15 cc/min. There is little difference for perfusion thermal event durations longer than 60s. Therefore, the thermal event duration was set to 60s for all the tests carried out experimentally and computationally. The computational model was made to run for 60 seconds with a time step of 0.1s, to match with the experimental results.

Because the convective perfusion probe and tissue phantom are square, a 3D model was initially used in Fluent. However, to conserve computational time, a 2D axis-symmetric model was also created. The parameter estimation code was used with the CFD results to estimate perfusion with the

same procedure described for experimental results. The comparison of the resulting perfusion estimates for the axis-symmetric and the 3D model are shown in Figure 11 over the range of flow rates used. The 2D axis-symmetric model results are in very good agreement with the 3D model. Consequently, the 2D axis-symmetric model was subsequently used.

The flow model allows for validation of the heat flux response of the phantom tissue test stand. Fluent is used to solve the momentum and energy equations to produce the corresponding heat flux curve. The parameter estimation procedure is then used to relate these results to a perfusion and contact resistance by the same method used for the experiments.

As a further validation of the CFD solutions, an additional computational model was created to provide a direct comparison between the Fluent model and the finite-difference parameter estimation code. In Fluent, perfusion can also be simulated by an energy source term as a function of the local temperature (which results directly in the Pennes bioheat equation). For this model, the inlet flow is set to zero and contact resistance and perfusion values are input directly. The resulting heat flux curve is then used to estimate the perfusion and contact resistance by the parameter estimation procedure. The values obtained from this model are compared with the perfusion values that were input to the Fluent model as shown in Table 2. The estimates obtained are in good agreement with the perfusion values input to the model, with maximum relative error of 9 % with respect to the obtained estimates. Therefore, the Fluent models can be used with the parameter estimation procedure to confirm the effective correspondence between flow rate and perfusion for the phantom tissue system.

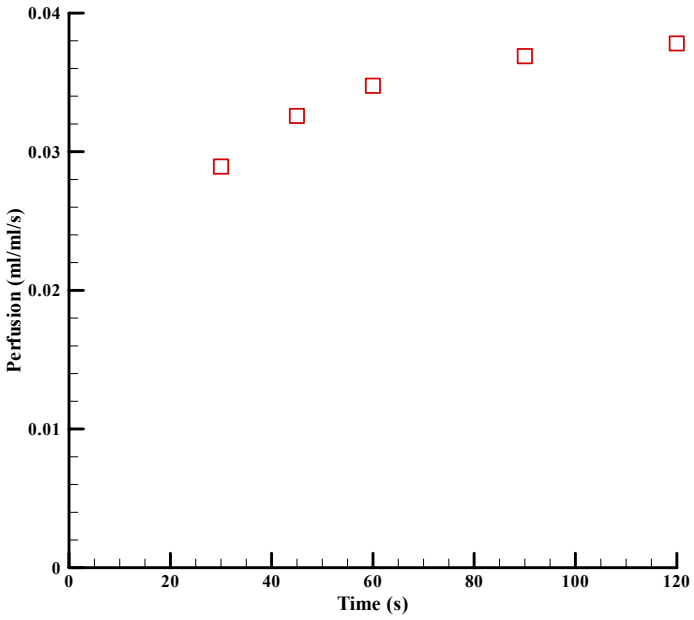

Figure 10: Perfusion estimates for different thermal event durations

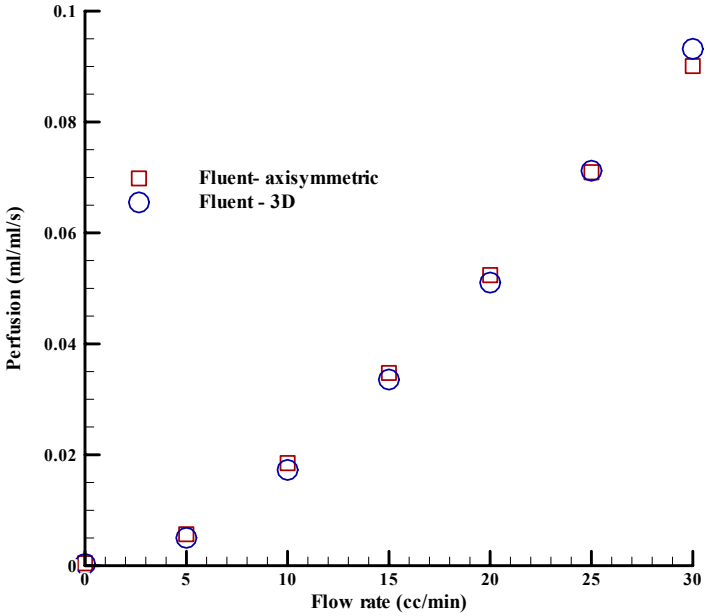

Figure 11: Perfusion estimate comparison for Fluent axis-symmetric and 3-D flow model

The heat flux response of the tissue from the Fluent flow model is shown in the Figure 12. It can be seen from the plot that the heat flux increases with increasing flow rate, and the curves becomes flatter sooner.

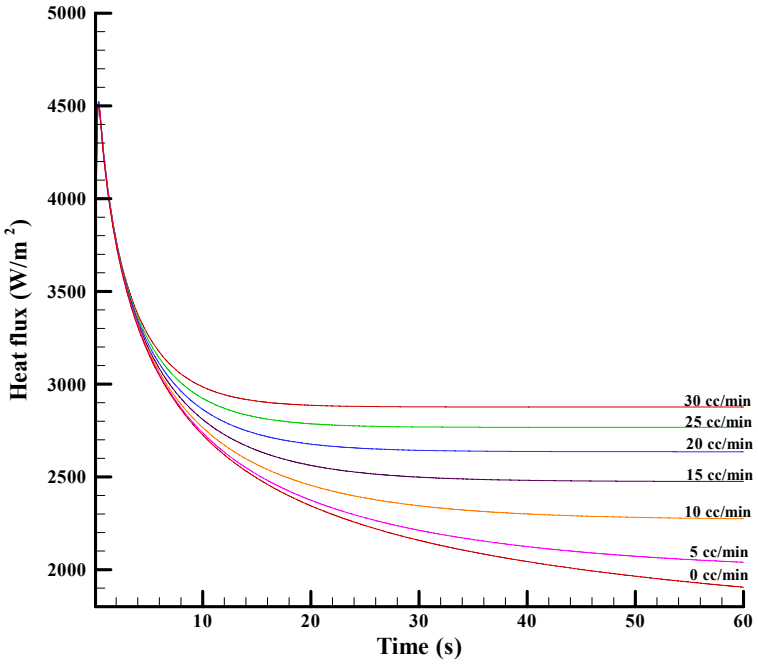

Figure 12: Heat flux response from the Fluent flow model

Table 2: Comparison of Fluent Pennes model with Parameter estimates

Input to Fluent model perfusion (ml/ml/s)	Output from Parameter Estimation code perfusion (ml/ml/s)
0.00567	0.00533
0.01849	0.01864
0.03475	0.03328
0.05238	0.04912
0.07094	0.06577
0.09008	0.08293

As seen from Figure 12 the heat flux curves for the different flow rates are almost identical for the first five seconds of the thermal event. After that the heat flux curves spread out depending on the flow rates. Sensitivity analysis was carried out to quantify the effects of perfusion and contact resistance on the heat flux curves. A dimensionless sensitivity coefficient, X_i^+, was defined as

$$X_i^+ = \frac{\delta q''^+_i}{\delta \beta_i^+} = \frac{\Delta q''^+_i}{\Delta \beta_i^+} \tag{3.2}$$

$$\Delta q''^+_i = \left| \frac{q''_{Pi} - q''_{Ni}}{q''_{Ni}} \right| \tag{3.3}$$

where $\Delta q''^+_i$ is the dimensionless change in heat flux for a perturbed value of the parameters, β. The subscripts Ni and Pi represent the nominal and perturbed values, respectively. The dimensionless difference of the nominal and perturbed perfusion and contact resistance values are represented by $\Delta \beta_i^+$ as calculated by

$$\Delta \beta_i^+ = \left| \frac{\beta_{Pi} - \beta_{Ni}}{\beta_{Ni}} \right| \tag{3.4}$$

The results of sensitivity analysis for the Fluent flow model at a flowrate of 15 cc/min are shown in Figure 13. It is evident that the sensitivity coefficient for contact resistance starts high and then becomes constant after the first 5 seconds. The perfusion sensitivity coefficient keeps on increasing with time, making it clear that perfusion is best estimated at longer times. It is therefore important to estimate the contact resistance, between the heat flux gage and the tissue along with the perfusion.

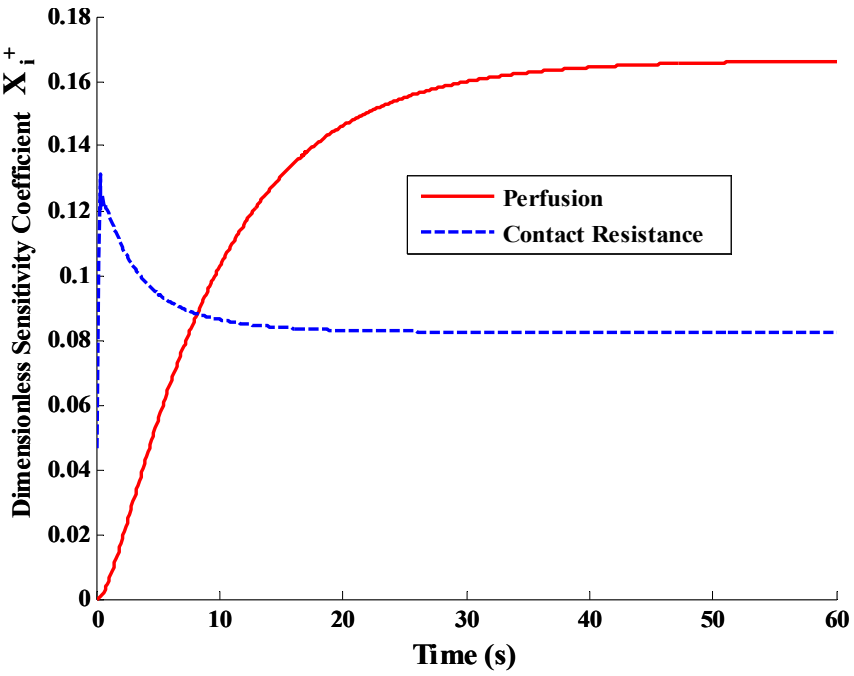

Figure 13: Sensitivity analysis for blood perfusion and contact resistance

3.9 Experimental Procedure

To ensure repeatability the same experimental procedure was used for all tests. Table 3 summarizes the experimental procedure timeline that was used for all phantom tissue tests. The first step is to equilibrate the temperature within the porous matrix by flushing at a maximum flow rate for 20 seconds. Then the flow rate is set and the system is allowed to equilibrate for the next 40 seconds. Data acquisition begins after one minute. The first minute of data acquisition is used to determine the offset in the heat flux signal. Next, the thermal event is started in the second minute of data acquisition and is recorded for 1 minute.

Ninety-one total tests were completed on the phantom tissue test stand. Tests were completed at 7 different flow rates ranging from 0 cc/min to 30 cc/min in increments of 5 cc/min. At each flow rate, 13 tests were completed to test the repeatability of the test stand. The testing was completed on 3 different days to test the effects of changing environmental conditions (especially air temperature).

Table 3: Summary of the experimental procedure for the phantom test

Step	Procedure	Time
1	Set the flow meter to maximum flow possible	0 sec
2	Set the flow rate to the desired flow rate for experimental run	20 sec
3	Start the data acquisition (heat flux and temperature)	60 sec
4	Turn the air supply on	120 sec
5	Turn the air supply off	180 sec
6	Data acquisition stops. Save the data files.	180 sec

3.10 Results

3.10.1 Experimental Heat Flux Results

One of the main design criteria for the phantom tissue test stand was to give repeatable experimental conditions, eliminating physiological variability. Figure 14 shows an example of the heat flux curves produced by the convective perfusion probe for the three different days of testing. With an inlet flow rate of 15 cc/min it can be seen that the heat flux results from day one are slightly lower than the other two days. This difference is due to a higher convective air temperature for the first day and a higher thermal contact resistance, possibly due to probe positioning. Overall, these curves showed very good repeatability. The curves are representative of the repeatability results from all of the different flow rates.

Another goal of the phantom tissue test stand was to have easily varied flow rates. To determine if the changes in inflow were detectable by the perfusion probe a comparison of the experimental heat flux at different flow rates is presented in Figure 15. The shape of the heat flux curves for the three different flow rates are decidedly different. This was to be expected and correlates to the different perfusion values. This shows the sensitivity of the blood perfusion probe for change in flow rate, which is directly related to perfusion.

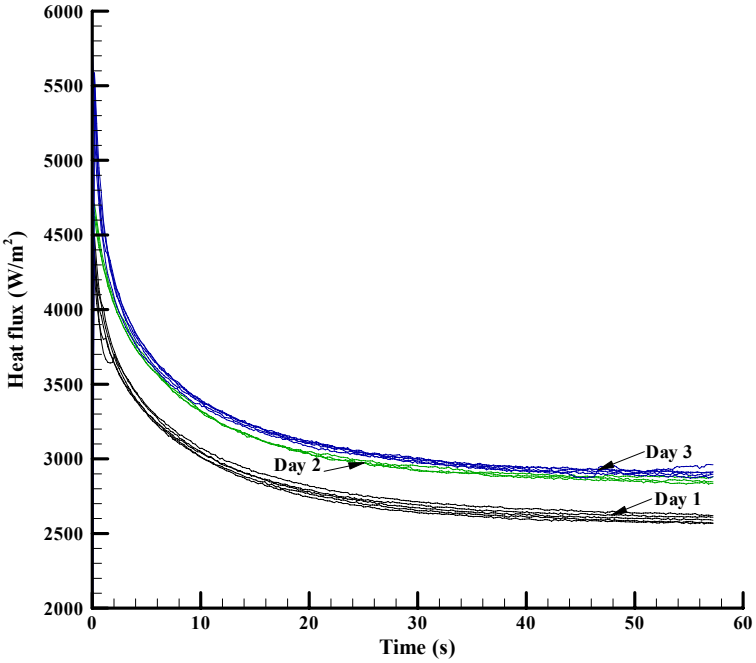

Figure 14: Repeatability of the experimental heat flux for 15 cc/min flow rate

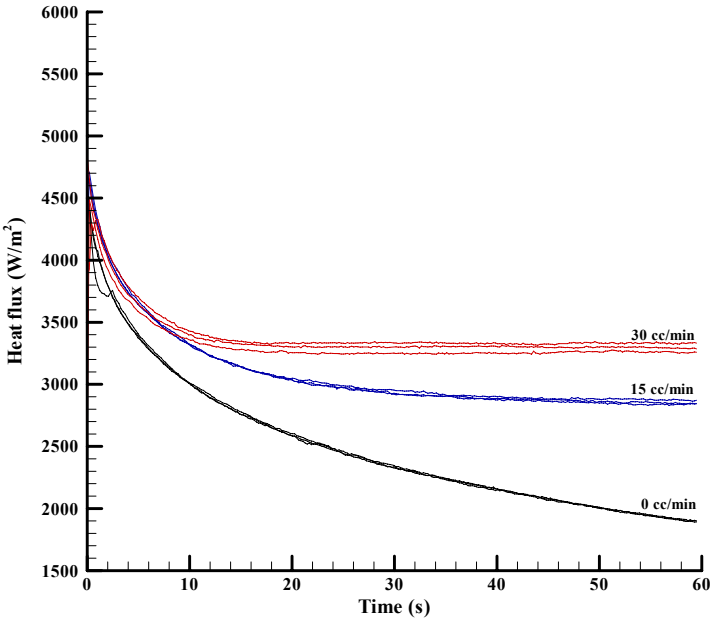

Figure 15: Heat flux sensitivity for phantom tissue test stand

3.10.2 Results of the Perfusion and Contact Resistance Estimates

The parameter estimation code was used to determine the experimental perfusion in the phantom tissue test stand for all of the tests at the different flow rates. The results are shown in Figure 16 from the experimental runs for day one, day two and day three for all the flow rates ranging from 0 – 30 cc/min, in increments of 5 cc/min. It is clear that the probe displays good measurement repeatability, as the perfusion values for different flow rates follow the same trend for all three days. There is higher variation in the estimates at higher flows, specifically, at 25 and 30 cc/min.

The average experimental perfusion values with 95% confidence intervals are shown in Figure 17, along with the perfusion estimates from the Fluent CFD model. The perfusion estimates for the no flow case in the experimental phantom tests were slightly negative. The offset was removed by subtracting the average perfusion estimated for the no flow case in phantom tissue (-0.00652 ml/ml/s) from all the results. The CFD flow model perfusion was 0.00043 ml/ml/s for the no flow case. This value is small relative to the perfusion measurements for the other flow rates and hence was assumed to be negligible. Figure 17 show that perfusion increases almost linearly with flow rate, as expected. The experimental perfusion estimates are in good agreement with that of the CFD flow model up through a flow rate of 20 cc/min. For flow rates of 25 and 30 cc/min the variation in perfusion estimates are slightly higher. These results clearly indicate the direct relationship between perfusion and flow rate for flows greater than 5 cc/min, and provide an experimental and a theoretical validation of the probe. Higher differences at the higher flow rates could be due to the uncertainty in the experimental temperature measurements. From the sensitivity analysis it was found that the parameter estimation procedure is highly sensitive to these measurements. Even with these offsets, the fact that the estimates are close in magnitude proves the trends shown in Figure 16 are repeatable. This indicates that the blood perfusion probe can be used to consistently detect changes in perfusion by surface measurements.

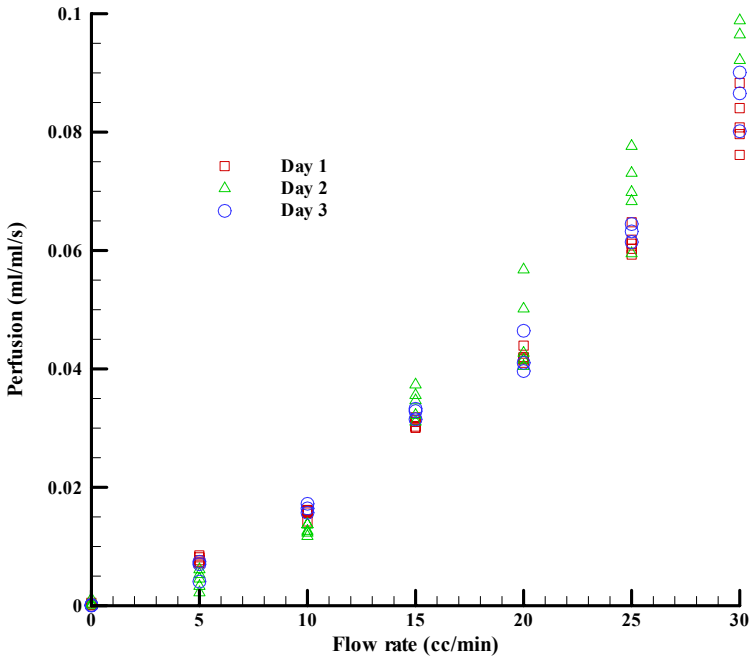

Figure 16: Perfusion estimated for the all the experimental tests conducted

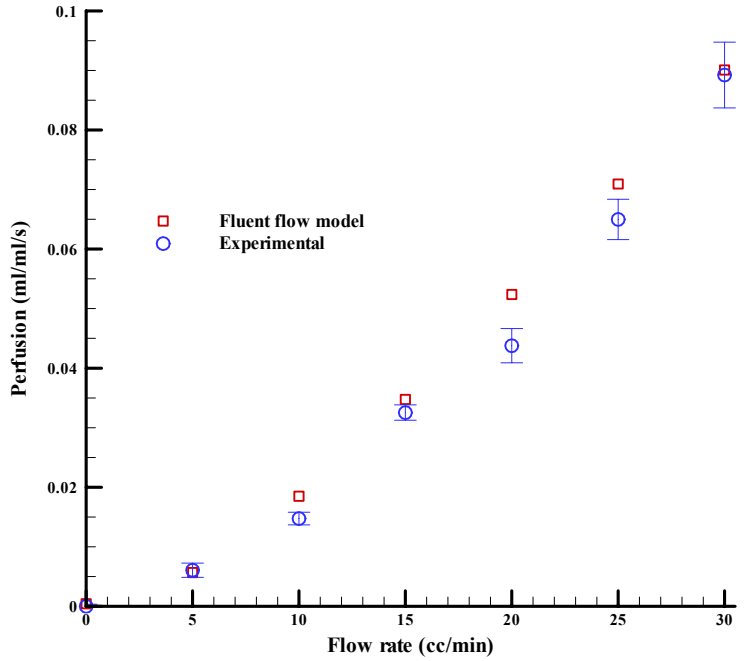

Figure 17: Comparison of perfusion estimates of Fluent flow model with Experimental test conducted on phantom tissue for different flow rates

The contact resistance estimated for the phantom tests is shown in Figure 18 with the 95% confidence intervals. It appears that there is no strong correlation between the contact resistance and the flow rate, although the points do exhibit some upward slope for flow rates greater than 10 cc/min. Statistical analysis was used to check the dependence of contact resistance on the perfusate flow rate. The statistical mean for all the flow rates is within 95% confidence intervals except for the flow rate of 10 cc/min. Therefore, it can be concluded that the differences in contact resistances are statistically insignificant and are generally independent of the inlet flow rate.

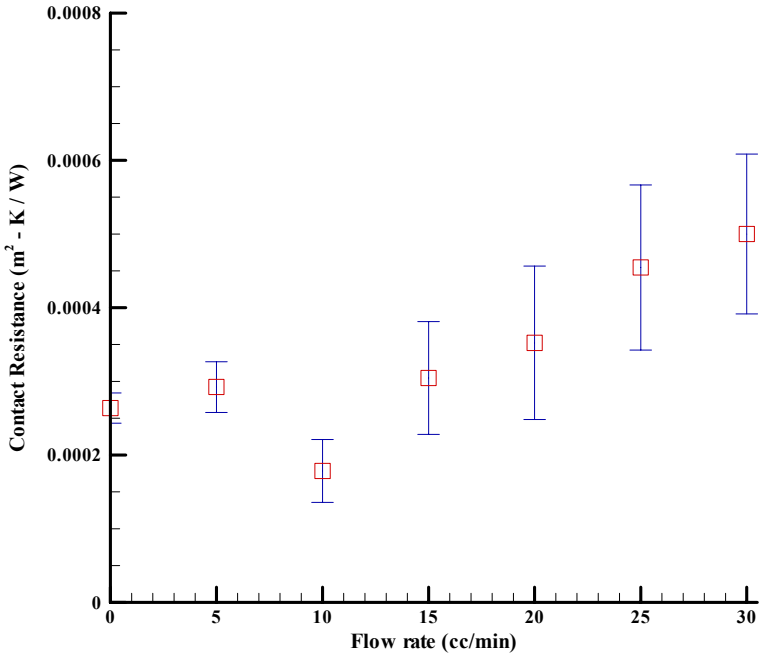

Figure 18: Contact resistance estimated for the phantom tissue test

3.11 Conclusions

The phantom tissue system proved to be a convenient, reliable test bed for surface perfusion measurements in an environment where physiological and pathological conditions are eliminated. The phantom tissue system was shown to be a valid calibration system using a combination of experimental and CFD results with the convective perfusion probe. The convective perfusion probe was shown to be sensitive and repeatable for perfusion measurements. The repeatability, sensitivity and good comparison with the CFD models demonstrates that perfusion can be reliably measured by the

convective perfusion probe. The phantom tissue system is a great device for testing and development of perfusion measuring devices.

3.12 Acknowledgements

This work has been supported by Grant No. EB03943-01 from the National Institutes of Health.

3.13 References:

P1.1 Schelbert, Heinrich R., 2000, "PET Contributions to Understanding Normal and Abnormal Cardiac Perfusion and Metabolism."*Annals of Biomedical Engineering*, Vo. 28, pp 922-929.

P1.2 Montet, X., M.K. Ivancevic, J. Belenger, M. Jorge-Costa, S. Pochon, A. Pechér, F. Terrier, and J. Vallé, 2003, "Noninvasive Measurement of Absolute Renal Perfusion by Contrast Medium-Enhanced Magnetic Resonance Imaging," *Investigative Radiology*, Vol. 38, No. 9, pp. 584-592.

P1.3 Prinzen, F. W., and J. B. Bassingthwaighte, 2000, "Blood flow distributions by microsphere deposition methods," *Cardiovascular Research*, Vol. 45, pp. 13-21.

P1.4 Vajkoczy, P., H. Roth, P. Horn, T. Lucke, C. Taumé, U. Hubner, G.T. Martin, C. Zappletal, E. Klar, L. Schilling, P. Schmiedek, 2000, "Continuous Monitoring of Regional Cerebral Blood Flow: Experimental and Clinical Validation of a Novel Thermal Diffusion Microprobe," *Journal of Neurosurgery*," Vol. 93, pp. 265-274.

P1.5 Niwayama, J., and T. Sanaka, 2005, "Development of a new method for monitoring blood purification: The blood flow analysis of the head and foot by laser Doppler blood flow meter during hemodialysis," *Hemodialysis International*, Vol. 9, pp. 55-62.

P1.6 Mileski, W. J. L. Atiles, G. Purdue, R. Kagan, J. R. Saffle, D. N. Herndon, D. Heimbach, A. Luterman, R. Yurt, C. Goodwin, J. L. Hunt, 2003, "Serial Measurements Increase the Accuracy of Laser Doppler Assessment of Burn Wounds," *Journal of Burn Care & Rehabilitation*, Vol. 24, pp. 187-191.

P1.7 Oltean, M. A. Aneman, G. Dindelegan, J. Mölne, M. Olausson, and G. Herlenius, 2005, "Monitoring of the Intestinal Mucosal Perfusion Using Laser Doppler Flowmetry After Multivisceral Transplantation," *Transplantation Proceedings*, Vol.37, pp 3323-3324.

P1.8 Leahy, M.J., de Mul, F.F.M., Nilsson, G.E., Maniewski, 1999, " Principles and Practice of the Laser-Doppler Perfusion Technique", *Technology and Health Care*, 7, pp. 143-162.

P1.9 Liebert, A., Leahy, M., Maniewski, R., 1995, " A Calibration Standard for Laser-Doppler Perfusion Measurements", *Rev. Sci. Instr.* 66(11), pp. 5169-5173.

P1.10 Machens, H., Pallua, N., Mailaender, P., Pasel, J., Frank, K., Reimer, R., Berger, A., 1996, "Measurements of Tissue Blood Flow by the Hydrogen Clearance Technique (HCT): A Comparative Study Including Laser Doppler Flowmetry (LDF) and the Erlangen Micro-Lightguide Spectrophotometer (EMPHO)," *Microsurgery*, Vol. 16, No. 12, pp. 808-817.

P1.11 Woodcock, J.P., 1985, "Noninvasive Blood Flow Measurement," *Critical Reviews in Biomedical Engineering,* Vol. 12, No. 3, pp. 201-235.

P1.12 Valvano, J.W., J.T. Allen, H.F. Bowman, 1984, "The Simultaneous Measurement of Thermal Conductivity, Thermal Diffusivity, and Perfusion in Small Volumes of Tissue," *Journal of Biomechanical Engineering*, Vol. 106, pp. 192-197.

P1.13 Bowman, H., 1985, "Estimation of Tissue Blood Flow," in: *Heat Transfer in Medicine and Biology*, eds. A. Shitzer and R. Eberhart, Vol. 1, Chap. 9, Plenum Press, pp 193-203.

P1.14 Khot. M. B., P. K. M. Maitz, B. R. Phillips, H. F. Bowman, J. J. Pribaz, D. P. Orgill, 2005, "Thermal Diffusion Probe Analysis of Perfusion Changes in Vascular Occlusions of Rabbit Pedicle Flaps," *Plastic Reconstructive Surgery.,* Vol. 115, No. 4, pp. 1103-1109.

P1.15 Cardinali, A.V., Lanz, O.I., Diller, T.E., Scott, E.P., 2002, "Validation of a Noninvasive Blood Perfusion Measurement System using a Canine Medial Saphenous Fasciocutaneous Free Tissue Flap Model", *Proceedings of the ASME, IMECE'02, New Orleans*, Nov 17- 22, Paper No. 32354 .

P1.16 Heymann, M. A., B. D. Payne, J. I. Hoffman, A. M. Rudolph, 1977, "Blood flow measurements with radionuclide-labeled particles," *Prognoses of Cardiovascular Disease,* Vol. 20, pp. 55-74.

P1.17 Juillard, L., Janier, M.F., Fouque, D., Lionnet, M., Bars, D.L., Cinotti, L., Barthez, P., Gharib, C., Laville, M., 2000, " Renal Blood Flow Measurement by Positron Emission Tomography using ^{15}O – labeled Water", *Kidney International*, Vol. 57, pp. 2511 – 2518.

P1.18 Monnet, E., Pelsue, D., Macphail, C., 2006, " Evaluation of Laser Doppler Flowmetry for Measurement of Capillary Blood Flow in the Stomach Wall of Dogs During Gastric Dilatation – Volvulus", *Veterinary Surgery*, Vol. 35, pp. 198-205.

P1.19 Martin, G. T. and Bowman, H. F., 2000, "Validation of Real-Time Continuous Perfusion Measurement," *Med. Biol. Eng. Comput.*, Vol. 38, pp. 319-327.

P1.20 Robinson, P.S., Scott, E.P., Diller, T.E., 2006, " Testing of Non-Invasive Probe for Measurement of Blood Perfusion", *Submitted to Journal of Medical Devices*.

P1.21 Pennes, H. H., 1948, "Analysis of Tissue and Arterial Blood Temperatures in the Resting Human Forearm," *J. Appl. Physiol.*, Vol. 1, pp. 93-122.

P1.22 von Rosenberg, D.U., 1969, Methods for Numerical Solution of Partial Differential Equations, pp. 84-89.

P1.23 Scott, E.P., Robinson, P.S., and Diller, T.E., 1998, "Development of Methodologies for the Estimation of Blood Perfusion Using a Minimally Invasive Probe", *Measurement Science and Technology*, (Invited Paper – Special Edition), Vol 9, No. 6, pp. 888-897.

Chapter 4

Paper 2: Non – Invasive Blood Perfusion Measurements of an Isolated Rat Liver and an Anesthetized Rat Kidney

To be submitted to Journal of Biomechanical Engineering[+]

4.1 Abstract

A simple, cost effective, and noninvasive blood perfusion system has been developed and tested in animal models. The system uses a small sensor to measure the heat transfer response to a small thermal event (convective cooling) imposed on the tissue surface. Heat flux data are compared with a mathematical model of the tissue to estimate both blood perfusion and contact resistance between the tissue and the probe. The perfusion system was evaluated for repeatability and sensitivity using isolated rat liver and exposed rat kidney tests. Perfusion in the isolated liver tests was varied by controlling the flow of the perfusate into the liver, and the perfusion in the exposed kidney tests was varied by temporarily occluding blood flow through the renal artery and vein. The perfusion estimated by the convective perfusion probe was in good agreement with that of the metered flow of perfusate into the liver model. The liver tests indicated that the probe can be used to detect small changes in perfusion (0.005 ml/ml/s). The probe qualitatively tracked the changes in the perfusion in the kidney model due to occlusion of the renal artery and vein.

[+] Co – authors: Brent E. Ellis, Patricia L. Ricketts, Dr. Elaine P. Scott, Dr. Thomas E. Diller, Department of Mechanical Engineering , Virginia Tech
Dr. Otto I. Lanz, Department of Small Animal Clinical Sciences, Virginia Tech
Dr. Charles Y. Lee, Department of Mechanical Engineering Science, UNC Charlotte

4.2 Introduction

Blood perfusion, defined as the blood volume flow exchange through a given volume or mass of tissue (in units of ml/ml/s or ml/100g/min), represents local blood flow through the capillary network and extracellular spaces in the tissue. It is important for normal tissue physiology, including the transport of oxygen, nutrients, and waste products, and is part of the temperature regulatory system of the body. Changes in blood perfusion are associated with a variety of pathologic processes, including burn and other traumatic wound healing, head traumas, and tumor growth.

As such, measurement of blood perfusion is a valuable medical diagnostic. For example, perfusion measurements can determine the success or failure of skin grafts and any related healing. The ability to measure perfusion is fundamental to an improved understanding of both normal and pathologic physiology, as well as the diagnosis and management of numerous medical conditions, including shock and tissue viability subsequent to traumatic injury, transplantation, and non-surgical treatments of cancer. Thus, knowledge of perfusion could be used to determine areas of tissue damage, regions of elevated healing response, or inconsistencies in expected function.

A noninvasive convective blood perfusion probe (CPP) has been developed to provide local surface perfusion estimates. To operate the system, a thermal event is imposed on the surface of the tissue, and the resultant heat flux is measured using a probe instrumented with a small sensor, as shown in Figure 19. Perfusion values are estimated from these heat flux measurements and corresponding calculated values from a mathematical model of the system using a minimization procedure. The objectives of this research are to evaluate the sensitivity and repeatability of the thermal blood perfusion system under physiological conditions using two animal tissue models: an exposed rat kidney and an isolated rat liver.

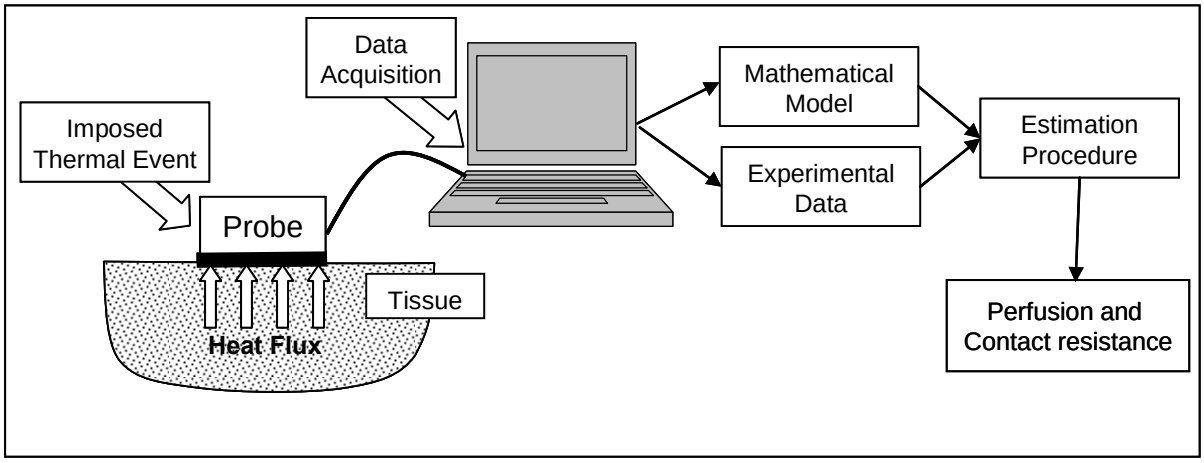

Figure 19: Schematic of Convective Blood Perfusion Probe (CPP) system

4.3 Background on Perfusion Measurements

Both thermal and non-thermal approaches have previously been attempted to measure blood perfusion. Thermal perfusion measurement methods are based on the clearance of thermal energy and usually require the insertion of a probe into the tissue. This not only disturbs the tissue to be measured, but causes discomfort and allows for the possibility of infection in the patient. However, these methods can be advantageous for deep tissue measurements such as in the brain *e.g.*, [P2.1- P2.3].

The most common of these methods is the Thermal Diffusion Probe (TDP) [P2.4-P2.7] consisting of a thermistor bead situated at the end of a hypodermic needle. The thermistor is used to both deposit thermal energy into the tissue and measure the temperature response. The power deposition is controlled as a specified function. The main advantage of the thermal diffusion probe is that it can provide absolute perfusion measurements. Khot *et al*. [P2.6] demonstrated that this technique was viable for rabbit pedicle flaps. Also, Kamiya *et al*. [P2.8] compared the thermal diffusion probe to the hydrogen clearance method and verified that these two methods produced similar perfusion measurements. The biggest drawback for widespread clinical use is that the probe is invasive and limited to depths greater than 5 mm. This is undesirable not only for the discomfort and danger to the patient, but also because of the trauma and disruption of the tissue that is being measured.

Several attempts have been reported to create instruments to thermally measure blood perfusion non-invasively. These generally have used a heater and temperature sensor on the surface of the tissue,

with some arrangement to minimize heat loss. Patel *et al*. [P2.9] and Li *et al.* [P2.10] used thermistor probes covered by insulation, while Walsh and Bowman (1984) [P2.11] used a second thermistor on top of the first to act as a guard heater. Castellana *et al*. [P2.12] used a thin-film resistor placed on the skin surface to provide heat and measure the temperature. Focused ultrasound was used by Anderson and Burnside [P2.13] as the heat source with a thermistor placed on the surface of the tissue to measure the temperature response. Holti and Mitchell [P2.14] used a thermopile between a heated copper piece and a surrounding piece of copper placed on the surface of the skin. They tried to relate the measured temperature difference established after several minutes of heating to the blood perfusion.

Noninvasive thermal techniques have had limited success because of several problems which are not present for the invasive techniques. The actual heat flux going into the tissue is difficult to determine because losses to the ambient are typically large. The heat losses are small for the invasive probes because they are not exposed to the environment. In addition, the thermal contact resistance between the probe and tissue surface is important and difficult to determine for the noninvasive probes. Because the invasive probes penetrate into the tissue, thermal contact is not an issue. Moreover, the mathematical modeling is simpler for the invasive probes because spherical symmetry can be assumed.

Common non-thermal perfusion measurement methods include imaging and laser Doppler methods. Magnetic Resonance Imaging (MRI) is a noninvasive technique to directly measure blood flow by utilizing arterial blood as an endogenous tracer. The arterial spin labeling (ASL) technique in MRI determines spatially and temporally resolved perfusion in tissue [P2.15-P2.17]. The clinical applications of perfusion MRI have been limited by number of factors, including relatively poor spatial resolution, limited volume coverage and low signal to noise ratio. It is difficult to improve any of these aspects because it requires rapid image acquisition. During the past decade, methodologies for ASL perfusion imaging have evolved from feasibility studies into practical usage. Although the use of MRI to measure perfusion yields accurate, repeatable and absolute results of perfusion, this method is limited to deep tissue [P2.18], and in general is inconvenient to use in critical settings, such as during surgery.

Positron Emission Tomography (PET) scans can be used to make relative measurements of blood perfusion, but require the introduction of a radioactive tracer into the blood supply. PET images begin with an injection of a solution of glucose (sugar) that has been "tagged" with a radioactive chemical isotope (generally fluorine 18, N-ammonia or O labeled water) [P2.19]. Metabolically active organs or tumors consume sugar at high rates, and as the tagged sugar starts to decay, it emits positrons. These positrons then collide with electrons, giving off gamma rays, and a computer converts the gamma

rays into images [P2.20-P2.21]. All of these imaging methods show promise, however, they are not feasible for blood perfusion measurements during surgery and they are limited by the cost, equipment size, and processing time.

Laser Doppler Flowmetry is an established technique for the real-time measurement of red blood cell motion in tissue. Laser Doppler Flowmetry (LDF) and Laser Doppler Imaging (LDI) [P2.22] work by illuminating the tissue with a laser. The perfusion measurement is derived from the product of the mean velocity and the concentration of the red blood cells within the volume of the tissue being measured [P2.22]. Laser Doppler signals from the tissue are recorded in BPU (Blood Perfusion Units) which is a relative units scale calibrated using a suspension of latex spheres undergoing Brownian motion. They have been used for monitoring dialysis [P2.23], assessing the extent of burn wounds [P2.24], and assessing transplant rejection [P2.25]. There are several difficulties associated with LDF technology. By its nature, LDF makes velocity measurements of red blood cells in only one direction and gives perfusion in relative values. Another problem is that LDF is highly sensitive to the optical properties of the tissue.

The convective perfusion probe system was developed to overcome some of the problems encountered in the existing perfusion measuring systems as described above. The significance of this system is that the fundamental design provides for practical, cost effective, noninvasive, absolute perfusion measurements on the tissue surface.

4.4 Design and Operation of Convective Perfusion Probe

In the convective perfusion probe system, a thermal event, in this case cooling, is imposed on the tissue surface. The resultant heat flux from the tissue is measured using a heat flux gage similar to Cardinali [P2.26], but smaller in size. The heat flux generates a temperature difference across the thickness of the heat flux gage, which appears as a voltage output (E) directly proportional to the heat flux, q''

$$q'' = \frac{E}{S_q} \tag{4.1}$$

where the constant, S_q, is the sensitivity factor of the heat flux gage.

The operation of the convective perfusion probe relies on the 10 to 15°C temperature elevation of the core body temperature above the usual air-conditioned environment temperature of 20°C to 25°C.

When not making a measurement, the sensor is in equilibrium with the surface temperature of the tissue with very little heat flux. The initiation of a measurement occurs when cooling is started. Here, cooling is achieved by forced convection from an air supply through the probe. This causes the sensor temperature to drop and the heat flux to increase because of the temperature gradient from the tissue. The temperature drop within the tissue is limited to less than 5°C to minimize temperature dependent effects on the perfusion. The heat flux measurements are recorded, along with air, skin surface, and core body temperatures, throughout each test. Once the air supply is turned off, the system comes back to equilibrium and is ready for another test. The process is painless and is barely detectable by the skin.

A schematic of the convective perfusion probe in operation is shown in Figure 20. A 10 mm × 10 mm heat flux gage (Vatell Corp. model BF-02) is mounted to the base of the probe housing, and a compressed air supply is connected to the housing and delivers room temperature air to provide convective cooling. The air is passed through a water bath to maintain it at a constant temperature before entering the probe housing. The air flows through a plate with nine holes (0.37 mm diameter) to create air jets which impinge onto the sensor causing a measurable heat flux response from the tissue. The air then exhausts through outlets in the housing. The probe sensor is affixed to the tissue using double-sided tape.

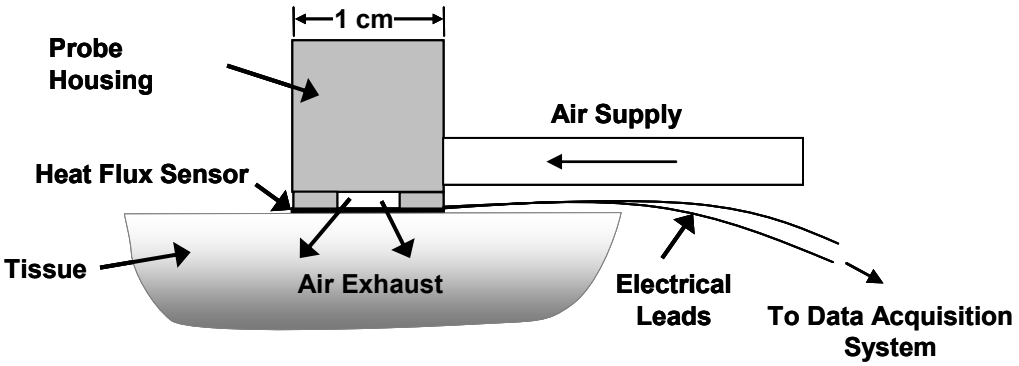

Figure 20: Convective Blood Perfusion Probe

4.5 Modeling and Parameter Estimation

Parameter estimation techniques are used to determine perfusion by minimizing an objective function containing both measured experimental and calculated heat flux data. The calculated heat flux data are obtained from a two-dimensional cylindrical finite-difference model of the probe and tissue based on the Pennes (1948) bioheat equation, neglecting metabolic heat generation.

$$(\rho C_p)_t \frac{\partial T_t}{\partial t} = k_t \nabla^2 T_t + (\rho C_p \omega)_b (T_a - T_v) \tag{4.2}$$

where T is temperature, t is time, ρ is density, C_p is specific heat, k is thermal conductivity, and ω is blood perfusion. The subscripts t, b, v and a, corresponds to tissue, blood, venous and arterial respectively. The tissue is assumed to be homogenous, and is supplied with arterial blood, at the body's core temperature. The blood perfusion is assumed to be uniform and the thermal properties of the tissue and the blood are also assumed to be constant.

The recorded air, arterial and tissue temperatures are used as input conditions for the model. By performing a sensitivity analysis, it was found that the parameter estimation procedure was highly sensitive to the air temperature measurements. To improve the parameter estimation routine, air temperature is recorded as a function of time all through the thermal event. The boundary conditions for the model are shown in Figure 21. An Alternating Directions Implicit (ADI) method is used to solve the discretized equations for the unknown temperature field. The Box-Kanemasu Method [P2.28] is used to perform the minimization procedure as shown in Figure 22. Note that both the perfusion and the unknown contact resistance at the probe/tissue interface are estimated. The independent estimate of the contact resistance is performed to eliminate the effects of differences in skin properties and surface characteristics.

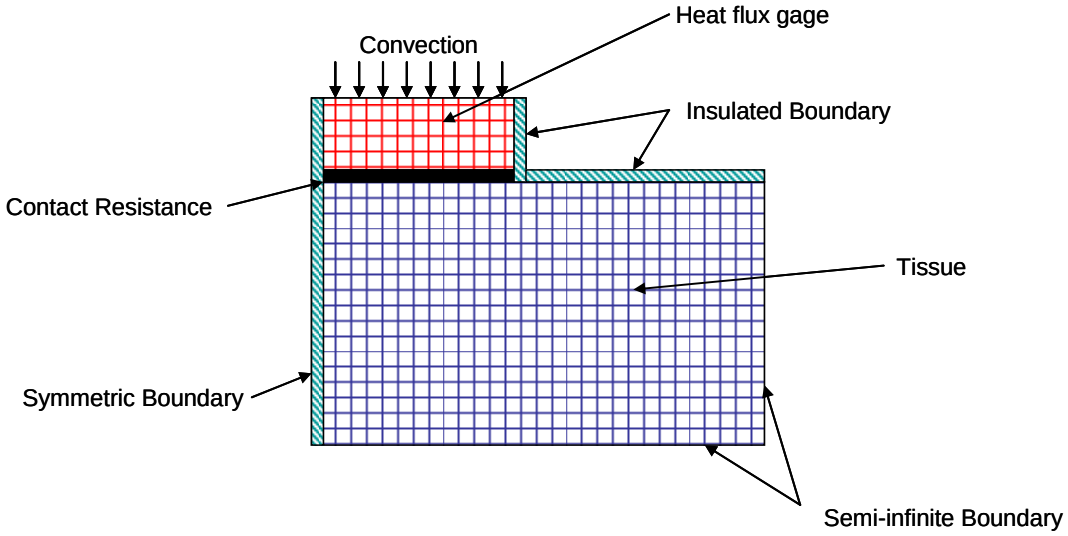

Figure 21: Schematic of Finite Difference Model of Sensor and Tissue

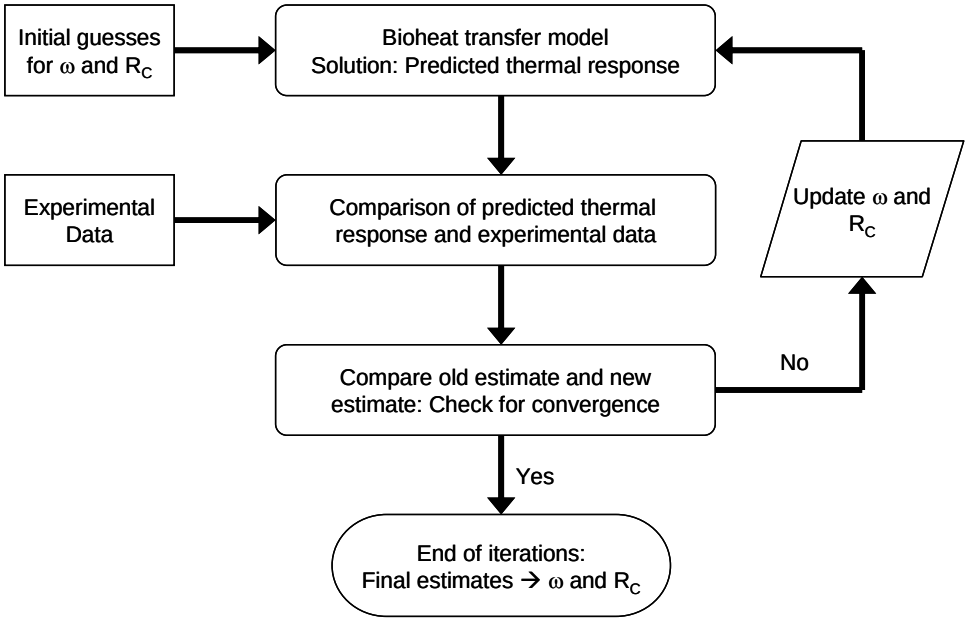

Figure 22: Model based estimation method used to estimate the unknown parameter, blood perfusion, ω, and contact resistance, R_C.

4.6 Data Acquisition Equipment

The data acquisition system used to record the heat flux and temperature data required for the estimation procedure is shown in Figure 23. A *P4*-2.8GHz laptop serves as the base. A 16 bit, USB high

performance multifunction data acquisition system is used to measure the voltage signals from the heat flux sensor and an inlet air thermocouple. These signals are amplified and passed through an A/D converter. National Instruments LabView 7.1 is used to control the data acquisition process. The other temperatures are measured by using a Doric thermocouple reader. The voltage signals from the heat flux sensor are converted to heat flux by multiplying the sensor sensitivity, and those from the thermocouple are converted to temperature by multiplying by the thermocouple sensitivity and adding the reference temperature (which is measured by the Doric).

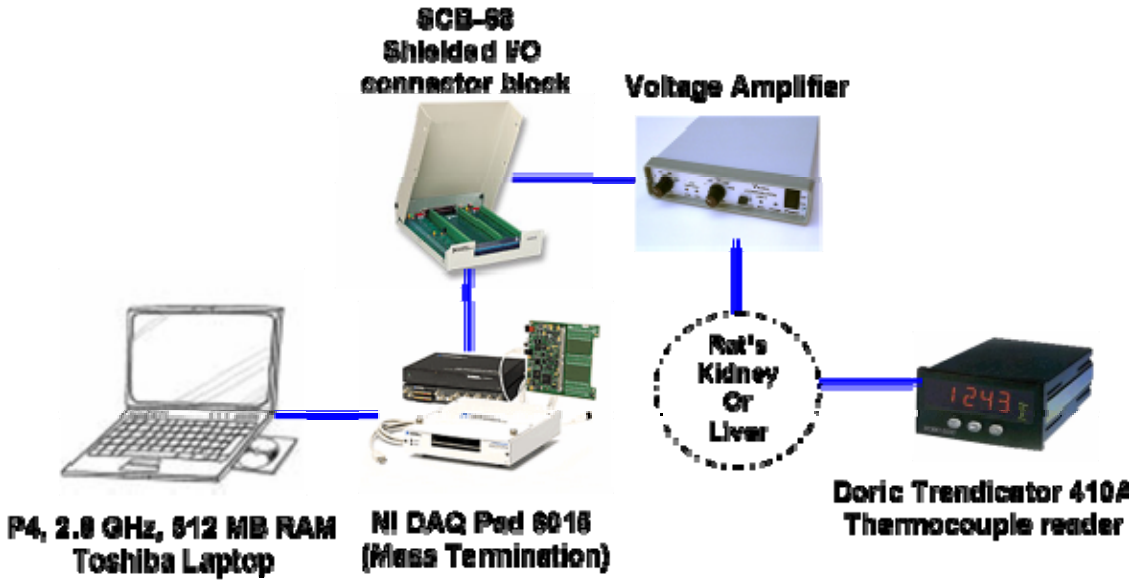

Figure 23: Data Acquisition used for Liver and Kidney Test

4.7 Experimental Methods

4.7.1 Isolated Liver Model

Experiments were performed using male Sprague-Dawley rats (Charles Rivers, Wilmington, MA, USA) weighing 270 g under isoflourane anesthesia, at the University of North Carolina, Charlotte. Animals were cared for and treated by protocol approved by National Institute of Health institutional animal use and care guidelines.

Isolation surgery started with a transverse abdominal incision. The portal vein, inferior vena cava and bile duct were exposed using moist gauze to move the bowel and the duodenum. The bile duct was

transected after distal ligation and a polyethylene tube (PE-10, BD-Clay Adams, Sparks, MD) was inserted into the lumen of the bile duct and secured with a circumferential 3-0 silk suture. One ml of saline containing 200 U of heparin was injected through the inferior vena cava. The portal vein was canulated using a 14 gauge catheter and secured with 3-0 silk suture. Then the inferior vena cava was closed with a 3-0 silk suture. A small incision was made on the suprahepatic vein, close to the heart. A 10 ml syringe filled with cold Krebs-Henseleit buffer solution was used to flush the blood out slowly. A 14 gauge catheter was inserted into the suprahepatic vena cava and tied tightly with a 3-0 silk suture.

The closed loop experimental arrangement for the liver is show in Figure 24. It was perfused with Krebs-Henseleit solution at a temperature of 37 $^{\circ}$C. A peristaltic pump monitored with an inline ultrasound flow transducer controls the flow rate. Inflow and outflow pressures are monitored with pressure transducers (not shown in figure). In order to keep the liver tissue alive, the perfusate passes through a gas exchanger with 95% O_2 and 5% CO_2 gas. After isolation, the liver was placed on a temperature-controlled stage as shown in Figure 25. The tissue was covered with clear plastic to prevent it from cooling and drying.

Tests were conducted at five different flow rates: 0, 5, 10, 15 and 20 ml/min with two to four repetitions at each flow rate. Liver temperature was monitored by placing a thermocouple on the tissue to be tested. The perfusate temperature was also recorded for each flow rate. The blood perfusion probe was affixed to the liver with a piece of two-sided tape. The DAQ typically runs for 120 seconds, the air is bled off through a three way valve for the first 60 seconds to remove any offset in heat flux. For the next 60 seconds, the air is forced to impinge on the sensor, eliciting a heat flux response from the tissue.

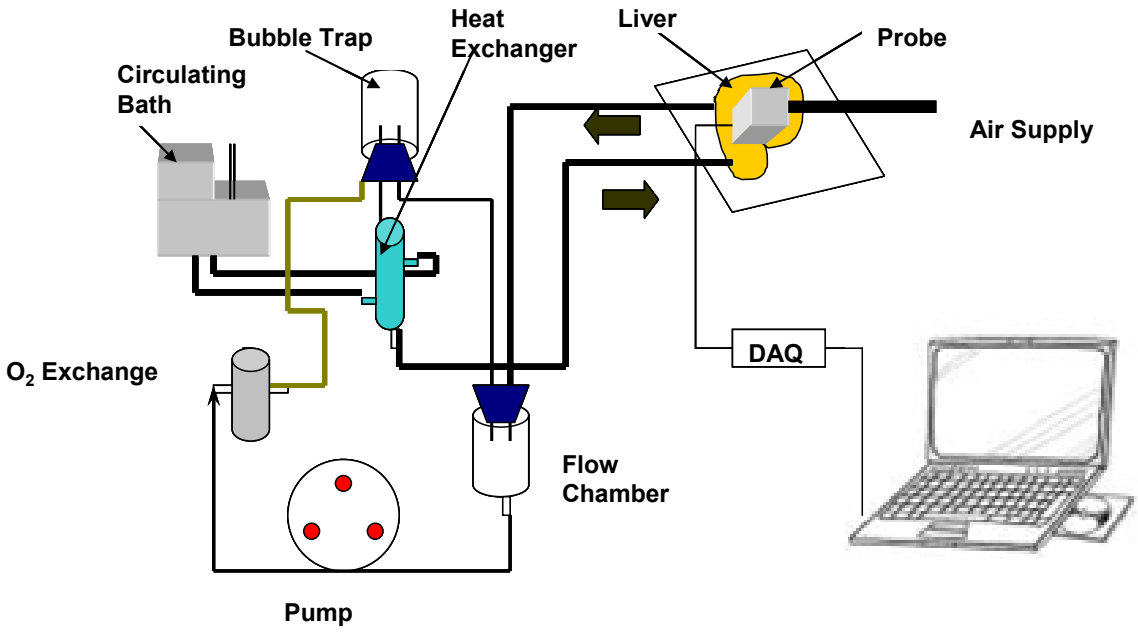

Figure 24: Experimental setup for the isolated liver test

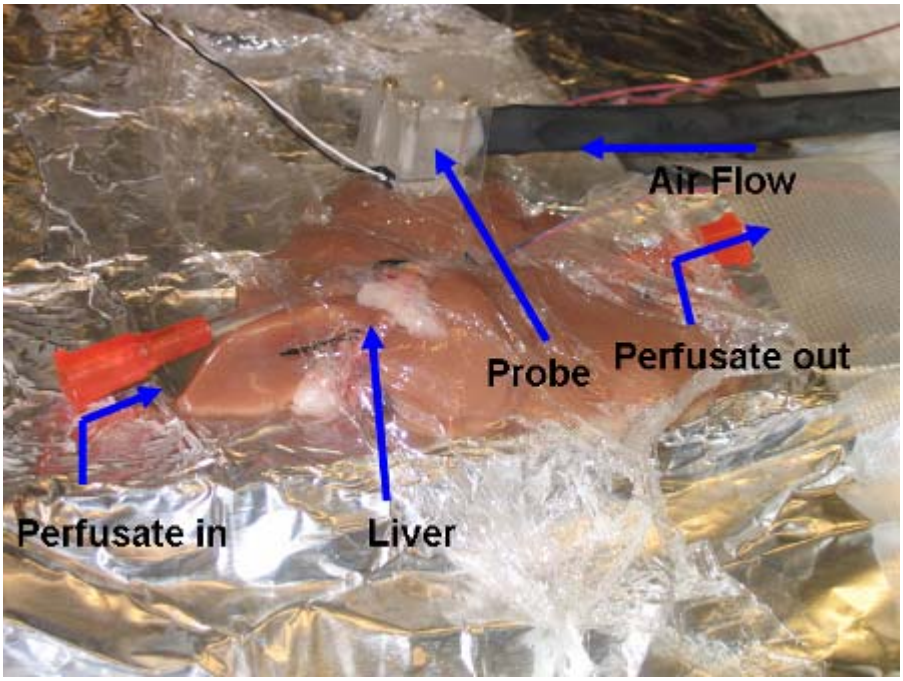

Figure 25: Probe on isolated liver for perfusion measurements

4.7.2 Exposed Kidney Model

The rat was anesthetized and maintained with isoflurane in 100% oxygen. The ventral abdomen was clipped from the xiphoid to the pubis and aseptically prepared for surgery. A sheet of ioban was used to drape the surgical site and an incision was made from the xiphpoid to the pubis using a number 15 scalpel blade. The left kidney was bluntly dissected and the renal vein and artery were isolated. Blood flow to the kidney was temporarily occluded using a microvascular clamp placed over the renal artery and vein. To re-establish blood flow, the microvascular clamp was removed from the renal artery and vein.

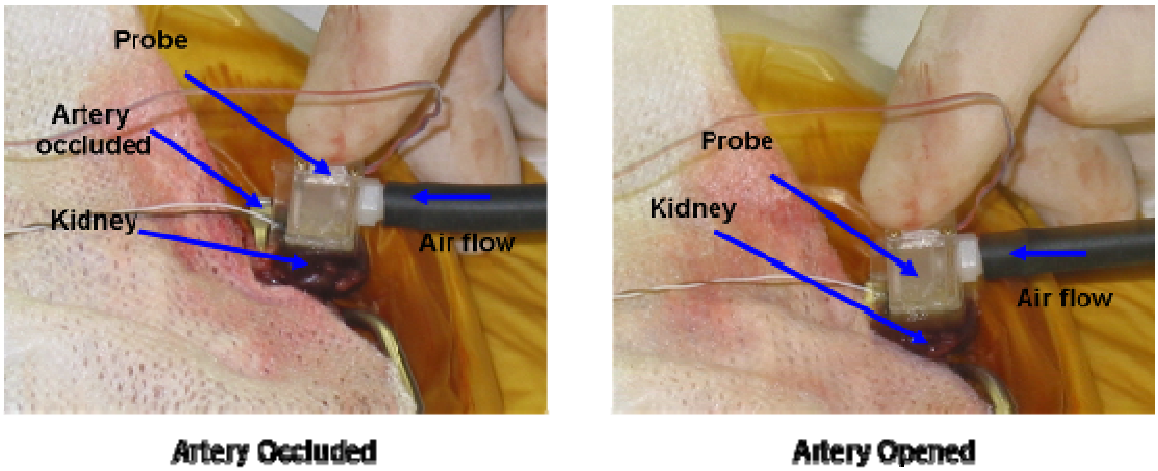

Figure 26: Experimental setup for the exposed kidney model

The data acquisition system ran for 120 seconds for each test. There is no air supplied for the first 60 seconds, which is done to remove any zero offset in the measured heat flux. After 60 seconds the air supply is switched on initiating the 60 second cooling event. A two minute break was allowed between each test to re-equilibrate the temperature in the tissue. Clamping both the artery and vein insures that flow both in and out of the tissue is stopped. The first three tests were done without occluding the artery to check the repeatability of the measured heat flux data from the blood perfusion probe. The next six tests were carried out by alternately occluding the artery and opening the artery. Figure 26 shows the probe placed on the kidney with the artery occluded.

4.8 Results and Discussions

4.8.1 Isolated Liver Model

The *ex vivo* liver model was used to provide a controlled perfusion in the living tissue and to validate the convective perfusion probe sensitivity and repeatability. Samples of the heat flux response during thermal events for perfusate flow rates of 5, 10, and 20 cc/min are shown in Figure 27. The curves for the different flow rates are clearly different and the repeatability for the same flow rate is reasonably good. Some of the variability in the heat flux for different flow rates is due to probe placement and surface contact resistance, which is quantified by the contact resistance. The initial rise and fall of the heat flux curve is due to the domination of contact resistance and conduction while the later part is influenced by blood perfusion [P2.29].

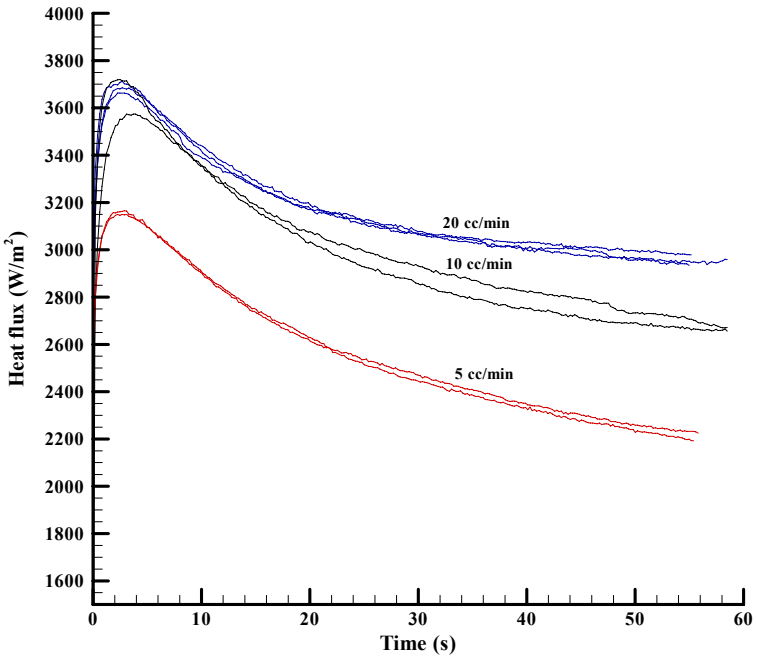

Figure 27: Repeatability and Sensitivity of the convective blood perfusion probe for different perfusate flow rate for liver model

Perfusion estimates were obtained for each of the different flow rates. The results for these are compared to the imposed flow rate with 95% confidence intervals indicated in Figure 28. The current

parameter estimation routine gives a slight offset in the perfusion values of -0.0087 ml/ml/s, which was removed from all of the results. The solid line indicates a one-to-one correspondence with the average perfusion values based on the measured flow rate and weight of the liver (15 grams). The perfusion estimates from the blood perfusion probe are in excellent agreement with the calculated average perfusion. It is also clear from the plot that the sensor can reliably detect a small change in blood perfusion (0.005 ml/ml/s). A statistical analysis was carried out to check the dependence of perfusion on the perfusate flow rate. It is also clear from Figure 28 that the statistical mean for all the flow rates are different up to perfusion estimates corresponding to 15 cc/min (0.017 ml/ml/s). Therefore, it is concluded that the measured perfusion is statistically significant over most of the range. More data sets are required at the higher flow rates.

Contact resistance was also estimated from the experimental measurements. As shown in Figure 29, the estimated contact resistance decreases with increase in perfusate flow rate up to 15 cc/min and then increases for 20 cc/min flow rate. These values are necessary for accurate estimates of the perfusion.

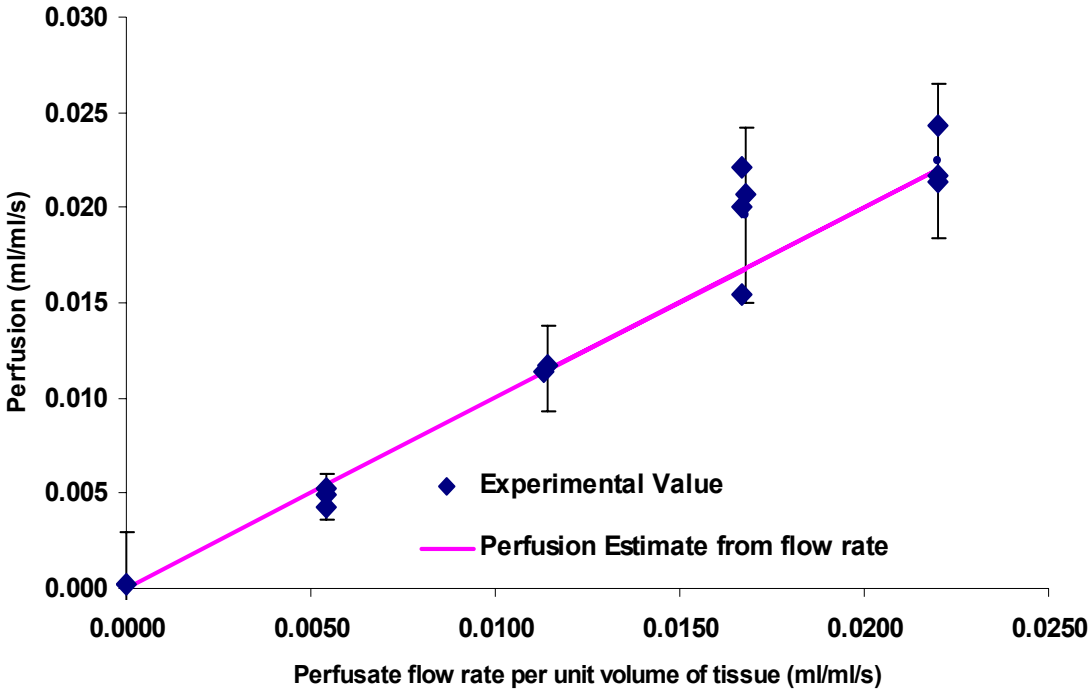

Figure 28: Perfusion estimates of liver with one to one correspondence

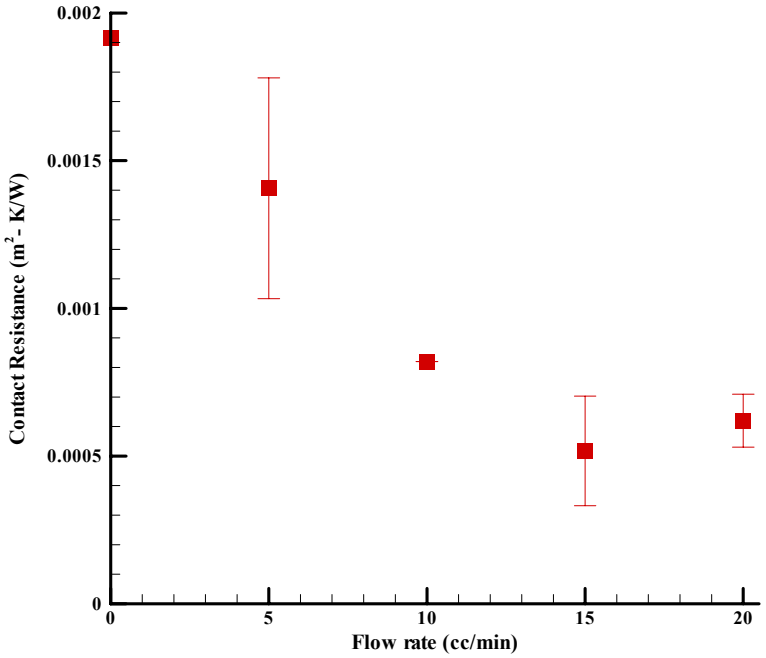

Figure 29: Contact resistance for liver tests with 95% confidence intervals

4.8.2 Exposed Kidney Model

Qualitative tests of the probe were done *in vivo* using the kidney model. The heat flux response is similar to that of the liver tests. The current numerical model for the probe and tissue gives a slight offset in the perfusion values of -0.00943 ml/ml/s for the kidney based on the occluded tests. This is very close to the value for the liver tests. It was subtracted from all of the perfusion estimates shown in Figure 30 and results in an average value of zero perfusion for the occluded cases. The accompanying table lists the perfusion values and the status of the kidney during the test. The tests are listed in sequential order of measurement. The first three tests show the repeatability of the measurements before the artery was clamped. These are typical perfusion values for the highly perfused tissue of the kidney. Tests 4 through 9 demonstrate the effects of occlusion. The perfusion values for the occluded tests drop substantially, as expected. The perfusion values when the artery is re-opened are slightly higher than for the three initial tests before occlusion (tests 1 through 3). This is a typical response following the sudden removal of the occlusion. The blood apparently rushes in when the clamp is removed to replenish the tissue, thereby increasing the blood perfusion in the tissue.

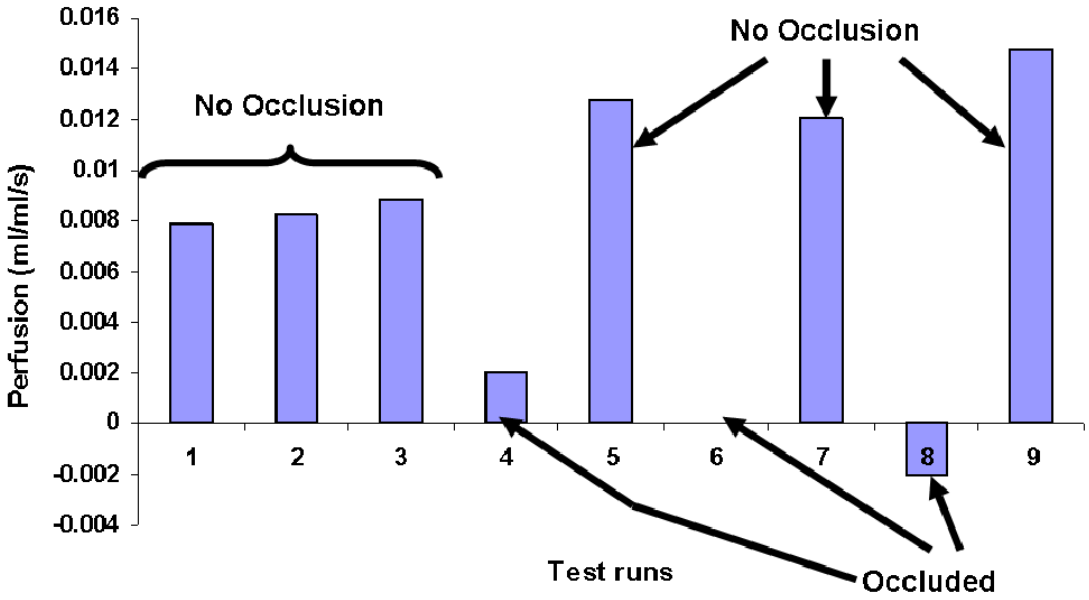

Figure 30: Average perfusion estimates for the rat kidney

Table 4: Perfusion estimates for the kidney tests

Tests	Artery	Perfusion ml/ml/s
1	open	0.00784
2	open	0.00825
3	open	0.00882
4	closed	0.00198
5	open	0.01274
6	closed	0.000
7	open	0.01203
8	closed	-0.00199
9	open	0.01478

To further demonstrate the effects of perfusion on the heat flux response a special test is shown in Figure 31. The artery was occluded for the first 60 seconds and then the artery was opened for the next 60 seconds. The heat flux for the first 60 seconds decreases steeply because there is no perfusion

due to the occlusion. The heat flux response increases immediately after the occlusion is removed, indicating that the perfusion quickly starts to warm the tissue. The corresponding perfusion estimates and model predictions are also shown for the comparison. Although the results don't match as well as the usual 60 s tests, the effects of perfusion are dramatic and generally predicted.

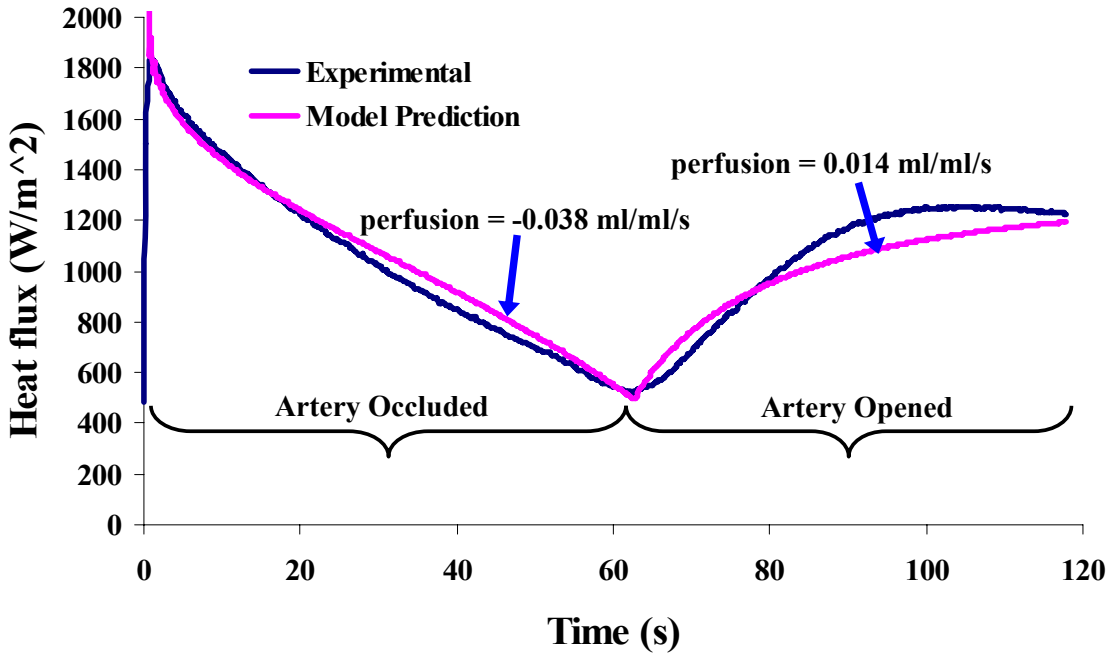

Figure 31: Heat flux response from the kidney model with artery occlusion followed by opening

4.9 Conclusions

The performance of the convective perfusion probe was successfully demonstrated on two animal models. The experimental measurements with an isolated liver were in good agreement with the average controlled flow of perfusate into the liver. The convective perfusion probe displayed good repeatability and sensitivity, reliably measuring changes in perfusion of the order of 0.005 ml/ml/s. The convective perfusion probe qualitatively assessed the perfusion changes in a rat kidney caused by the occlusion of the renal artery and vein. The repeatability, sensitivity and good agreement with the animal model results demonstrates that perfusion can be qualitatively and quantitatively measured by the convective perfusion probe.

.

4.10 Acknowledgements

This work has been supported by Grant No. EP03943-01 from the National Institutes of Health.

4.11 References:

P2.1 Chato, J.C., 1985, "Measurement of Thermal Properties of Biological Materials," in *Heat Transfer in Medicine and Biology*, eds. A. Shitzer and R. Eberhart, Vol. 1, Chap. 8, Plenum Press, NY, pp 167-192.

P2.2 Bowman, H., 1985, "Estimation of Tissue Blood Flow," in: *Heat Transfer in Medicine and Biology*, eds. A. Shitzer and R. Eberhart, Vol. 1, Chap. 9, Plenum Press, pp 193-203.

P2.3 Kress, R., and R. Roemer, 1987, "A Comparative Analysis of Thermal Blood Perfusion Measurement Techniques," *Journal of Biomechanical Engineering*, Vol. 109, No. 3, pp. 218-225.

P2.4 Valvano, J.W., J.T. Allen, H.F. Bowman, 1984, "The Simultaneous Measurement of Thermal Conductivity, Thermal Diffusivity, and Perfusion in Small Volumes of Tissue," *Journal of Biomechanical Engineering*, Vol. 106, pp. 192-197.

P2.5 Vajkoczy, P., H. Roth, P. Horn, T. Lucke, C. Taumé, U. Hubner, G.T. Martin, C. Zappletal, E. Klar, L. Schilling, P. Schmiedek, 2000, "Continuous Monitoring of Regional Cerebral Blood Flow: Experimental and Clinical Validation of a Novel Thermal Diffusion Microprobe," *Journal of Neurosurgery*," Vol. 93, pp. 265-274.

P2.6 Khot. M. B., P. K. M. Maitz, B. R. Phillips, H. F. Bowman, J. J. Pribaz, D. P. Orgill, 2005, "Thermal Diffusion Probe Analysis of Perfusion Changes in Vascular Occlusions of Rabbit Pedicle Flaps," *Plastic Reconstructive Surgery.,* Vol. 115, No. 4, pp. 1103-1109.

P2.7 Maitz, Peter K. M, M. B. Khot, H. F. Mayer, G. T. Martin, J. J. Pribaz, H. F. Bowman, D. P. Orgill, 2005, "Continuous and Real-Time Blood Perfusion Monitoring in Prefabricated Flaps," *Journal of Reconstructive Microsurgery.* Vol. 20, No. 1, pp. 35-41.

P2.8 Kamiya, Hinoryuki. G. Watanabe, T. Saito, T. Doi, S. Tomita, H. Ohtake, T. Kanamori, 2002, "Real-time and continuous monitoring of myocardial blood flow using a thermal diffusion method." *European Journal of Cardio-thoracic Surgery*, Vol. 21, pp. 748-752.

P2.9 Patel, P.A., J.W. Valvano, J.A. Pearce, S.A. Prahl, C.R. Denham, 1987, "A Self-Heated Thermistor Technique to Measure Effective Thermal Properties from the Tissue Surface," *Journal of Biomechanical Engineering*, Vol. 109, pp. 330-335.

P2.10 Li, H. J., X. X. Zhang, and Y. F. Yi, 2002, "Measurement of Blood Perfusion Using The Temperature Response to Constant Surface Heat Flux." *International Journal of Thermophysics, Vol 2*, No. 6, pp 1631-1644.

P2.11 Walsh Jr., J.T., and Bowman, H.F., 1984, "A Non-Invasive Method for Quantifying Tissue Perfusion", *Advances in Bioengineering*, pp. 5-6.

P2.12 Castallena, F.S., Skalak, R., Cho, J.M., Case, R.B., 1983, "Steady State Analysis and Evaluation of New Thermal Sensor for Surface Measurement of Tissue Perfusion", *Annals of Biomedical Engineering*, Vol. 11, pp. 101-115.

P2.13 Anderson, G.T., and G. Burnside, 1990, "A Noninvasive Technique to Measure Perfusion Using a Focused Ultrasound Heating Source and a Tissue Surface Temperature Measurement," *Advances in Measuring and Computing Temperatures in Biomedicine: Thermal Tomography Techniques, Bio-Heat Transfer Models*, eds. R.G. Roemer et al., ASME, pp. 31-35.

P2.14 Holti, G. and Mitchell, K.W., 1979, "Estimation of the Nutrient Skin Blood Flow using a Non-Invasive Segmented Thermal Clearance Probe", *Non-Invasive Physiological Measurements,* edited by E.P. rolfe, Vol. 1, Chap. 5, Academic Press, London, pp. 113-123.

P2.15 Liu, J., and Xu, L.X., 1999, "Estimation of Blood Perfusion Using Phase Shift in Temperature Response to Sinusoidal Heating at the Skin Surface", *IEEE Transactions on Biomedical Engineering*, Vol. 46, No. 9, pp. 1037-1043.

P2.16 Montet, X., Ivancevic, M.K., Belenger, J. Jorge-Costa, M., Pochon, S., Pechér, A., Terrier, F., Vallé, J., 2003, "Noninvasive measurement of absolute renal perfusion by contrast medium enhanced magnetic resonance imaging", *Investigative Radiology*, Vol. 38, No.9, pp. 584-592.

P2.17 Vallee, J.P., Lazeyras, F., Khan, H.G., et al., 2000, "Absolute blood flow quantification by dynamic MRI and Gd-DTPA", *European Radiology*, Vol. 10, No. 8, pp. 1245-1252.

P2.18 Dias, M., Hadgraft, J., Glover, P.M., McDonald, P.J., 2003, "Stray Field Magnetic Resonance Imaging: A Preliminary Study of Skin Hydration", *J. Phys*, Vol. 36, pp. 364-368.

P2.19 Schelbert, Heinrich R., 2000, "PET Contributions to Understanding Normal and Abnormal Cardiac Perfusion and Metabolism."*Annals of Biomedical Engineering*, nVo. 28, pp 922-929.

P2.20 Nuutilia, P. and K. Kalliokoski, 2000, "Use of positron emission tomography in the assessment of skeletal muscle and tendon metabolism and perfusion," *Scandinavian Journal of medicine & Science in Sports* Vol. 10, pp. 346-350.

P2.21 Boellaard, R., P. Knaapen, A. Rijbroek, G. J. J. Lutersema, A. A. Lammertsma, 2005, "Evaluation of Basis Function and Linear Least Squares Methods for Generating Parametric Blood

Flow Images Using ^{15}O-Water and Positron Emission Tomography" *Molecular Imaging and Biology.*

P2.22 Svedman, C., G.W. Cherry, E. Strigini, T.J. Ryan, 1998, "Laser Doppler Imaging of Skin Microcirculation," *Acta Dermato-Venereologica*, Vol. 78, pp. 114-118.

P2.23 Niwayama, J., and T. Sanaka, 2005, "Development of a new method for monitoring blood purification: The blood flow analysis of the head and foot by laser Doppler blood flow meter during hemodialysis," *Hemodialysis International*, Vol. 9, pp. 55-62.

P2.24 Mileski, W. J. L. Atiles, G. Purdue, R. Kagan, J. R. Saffle, D. N. Herndon, D. Heimbach, A. Luterman, R. Yurt, C. Goodwin, J. L. Hunt, 2003, "Serial Measurements Increase the Accuracy of Laser Doppler Assessment of Burn Wounds," *Journal of Burn Care & Rehabilitation*, Vol. 24, pp. 187-191.

P2.25 Oltean, M. A. Aneman, G. Dindelegan, J. Mölne, M. Olausson, and G. Herlenius, 2005, "Monitoring of the Intestinal Mucosal Perfusion Using Laser Doppler Flowmetry After Multivisceral Transplantation," *Transplantation Proceedings*, Vol.37, pp 3323-3324.

P2.26 Cardinali, A.V., Lanz, O.I., Diller, T.E., Scott, E.P., 2002, "Validation of a Noninvasive Blood Perfusion Measurement System using a Canine Medial Saphenous Fasciocutaneous Free Tissue Flap Model", *Proceedings of the ASME, IMECE'02, New Orleans*, Nov 17- 22, Paper No. 32354 .

P2.27 Pennes, H. H., 1948, "Analysis of Tissue and Arterial Blood Temperatures in the Resting Human Forearm," *J. Appl. Physiol.*, Vol. 1, pp. 93-122.

P2.28 Scott, E.P., Robinson, P.S., and Diller, T.E., 1998, "Development of Methodologies for the Estimation of Blood Perfusion Using a Minimally Invasive Probe", *Measurement Science and Technology*, (Invited Paper – Special Edition), Vol 9, No. 6, pp. 888-897.

P2.29 Mudaliar, A.V., Ellis, B.E., Ricketts, P.L., Lanz, O.I., Scott, E.P., Diller, T.E., 2006, "A Phantom Tissue System for the Calibration of a Perfusion System", *to be Submitted to ASME Journal of Biomechanical Engineering.*

Chapter 5
Conclusions and Recommendations

Blood perfusion is crucial for normal tissue physiology and is a chief component in the thermoregulatory system of the body. The ability to measure blood perfusion is a valuable medical diagnostic, as decreased perfusion is an indicator of microcirculation problems.

5.1 Overview of Phantom Tissue Test Results

The phantom tissue system proved to be a convenient, reliable test bed for surface perfusion measurements in an environment where physiological and pathological conditions are eliminated. The phantom tissue system was shown to be valid with a combination of experimental and CFD results using the convective perfusion probe. The experimental protocol for the duration of thermal event was concluded from the CFD study to be 60 seconds, beyond which the perfusion becomes independent of length of the thermal event. The CFD study proved that the 2D axis-symmetric model was in excellent agreement with that of 3D model, thus cutting down the computational time. The convective perfusion probe was shown to be sensitive and repeatable for perfusion measurements. The contact resistance calculated by the parameter estimation program is important but is generally independent of the flow rates. Contact resistance alters the magnitude of the heat flux curve, but the perfusion estimate remains the same. The CFD Pennes model is also in good agreement with parameter estimation results. The repeatability, sensitivity and good comparison with the CFD models proves that change in perfusion can be monitored by the convective perfusion probe. The phantom tissue system is a great device for testing and development of perfusion measuring devices.

5.2 Overview of Animal Model Test Results

The *ex vivo* liver test results of convective perfusion probe were in good agreement with average metered flow of the perfusate through the liver. The probe quantified the perfusion using liver model measuring changes in perfusion of the order of 0.005 ml/ml/s. The perfusion probe showed good repeatability and sensitivity for the perfusion measured. The convective perfusion probe displayed good repeatability and sensitivity for the liver model. The convective perfusion probe qualitatively assessed the perfusion changes in kidney caused by the occlusion of the renal artery and vein. The repeatability, sensitivity, and good agreement with the animal model results demonstrates that perfusion can be

qualitatively and quantitatively measured by the convective perfusion probe. The performance of the convective perfusion probe was successfully demonstrated on the two animal models.

5.3 Recommendations for Future Work

Recommendations for the model

The results obtained from the phantom tissue test as well as from CFD model using parameter estimation program shows that as perfusion increases (with increase in flow rate), the contact resistance also increases. The contact resistance should remain constant for the experimental setup based on the probe position. The increasing trend of the contact resistance with increase in the flow rate is due to the minimization model. New minimization techniques should be explored or should be attempted out and the results of the current Box-Kanemasu modified form of Gauss minimization technique should be compared to get better understanding of the mathematical model behavior. Also the current model is limited to measure average perfusion over the tissue volume, other methods should be tried out to predict the both spatial and temporal distribution of perfusion in the tissue during the thermal event.

In the previous work done in our lab, the perfusion was forced to zero whenever negative values were obtained from the parameter estimation routine. In the current study, the perfusion was allowed to go negative. For no flow cases in phantom tissue the parameter estimation predicted some offset which were eventually removed from rest of the data, this might be due to thickness of the porous matrix used. For flow rate up to 10 cc/min the flow was not able to reach near the top of the tissue where heat flux gage is placed. Also the maximum thermal penetration is about 1 mm, implying that 12.7 mm thick porous matrix has more thickness than required. Parameter estimation for porous matrix with different thickness should be carried out to check the effects of thickness on the model.

Recommendations for the phantom experiments

Presently thermocouples are being used to measure the temperatures at different locations to feed the recorded data as input to the parameter estimation program. The thermocouple signals are generally of the order of 40 μV for a degree change in temperature. Amplifiers are typically used to amplify the signals and they tend to be expensive, also there is noise issue when measuring such low signals. The use of thermistor is recommended to eliminate the need of amplifier and the noise issue. As the thermistor signals are much bigger and can be resolved easily by a 16 bit DAQ.

All the experiments conducted on phantom tissue with the sponge of 12.7 mm thick. It was observed both experimentally (dye test) and computationally that at flow rate less than 10 cc/min the

fluid jet coming from the inlet were unable to reach the top surface inside the sponge (porous matrix). Different thickness of the sponge should be investigated in both the phantom tissue experiments and CFD model.

Probe Design Recommendations

The current probe was designed based on the previous developed probes. The probe housing should be incorporated in CFD model to check how that actual probe behaves. The line pressure of the air supply can be used at the inlet boundary. Also this will help in improving the design of the probe housing.

Recommendations for Animal Model Studies

It was found that the perfusion and contact resistance were very sensitive to the placement of the probe. It is recommended to design a probe holder for conducting animal model tests. Also once the probe is place it should not be removed and placed again. There is also issue of noise when blood or other fluids come in contact with the heat flux gage or thermocouple. To avoid this it is suggested to use pressed sensor (Ellis, 2006) for the test. In presses sensor the heat flux gage is laminated with very thin (0.05 mm) Mylar sheet to avoid direct contact the fluids.

Also the perfusion estimated in the present work need to be validated with other existing perfusion measuring technique. Use of microsphere technique should be attempted on the ex vivo and in vivo model.

Appendix A
Convective Perfusion Probe Design

A.1 Virginia Tech Bioprobe History

The first application of heat flux sensors to the blood perfusion measurement problem, and the inaugural research for the bioprobe, is described in Michener et al. (1991). His work describes the mathematical model of the Pennes bioheat equation, which is the basis of the operation for the sensor and is discussed in detail in chapter 3. Additional research and development by Fouquet et al. (1993) and O' Reilly et al. (1996) resulted in a fully functional sensor prototype. Robinson (1998) continued the work by developing the biothermal model and parameter estimation routine, and validated the concept of the blood perfusion probe by developing and carrying out experimental protocols for both living tissue and non-biologic tissue [45]. Robinson used the sum of the squares error on both experimental heat flux and temperature data, and calculated the heat flux and temperature data for the objective function in the parameter estimation routine. Cardinali (2002) found that the perfusion is more sensitive to heat flux than to the temperature. The parameter estimation routine was modified by Cardinali using the sum of squares error of the heat flux for the objective function. Cardinali further worked on validating the blood perfusion probe and established the feasibility of using the blood perfusion probe in a clinical setting, as it was tested on canine legs during laparoscopic spay surgery and on canine medial saphenous fasciocutaneous free tissue flaps.

The further validation of the probe was carried out by Ballmer (2003a and 2003b) by testing the probe on Madden's (2003) agar phantom tissue test stand. Ballmer also assessed the probe's consistency of measurement through testing on the medial aspect of the thoracic and pelvic limbs of six canines. During these tests epidurals were administered in order to induce vasoconstriction in the pelvic limb. It was concluded that the probe demonstrated consistent results for multiple canines, as the trends in perfusion pre-epidural were similar for all six canines, however the post-epidural trends were found to be inconsistent from canine to canine. The most recent developments are described in Comas (2005). Comas assessed the measurement repeatability and sensitivity of a slightly modified sensor by testing it on a controlled perfusion phantom tissue test stand, such that the effect of physiologic and pathologic conditions could be eliminated. The heat flux gage in the probe used by Comas was had larger sensing area than the previously used gages, also the thermocouple on the gage was located at the edge near the wire terminals of the gage. The aluminum foil on the bottom face of the sensor was removed. The air

temperature was monitored by a thermocouple placed inside the tube connected to air supply. Preliminary *in vivo* study using rats was conducted to establish experimental protocol for future testing. Comas also measured the relationship between the inflow rate to the test section and the perfusion values.

A.2 Blood Perfusion Probe Design

The concept of the heat flux probe to measure blood perfusion is based on the fundamental tenet that heat will flow along a negative temperature gradient. A temperature gradient is created across a sensor that measures heat flux. This temperature difference is due to warm tissue containing warm fluid flow on one side of the sensor. In the current research, jets of room temperature air provide convective cooling on the other side of the sensor surface. The sensor then measures the heat flux response from the tissue. The amount of the heat flux available to equilibrate and/or recover the cooling effect is related to the blood perfusion in the local region.

The core of the heat flux sensor is a thin (0.25 mm) thermopile. This thermopile is comprised of small bimetallic junctions arranged in pairs across a thin resistive layer. Since the thermopile junctions produce a voltage related to their temperature, the difference in voltages between two paired junctions represents the local temperature difference across the resistive layer. The sum of these voltage differences between all of the junction pairs yields an average temperature difference across the entire thermopile. Based on Fourier's Law of conduction for a steady-state, one dimensional system,

$$q'' = \frac{k}{L}\Delta T \qquad \text{(A.1)}$$

heat flux is directly proportional to the temperature difference. Therefore, the voltage output measured across the thermopile is proportional to the heat flux through the thermopile.

$$q'' = \frac{E}{S_q} \qquad \text{(A.2)}$$

Where q" is the heat flux, E is the voltage output, S_q is the sensitivity, or calibration coefficient, of the sensor.

The current design of the sensor is shown in Figure 32, the thatched area indicate the sensing area i.e. the thermopile area. The heat flux gage is 10 mm x 10 mm in area and 0.25 mm in thickness. The sensing area is about 57.4 mm^2.

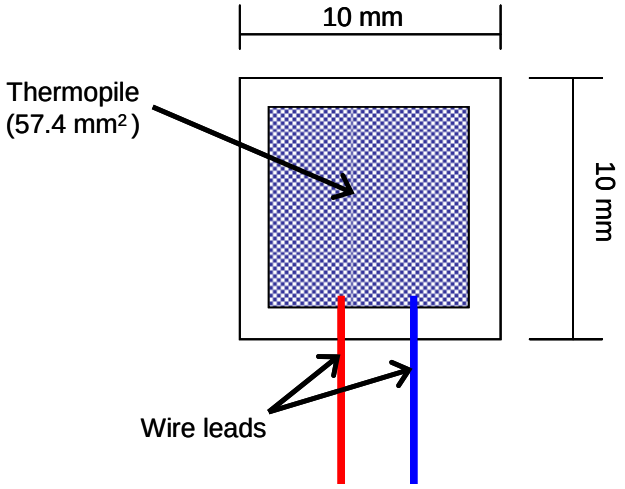

Figure 32: Heat flux gage used in the convective perfusion probe

Table 5: Thermal and physical properties of the current heat flux gage

Property	Values
Length	10 mm
Width	10 mm
Sensing Area	57.4 mm^2
Thickness	0.25 mm
Density	1250 kg/ m^3
Specific Heat	1340 J/kg-K
Conductivity	0.25 W/m-K

A.3 Previous convective perfusion probes

The current blood perfusion probe is a second generation design with a smaller housing and heat flux sensor than Robinson (1998), Cardinali (2002), Ballmer (2003a, b) and Comas (2005). The probes used by Robinson, Cardinali, Ballmer contained a thin layer of aluminum foil on the bottom of the side of the heat flux gage shown in Figure 33, whereas the one used by Comas shown in Figure 34 did not have the foil. The probe housing used by all of them was made of aluminum.

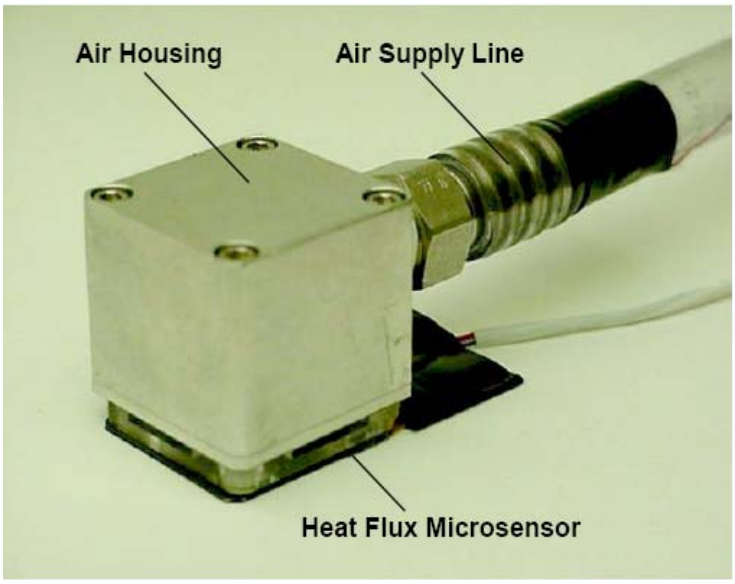

Figure 33: Convective probe used by Robinson (1998), Cardinali (2002) and Ballmer (2003a, b)

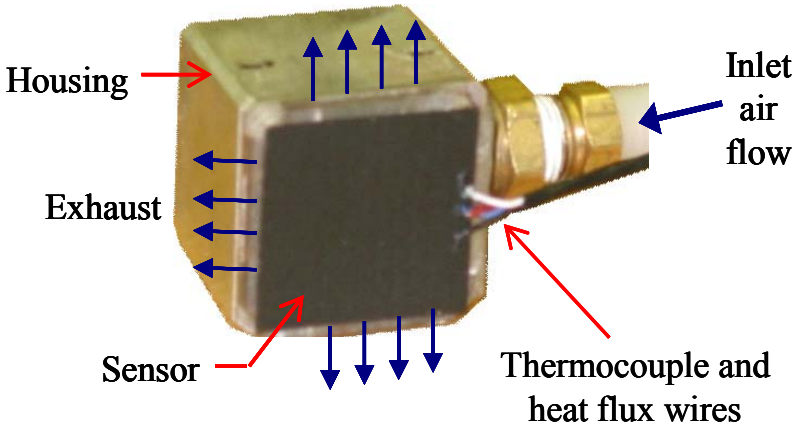

Figure 34: Perfusion Probe used by Comas (2005)

A.4 Present convective perfusion probe

The bigger probe had contact surface area of 645 mm^2 and was difficult to place it on rats; therefore a probe with smaller contact surface area of 100 mm^2 was developed. This smaller convective probe can be used with ease on both in vivo and ex vivo tests on rats. The convective perfusion probe is shown in Figure 35. The probe housing dimensions are 12.7 mm × 12.7 mm × 10.2 mm. A Vatell heat flux gage (10 mm × 10 mm × 0.25 mm) is placed on the housing which is connected to an air supply. The current probe housing made of plastic (Lexan), to avoid heat loss from the housing. A compressed air supply is connected to the housing and delivers room temperature air to provide convective cooling. The air is passed through a water bath before entering into the probe housing to maintain it at a constant temperature. In operation, the probe is affixed to the tissue using double-sided tape. Air then flows into the housing and through a plate with nine holes (0.37 mm diameter) to create air jets which impinge onto the sensor causing a measurable heat flux response from the tissue. The air then exhausts through outlets in the housing shown in the Figure 35.

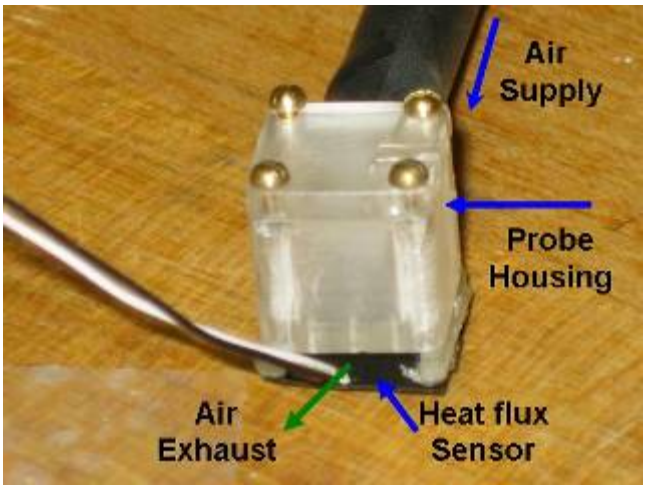

Figure 35: Present convective perfusion probe

Appendix B

Bioheat Transfer Model and Parameter Estimation

B.1 Bioheat transfer model

Due to the complexity of modeling heat transfer in living tissue, there has been much literature devoted to the development of the biothermal models. Much of the work in the field of bioheat transfer model describes blood perfusion based on the early work of Pennes (1948).

$$(\rho C_p)_t \frac{\partial T_t}{\partial t} = k_t \nabla^2 T_t + (\rho C_p \omega)_b (T_a - T_v) \qquad \text{(B.1)}$$

where T is temperature, t is time, ρ is density, C_p is specific heat, k is thermal conductivity, and ω is blood perfusion. The subscripts t, b, v and a, corresponds to tissue, blood, venous and arterial respectively. The heat generated due to metabolic activity is assumed to be negligible.

In the Pennes bioheat equation the first term on left hand side is the storage term and on the right hand side the first term is heat conduction in the tissue and the second term is the energy loss due to blood flow by including the blood perfusion term. The Pennes bioheat model is generally used as the benchmark for the recently developed model for comparisons.

An overview of several bioheat transfer models, including the Pennes model, is presented in Charney, 1992. Charney's review also includes models by Wulff, Klinger, and Chen and Holmes. Wulff and Klinger used a blood velocity within a temperature gradient for convective term, instead of the perfusion term defined in Pennes model. Other approaches at modeling bioheat transfer have also been explored. Weinbaum and Jiji (1985) developed a more complex model, involving heat exchange between the blood vessels, which acts as counter-current pairs. Roemer et al. (1985) developed a model of calculating blood perfusion based on the energy balance of power absorbed by tissue from a heat source. Another model proposed by Brinck and Werner (1994) simply improves upon the Pennes approach to model bioheat transfer by introducing a correction factor to be used with convective blood perfusion term.

A later study by Weinbaum et al., in 1997, it was found that for certain condition the Weinbaum and Jiji (1985) model reduces to the Penne's bioheat equation. Consequently, it has been concluded that although more complex models have been proposed for biothermal predictions, the Penne's bioheat equation is simple, and adequately models the bioheat transfer in living tissue.

B.2 Assumptions

As stated earlier, the Penne's bioheat equation is an often used as the model for explaining heat transfer through biological tissue. The Penne's bioheat equation is based on conservation of mass and energy, the control volume of tissue is assumed to be homogenous, and is supplied with arterial blood, which is at the body's core temperature. The temperature difference between arterial and venous blood drives the heat exchange in the tissue. Figure 36 shows a graphical representation of the heat exchange between the blood and tissue. The blood flow is assumed to be uniform and the thermal properties of the tissue and the blood are also assumed to be constant. Under the mentioned assumptions the conservation of energy yields the Penne's bioheat equation (equation. B.1), which describes temperature of the tissue volume.

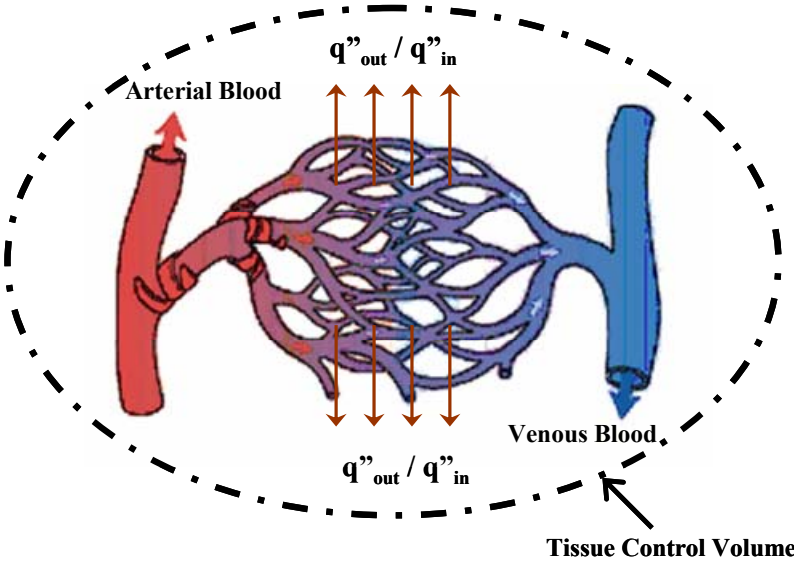

Figure 36: Heat exchange in a control volume of tissue for Penne's bioheat model

B.3 Finite difference formulation

The numerical approach was chosen to solve the bioheat transfer model, as an analytical solution is impractical in this case due to the nature and complexity of the problem. To solve the governing equation as discussed before, a two-dimensional finite difference solution was used. A cylindrical coordinate system was chosen due the simplicity. The schematic representation of the sensor, contact resistance and tissue is shown in the Figure 37. An Alternating Directions Implicit

(ADI) method was used to solve the discretized equations for the unknown temperature field. The ADI method allows for a two dimensional problem to appear as a one dimensional problem, thus facilitating the solution algorithm. To make the two-dimensional problem appear as one-dimensional problem orthogonal sweeps, first in the axial direction and then in the radial directions are performed over half time steps. By marching through sweeps in one direction and then the other time is advanced by one full time step, and the transient temperature field can be solved for.

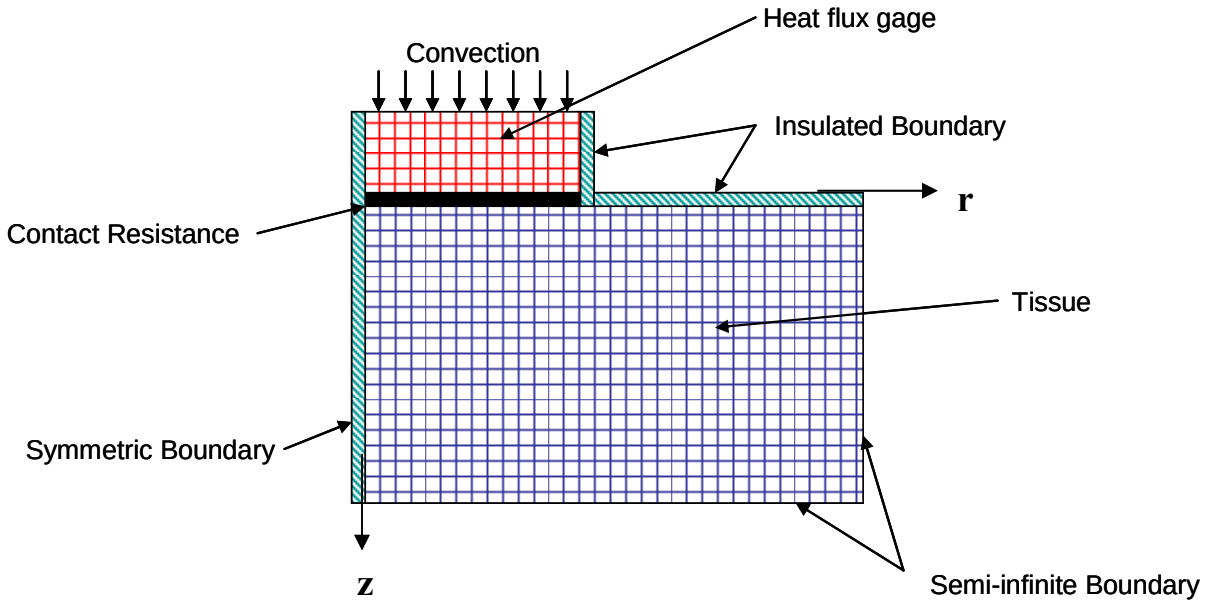

Figure 37: Schematic of finite difference model of tissue and sensor

Robinson (1998), developed the dimensionless finite-difference code for the parameter estimation in FORTRAN, Comas (2005) rewrote this code in Matlab to make the data reduction and processing simpler. This old code was based on non-dimensional Pennes bioheat equation; it was difficult to control the parameter which were most sensitive to perfusion measurements. In the old code the sensor and the tissue were assumed to have same initial temperature, which actually is not true. Also there were minor problems in calculating the heat flux measurements, as the finite difference model was in cylindrical coordinate the heat flux was calculated as an average value rather than area weighted average. The approach for calculating results on the boundary cells were based on the ghost cells (imaginary cells). The code was tedious to run since it was not capable of running multiple files

together and for every heat flux data the starting and the ending point of the thermal event has to be fed to the code.

The new finite-difference code is in dimensional form was developed, to make it user friendly and easier a new driver program has been developed to read all the experimental heat flux and temperature data file together in parameter estimation program. The driver program runs the parameter estimation routine and saves all the perfusion estimates, contact resistance and sum of the squares and the convergence plot for each case in a file. Also, with this code there is no need of entering the starting and ending point of the thermal event for each case, it detects by itself the starting and ending point of the thermal event based on the experimental heat flux values.

The present code developed also has the capability to assign different initial condition for the sensor and the tissue. The tissue initial condition is based on the temperature gradient measured by the thermocouples placed on the top of the tissue and at the inlet. It was reported that the perfusion estimates were highly sensitive to air temperature therefore provision was made to incorporate actual air temperature in the finite-difference model. With the old 24 bit DAQ the air temperature was sampled at 5 Hz it was curve fitted using cubic spline to generate the data for 10 Hz frequency for 60 s of thermal event. The finite-difference code was solved using half of the experimental time step to match the sampling frequency of 10 Hz. The new 16 bit DAQ has the ability to sample each individual channel at 10 Hz therefore an option is provided to select the DAQ used in experiments.

In the previous code, all the boundary conditions the temperatures were calculated using imaginary cells. But in the present code the imaginary cells are used only at the symmetric, insulated and semi-infinite boundaries. At the convective surface and the interface between the heat flux gage and tissue thermal resistance concept was used shown in the Figure 38 and Figure 39. The heat flux was measured as conductive heat flux based on Fourier law. The average area weighted temperature difference was used to calculate the heat flux from the gage as the model is in cylindrical coordinate. In the previous code just mean temperature was used.

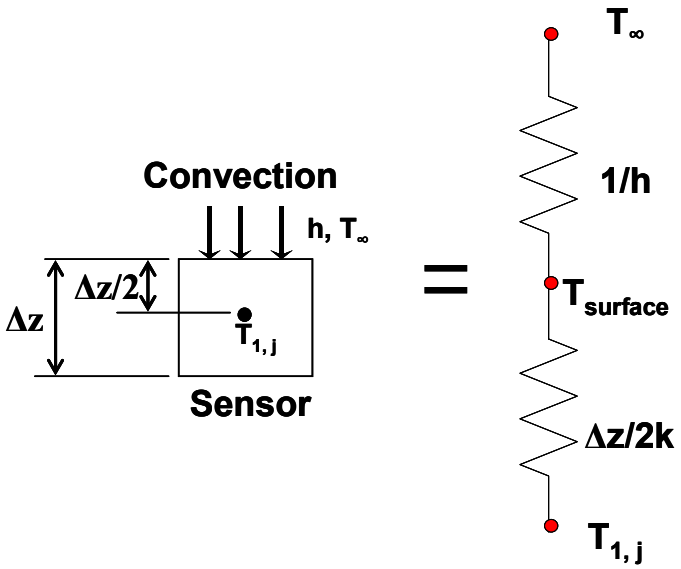

Figure 38: Thermal circuit for the convective boundary on the surface of the sensor

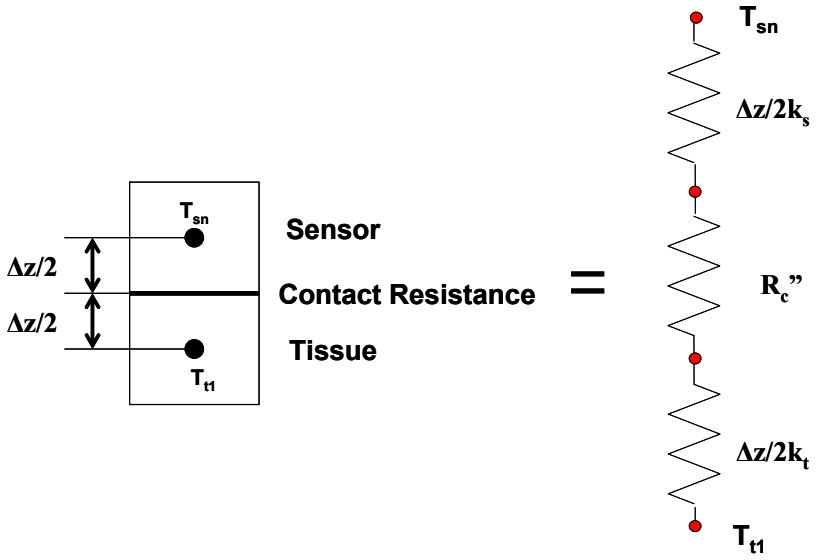

Figure 39: Thermal circuit at the interface of the sensor and tissue with contact resistance incorporated between them

B.4 Numerical Discretization

The Pennes bioheat equation and the probe governing equation can be fully discretized by integrating each term in space and time. For example:

$$\int_{r=0}^{r_{max}} \int_{z=0}^{z_{max}} \int_{p}^{p+1} \frac{\partial T(r,z,t)}{\partial t} dt\, dz\, dr = \tag{B.2}$$

$$\int_{r=0}^{r_{max}} \int_{z=0}^{z_{max}} \int_{p}^{p+1} \left[\frac{1}{r} \frac{\partial}{\partial r} \left(r \frac{\partial T(r,z,t)}{\partial r} \right) + \frac{\partial^2 T(r,z,t)}{\partial z^2} + \omega \left(T_a - T(r,z,t) \right) \right] dt\, dz\, dr$$

To achieve the time discretization, a Crank-Nicolson implicit method was chosen. In this method a linear variation between the temperature at the present time and the temperature at the next time step is assumed, as shown mathematically in equation. (B.3) (Patankar, 1980).

$$\int_{p}^{p+1} T_{i,j}\, dt = \left(\frac{1}{2} T_{i,j}^{p+1} + \frac{1}{2} T_{i,j}^{p} \right) \Delta t \tag{B.3}$$

B.5 Finite Difference Equations

The resulting finite difference equations from the numerical discretization are shown here

B.5.1 Finite Difference Equation for Heat flux gage

Energy equation in heat flux gage

$$\frac{\partial T}{\partial t} = \alpha_S \left(\frac{1}{r} \frac{\partial T}{\partial r} + \frac{\partial^2 T}{\partial r^2} \right) + \alpha_S \left(\frac{\partial^2 T}{\partial z^2} \right)$$

Axial sweep in heat flux gage

$$A_S\, T_{i-1,j}{}^{n+\frac{1}{2}} + B_S\, T_{i,j}{}^{n+\frac{1}{2}} + A_S\, T_{i+1,j}{}^{n+\frac{1}{2}} =$$
$$C_S(j)T_{i,j-1}{}^{n} + D_S\, T_{i,j}{}^{n} + E_S(j)T_{i,j+1}{}^{n}$$

Boundary conditions for axial sweep in gage

Convection

$$T_{1,j}^{n+\frac{1}{2}}\left(h+\frac{k_s}{\Delta z}\right) - T_{2,j}^{n+\frac{1}{2}}\left(\frac{k_s}{\Delta z}\right) = hT_\infty$$

Contact Resistance

$$T_{ns,j}^{n+\frac{1}{2}}\left(1+\frac{k_s}{\Delta z}\left(\frac{\Delta z}{2k_s}+R_c^{"}+\frac{\Delta z}{2k_t}\right)\right) - T_{ns-1,j}^{n+\frac{1}{2}}\frac{k_s}{\Delta z}\left(\frac{\Delta z}{2k_s}+R_c^{"}+\frac{\Delta z}{2k_t}\right) = T_{t1,j}^{n}$$

Radial sweep in heat flux gage

$$C_S(j)\,T_{i,j-1}{}^{n+1} + (2-D_S)\,T_{i,j}{}^{n+1} + E_S(j)\,T_{i,j+1}{}^{n+1} =$$
$$-A_S\,T_{i-1,j}{}^{n+\frac{1}{2}} + (2-B_S)\,T_{i,j}{}^{n+\frac{1}{2}} - A_S\,T_{i+1,j}{}^{n+\frac{1}{2}}$$

Boundary conditions for radial sweep in gage

Symmetric Boundary

$$T_{i,1}^{n+1} = T_{i,2}^{n+1}$$

Insulated Boundary

$$T_{i,ms}^{n+1} = T_{i,ms-1}^{n+1}$$

where

$$A_S = \left[-\frac{\alpha_S \Delta t}{2\Delta z^2} \right]$$

$$B_S = \left[1 + \frac{\alpha_S \Delta t}{\Delta z^2} \right]$$

$$C_S = \left[\frac{\alpha_S \Delta t}{2\Delta r} \left(\frac{1}{\Delta r} - \frac{1}{2r(j)} \right) \right]$$

$$D_S = \left[1 - \frac{\alpha_S \Delta t}{\Delta r^2} \right]$$

$$E_S = \left[\frac{\alpha_S \Delta t}{2\Delta r} \left(\frac{1}{\Delta r} + \frac{1}{2r(j)} \right) \right]$$

B.5.2 Finite Difference equation for the tissue

Energy equation in the tissue (Pennes bioheat equation)

$$\frac{\partial T}{\partial t} = \alpha_t \left(\frac{1}{r} \frac{\partial T}{\partial r} + \frac{\partial^2 T}{\partial r^2} \right) + \alpha_t \left(\frac{\partial^2 T}{\partial z^2} \right) + \omega \left(T_a - T \right)$$

Axial sweep in tissue

$$A_{1t}\, T_{i-1,j}^{\,n+\frac{1}{2}} + B_{1t}\, T_{i,j}^{\,n+\frac{1}{2}} + A_{1t}\, T_{i+1,j}^{\,n+\frac{1}{2}} =$$

$$C_{1t}(j)\, T_{i,j-1}^{\,n} + D_{1t}\, T_{i,j}^{\,n} + E_{1t}(j)\, T_{i,j+1}^{\,n} + \frac{\omega \Delta t}{2} T_a^{\,n}$$

Boundary conditions for axial sweep in tissue

ContactResistance

$$T_{t1,j}^{n+\frac{1}{2}}\left(1+\frac{k_s}{\Delta z}\left(\frac{\Delta z}{2k_s}+R_c^{"}+\frac{\Delta z}{2k_t}\right)\right)-T_{t1+1,j}^{n+\frac{1}{2}}\frac{k_t}{\Delta z}\left(\frac{\Delta z}{2k_s}+R_c^{"}+\frac{\Delta z}{2k_t}\right)=T_{ns,j}^{n}$$

Insulated Boundary

$$T_{t1}^{n+\frac{1}{2}}=T_{t1+1}^{n+\frac{1}{2}}$$

Semi – infinite Boundary (zero heat flux)

$$T_{nt,j}^{n+\frac{1}{2}}=T_{nt-1,j}^{n+\frac{1}{2}}$$

Radial sweep in tissue

$$C_{1t}(j)T_{i,j-1}^{n+1}+D_{2t}T_{i,j}^{n+1}+E_{1t}(j)T_{i,j+1}^{n+1}=$$

$$-A_{1t}T_{i-1,j}^{n+\frac{1}{2}}+B_{2t}T_{i,j}^{n+\frac{1}{2}}-A_{1t}T_{i+1,j}^{n+\frac{1}{2}}+\frac{\omega\Delta t}{2}T_a$$

Boundary conditions for radial sweep in tissue

Symmetric Boundary

$$T_{i,1}^{n+1}=T_{i,2}^{n+1}$$

Semi - infinite Boundary

$$T_{i,mt}^{n+1}=T_{i,mt-1}^{n+1}$$

where

$$A_{1t} = \left[-\frac{\alpha_t \Delta t}{2\Delta z^2} \right]$$

$$B_{1t} = \left[1 + \frac{\alpha_t \Delta t}{\Delta z^2} + \frac{\omega \Delta t}{2} \right]$$

$$B_{2t} = \left[1 + \frac{\alpha_t \Delta t}{\Delta r^2} + \frac{\omega \Delta t}{2} \right]$$

$$C_{1t} = \left[\frac{\alpha_t \Delta t}{2\Delta r} \left(\frac{1}{\Delta r} - \frac{1}{2r(j)} \right) \right]$$

$$D_{1t} = \left[1 - \frac{\alpha_t \Delta t}{\Delta r^2} \right]$$

$$D_{2t} = \left[1 - \frac{\alpha_t \Delta t}{\Delta z^2} \right]$$

$$E_{1t} = \left[\frac{\alpha_t \Delta t}{2\Delta r} \left(\frac{1}{\Delta r} + \frac{1}{2r(j)} \right) \right]$$

B.6 Validation of Finite Difference code

The results from the finite difference model needs to be validated with the analytical solution in order to have confidence. Also the tissue thickness required to model it as semi-infinite needs to be validated. To model the finite difference code as semi-infinite solid, the sensor was removed from the finite difference model discussed before and the whole tissue top surface was imposed with a convective boundary. The semi-infinite analytical solution for a convective boundary with no perfusion and contact resistance with constant thermal properties is shown in equation B.4. Thermal properties applied to the tissue and the temperatures used are presented in Table 6. From the Figure 40 it can be seen that the heat flux calculated by finite difference code is in excellent agreement with the analytical solution.

$$T(t) = T_{init} + (T_\infty - T_{init}) \left\{ 1 - \left[\exp\left(\frac{h^2 \alpha_t t}{k_t^2} \right) \right] \left[erfc\left(\frac{h\sqrt{\alpha_t t}}{k_t} \right) \right] \right\} \qquad \text{(B.4)}$$

Table 6: Parameter values of the tissue and the convective boundary details used to solve the 1D semi-infinite analytical solution

Parameter	Value
T_{init}	35 °C
T_{∞}	23.96 °C
α_t	0.144×10^{-6} m^2/s
h	1000 $W/m^2 - K$
k_t	0.5723 W/m-K

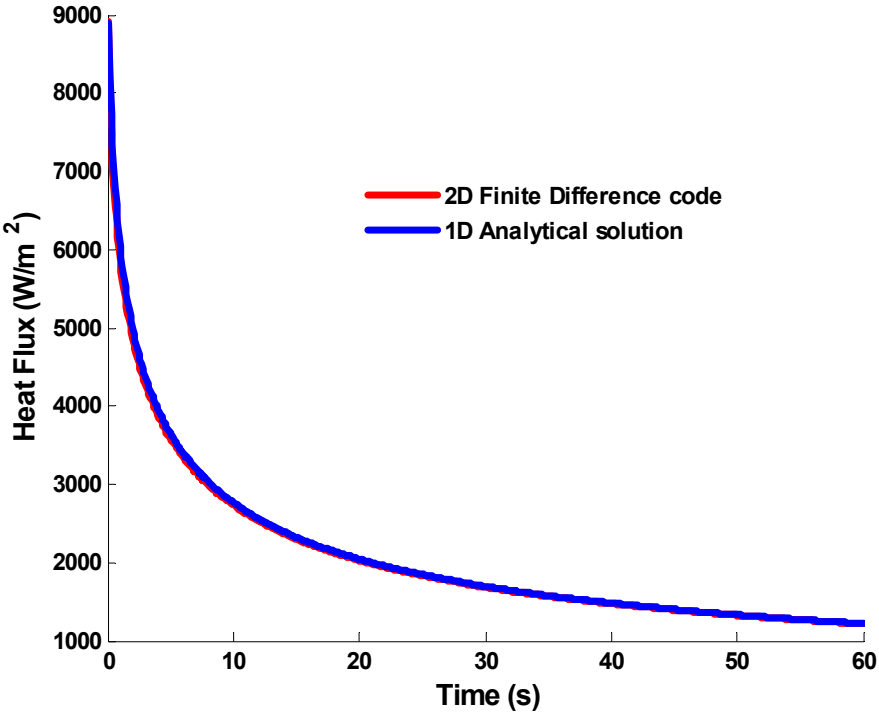

Figure 40: Heat flux comparison of 2D Finite difference model without sensor, with 1D analytical solution for semi-infinite wall with convective boundary

B.7 Parameter Estimation Procedure

The parameter estimation program used for this thermal analysis is based on Gauss minimization with Box-Kanemasu modification. This method attempts to adjust the model parameters to obtain a match between the model output and experimental data. This match is achieved by minimization of an objective function that related model and experimental data. The objective function used for this purpose is a sum of squares error between the calculated and measured data:

$$S = \sum_{i=1}^{N} \frac{(\vec{q}''_{m_i} - \vec{q}''_{c_i})}{\vec{\sigma}^2_{q_i}} \tag{B.5}$$

where *q"* represents heat flux. The subscripts *m* and *c* represent measured and calculated, respectively. The variance of the experimental heat flux is denoted by σ_q^2. Note, that all of the quantities in equation B.5 are vectors. Since the variance of a data set is a single number, we take $\vec{\sigma}^2_{q_i}$ to be an array of the same length as the number of data points, with all terms equal to the value of the variance. This variance vector can than be multiplied by a factor for certain data points in order to emphasize areas where minimization of the error between the experimental and calculated data is not as important (i.e. the time over which contact resistance dominates). Using a vector rather than a scalar quantity for the variance allows for certain data points to carry more weight in the objective function, as it is a summation of all the data points.

Ideally, the objective function displays a parabolic shape, with one distinct minimum point, as shown in Figure 41. Difficulties can occur when the slope of the objective function is relatively flat (insensitivity) or when multiple minimums exist (non-uniqueness).

In the Gaussian method, the minimum value of the objective function is found by setting the derivative of *S* with respect to the estimated parameter vector, β, to zero. For the objective function shown in equation B.5 this process yields equation B.6.

$$\nabla_\beta S = \frac{2}{\sigma_q^2}\left(-\nabla_\beta \vec{q}''_c(\beta)^{\mathrm{T}}\right)\left(\vec{q}''_m - \vec{q}''_c(\beta)\right) \tag{B.6}$$

where $\nabla_\beta q''_c(\beta)$ is defined as the sensitivity vector for heat flux, $\vec{\mathrm{X}}_q(\beta)$. At this point two approximations are made. The first is that the sensitivity vector, $\vec{\mathrm{X}}_q(\beta)$ is approximated as $\vec{\mathrm{X}}_q(b)$, where the vector, $\vec{b}$ is an approximation of β. In this work, the vector $\vec{b}$ consists of the estimates of perfusion and contact resistance. The second approximation is that $\vec{q}''_c(\beta)$ is taken to be the first two terms of a

Taylor series expansion about $\vec{b}$. In order to solve for the next parameter estimates, $\beta = \vec{b}^{k+1}$, given the previous values, $\vec{b} = \vec{b}^{k}$, the approximations explained above are substituted into equation B.6. This process yields

$$\vec{b}^{k+1} = \vec{b}^{k} + \Delta\vec{b}^{k} \tag{B.7}$$

Where $\Delta\vec{b}^{k}$ is given by

$$\Delta\vec{b}^{k} = \left(\frac{1}{\vec{\sigma}_q^2} \vec{\mathrm{X}}_q(\vec{b})^{\mathrm{T}} \vec{\mathrm{X}}_q(\vec{b}) \right)^{-1} \cdot \left(\frac{1}{\vec{\sigma}_q^2} \vec{\mathrm{X}}_q(\vec{b})^{\mathrm{T}} (\vec{q}_m'' - \vec{q}_c''(\vec{b})) \right) \tag{B.8}$$

The Gauss iterative estimates are continued until a parameter convergence is reached, or until the number of maximum allowed iterations has been reached. The convergence criterion for this case is shown in equation B.9.

$$\frac{b^{k+1} - b^{k}}{b^{k}} \leq 0.001 \tag{B.9}$$

In this research, the convergence criteria shown in equation B.9 must be met for both the perfusion and contact resistance estimates independently.

For this work the Gaussian Minimization method is implemented using a whole domain method (Robinson, 1998), rather than sequentially. In the sequential method, a set of parameters is estimated for each data point. This means that for each data point, the bioheat transfer model is solved up to the time at which the data point takes place. This leads to very long computational times for solving the parameter estimates of the entire data set when using finite difference or other numerical methods. In the whole domain method the bioheat transfer model is run once with a given estimate for perfusion and contact resistance for each Gaussian iteration. That is, that one set of parameters is estimated for the entire data set. A flowchart of the parameter estimation procedure, using the whole domain method, has been presented in Figure 42

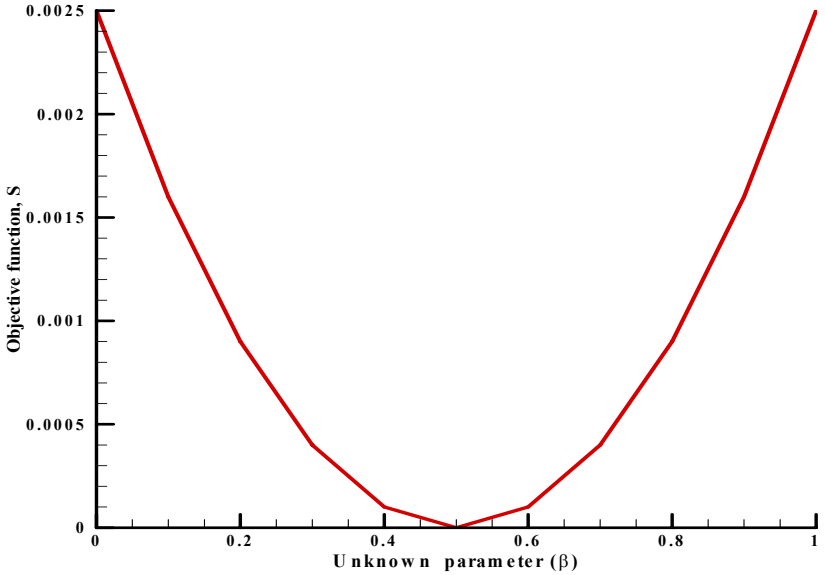

Figure 41: Plot of ideal objective function, showing a distinct minimum point for the objective function at a given value of parameter being estimated

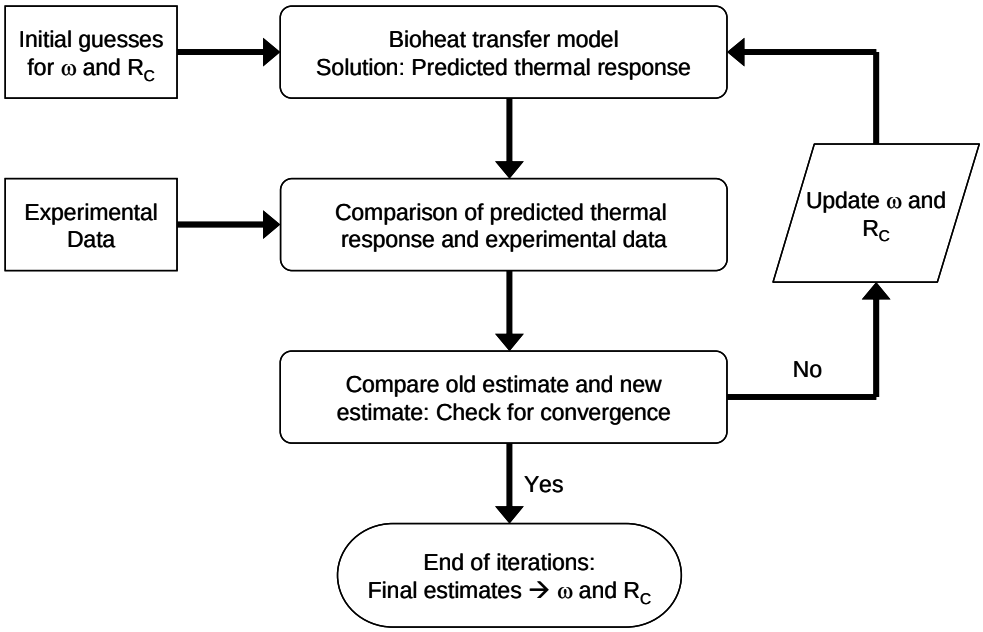

Figure 42: Example plot of the ideal objective function, showing a distinct minimum point for the objective function at a given value of the parameter being estimated

Appendix C

Parameter Estimation, Finite Difference and Related Program

The parameter estimation routine and other related program are that work together is presented here. Figure 43 shows the flow sheet of the program developed

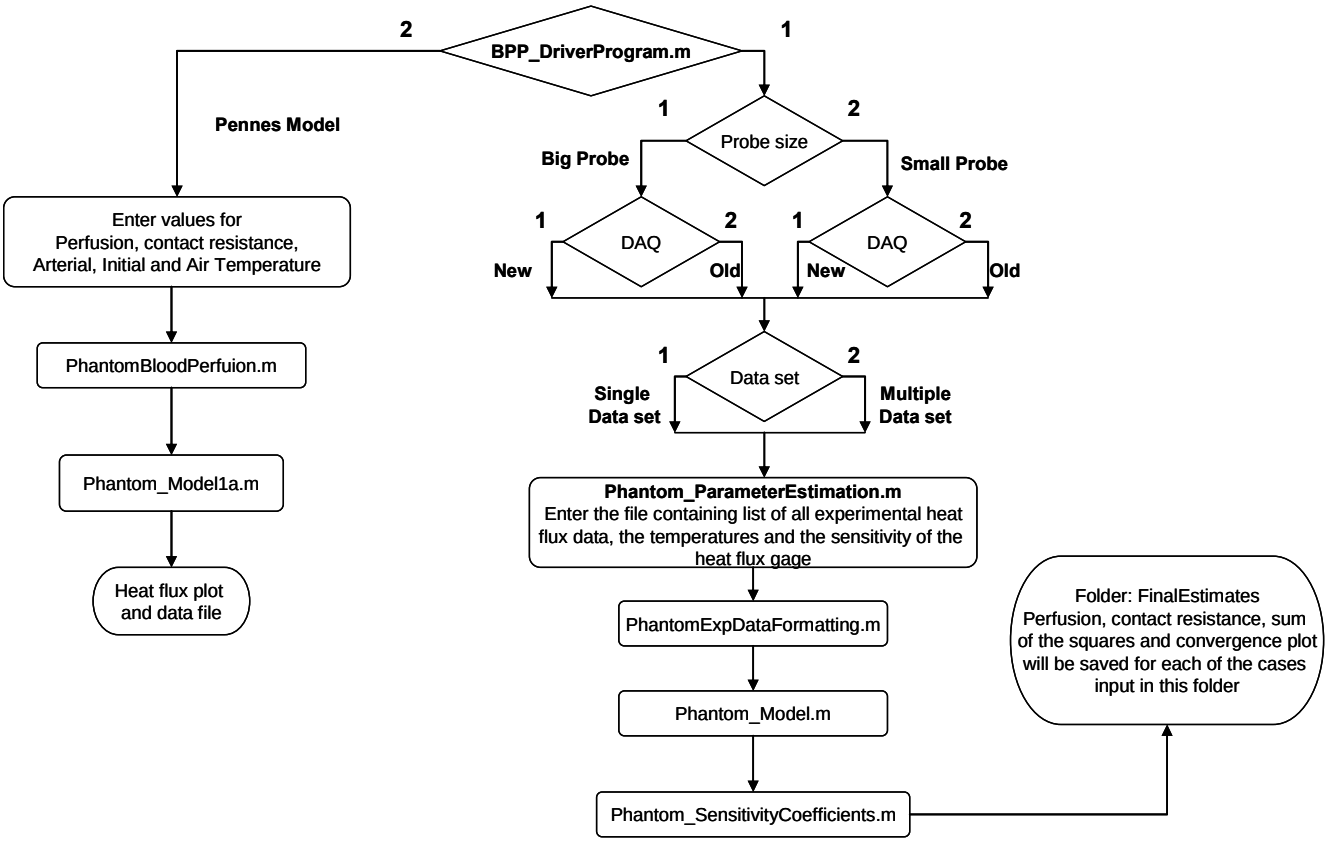

Note:
New: It will allow to acquire signals at sampling frequency of 10 Hz/channel
Old: It will allow to acquire signals at sampling frequency of 10 Hz/ 2 channel

Figure 43: Flow sheet of how the Pennes model and parameter estimation programs work together within the BPP_DriverProgram.m

C.1 BPP_DriverProgram.m

```
function BPP_DriverProgram
global R_Temp Art_Temp Top_Temp Skin_Temp Rs MFP MFS MFT
clear all;
close all;
clc;
% This driver program written by Ashvin Mudaliar on 27th of May 2006. This
% code is used to run one or multiple set of experimental data at one shot.
% R_Temp = Reference Temp
% Art_Temp = Arterial Temp
% Top_Temp = Top thermocouple Temp
% Skin_Temp = Skin Temp
% Rs = Sensor Equivalent Radius
% MFP = Multiplication factor for Probe (MFP_bp = 1.2 and MFP_sp = 1)
% MFS = Multiplication factor for sensor to convert volts into W/m^2

Run_Choice = input('Enter 1 to run Parameter Estiamtion and 2 Finite Difference Model:  ');
 if Run_Choice == 2
   Phantom_BloodPerfusion;
else

   Probe_Choice = input('Enter 1 for big probe and 2 for small probe:  ');

   if Probe_Choice == 1
      Rs = 0.00953; % Radius of the cut out section in the probe housing
      MFP = 1.2; % Since the sensing are of the sensor is bigger than the
            % area exposed to air jets, so the heat flux measured will
            % be higher than the measured
   elseif Probe_Choice == 2
      Rs = 0.004275; % Equivalent radius based on sensing area of 57.4 mm^2
      MFP = 1; %Whole of the senor is exposed to the air jets
   end

   MFS = input('Enter the multipication factor of the sensor:  ');

   DAQ_Choice = input('Enter 1 for New DAQ and 2 for Old DAQ:  ');
   if DAQ_Choice == 1
      MFT = 1;
   elseif DAQ_Choice == 2
      MFT = 2;
   end

   Input_Choice = input('Enter 1 for one set of data and 2 for multiple set of data:   ');

   a = '.txt';

   if Input_Choice == 1
      R_Temp = input('Enter the Reference Temperature in deg C:   ');
      Art_Temp = input('Enter the Arterial Temperature in deg C:   ');
      Skin_Temp = input('Enter the Skin Temperature in deg C:   ');
      Test_type = input('Enter 1 for phantom test and 2 for animal test:  ');
      if Test_type == 1
       Top_Temp = input('Enter the Top Thermocouple Temperature in deg C:   ');
```

```
    elseif Test_type == 2
       Top_Temp = Skin_Temp;
    end

    filenamenumber = input('Enter the filename: ');
    d = num2str(filenamenumber);
    z = char(d);
    q = [z,a];

    [FinalP2, FinalCR2, FinalSS2] = Phantom_ParameterEstimation(q,R_Temp,Art_Temp,Top_Temp,Skin_Temp,Rs,MFP,MFS,MFT,d);
    else

    filename = input('Enter the text file having heat flux and temperature info:    ');
    NumofData = input('Enter the number of Experiments:  ');
    char d;
    y1 = load(filename, '%f');

    for count = 1:NumofData
       filenamenumber = y1(count,1);
       d = num2str(filenamenumber);
       z = char(d);
       q = [z,a];
       R_Temp = y1(count,2);
       Art_Temp = y1(count,3);
       Top_Temp = y1(count,4);
       Skin_Temp = y1(count,5);

       [FinalP2, FinalCR2, FinalSS2] = Phantom_ParameterEstimation(q,R_Temp,Art_Temp,Top_Temp,Skin_Temp,Rs,MFP,MFS,MFT,d);
       Perfusion(count) = FinalP2;
       CR(count) = FinalCR2;
       SS(count) = FinalSS2;
    end

    filepath = 'C:\MATLAB701\work\NewDAQ\FinalCode\FinalResults\FinalEstimates';
    suffix = '.txt';
    fulloutputname = strcat(filepath,suffix);
    fid = fopen(fulloutputname,'w');
    fprintf(fid,'***Parameter Estimation for All Runs***\n\n');
    fprintf(fid,'Perfusion (ml/ml/s) \t Contact Resistance (m^2-K/W) \t Sum of the Squares \n');
    fprintf(fid,'--------------------\t ---------------------------- \t --------------------\n');

    for count = 1:NumofData
       fprintf(fid,'%10.5f \t %28.5f \t %26.5f \n', Perfusion(count), CR(count), SS(count));
    end
    fclose(fid);
  end
end
```

C.2 Phanton_ParameterEstimation.m

```
function[FinalP, FinalCr, FinalSS] =
Phantom_ParameterEstimation(filename1,R_Temp,Art_Temp,Top_Temp,Skin_Temp,Rs,MFP,MFS,MFT,d)

% ************************************************************************** %
%% PARAMETER ESTIMATION ROUTINE
%%          by Ashvinikumar Mudaliar
%% This program is modified from Caroline program to take the air
%% temperature variation and inital temperature for sensor and tissue

%% This is the program that executes the paramter estimation routine if
%% decision = 2 in BloodPerfusion.m.  It takes in the experimental heat
%% flux data and compares it to the data from the model.  The unknown parameter
%% values, perfusion and contact resistance are adjusted accordingly after each
%% iteration in order to achieve convergence between the experimental and
%% calculated heat flux data.
%%
%%
%%     Inputs: filename1: filename of the file containing the experimental
%%                 heatflux data (written as a string i.e.
%%                 filename1.txt')
%%             filename2: filename of the file containing the experimental
%%                 temperature data (written as a string i.e.
%%                 'filename1.txt')\
%%
%%     Outputs: opens Estimates.txt in a new m-file window.  This file contains
%%        the parameter estimates and sum of squares for each iteration and
%%        the final perfusion and contact resistance estimates.  It also
%%        contains the heat flux convergence plot data (time, experimental q"
%%        and calculated q").  The convergence plot is also opened when
%%        the program is done running.\
% ************************************************************************** %

global N NP temperatures
global start stop

    % starts clock for program run-time

% ********************** Call ExpDataFormatting m-file ********************** %
%[variables,initial_guesses,temperatures,dataout] = ExpDataFormatting_SP(filename1,filename2);
[time,FD_tstp,initial_guesses,temperatures,variance,SmoothAirTemp,heat_flux,const5] =
Phantom_ExpDataFormatting(filename1,R_Temp,Art_Temp,Top_Temp,Skin_Temp,Rs,MFP,MFS,MFT,d);

Y = heat_flux';
NTSTP = const5;
%Var = dataout(3,:)';
Var = variance';
MaxIt = 30;
BS = initial_guesses;
NP = 2;
Tair = temperatures(1); Tart = temperatures(2); Tinit1 = temperatures(3); Tinit2 = temperatures(4);Tsensor = temperatures(5);
Tair_smooth = SmoothAirTemp;
% ************************************************************************** %
```

```
%%%  Create text file where output data will be saved
%filepath='C:\MATLAB701\work\Plasticprobecode\Estimates';   % ---> Make sure you have the correct
% filepath='C:\MATLAB701\work\Imaginary_cell_code\Estimates';   % ---> Make sure you have the correct
% suffix='.txt';                          % directory name for MatLab on
% fulloutputname=strcat(filepath,suffix);       % the computer you are using.

z='C:\MATLAB701\work\NewDAQ\FinalCode\FinalResults\Estimates';
q=[z,d];
filepath=q;   % ---> Make sure you have the correct
suffix='.txt';                          % directory name for MatLab on
fulloutputname=strcat(filepath,suffix);       % the computer you are using.

fid=fopen(fulloutputname,'w');
fprintf(fid,'***PARAMETER ESTIMATION ROUTINE*** \n\n');
fprintf(fid,'Input Files: %s, ', filename1); %fprintf(fid,'%s \n', filename2);
fprintf(fid,'Date & Time: %4.0f/%02.0f/%02.0f, %02.0f:%02.0f:%02.0f\n\n', clock);
fprintf(fid,'T_arterial = %4.2f \n',Tart);
fprintf(fid,'T_air = %4.2f \n',Tair);
fprintf(fid,'T_TopThermocouple = %4.2f \n',Tinit2);
fprintf(fid,'T_BottomThermocouple = %4.2f \n',Tinit1);
fprintf(fid,'T_Sensor = %4.2f \n\n',Tsensor);
fprintf(fid,'Starting Line #: %5.0f \n', start);
fprintf(fid,'Ending Line #: %5.0f \n\n', stop);
fprintf(fid,' Perfusion (mL/mL/s) \t Contact Resistance (m^2-K/W) \t Sum of Squares\n');
fprintf(fid,'---------- \t ---------- \t ---------- \n');


% ************************************************************************** %
% ************** Start of Sequential Gauss Estimation Scheme ***************** %

ConvTest = 0;
control =1;

while control < MaxIt

   if ConvTest == 0


% ************************** Call MODEL m-file ****************************** %
      [TIME, SMOOTHPQ] = Phantom_MODEL(BS, temperatures, NTSTP,Tair_smooth, FD_tstp, Rs, MFT);
% ************************************************************************** %
      Qpredicted = SMOOTHPQ;          % save for plotting on final iteration

% ***************** Call SENSITIVITY COEFFICIENTS m-file ******************** %
      SC = Phantom_SensitivityCoefficients(BS,temperatures, SMOOTHPQ, NTSTP,Tair_smooth, FD_tstp, Rs, MFT);
% ************************************************************************** %

%% ----- Calculate the sum of squares (SSy)
      Resid = (Y - SMOOTHPQ);
      SSy = sum(Resid.^2./Var);
%       RSSy = sum(RS.^2);
%
%% ----- Calculate the "C" matrix
      for k = 1:NP
```

```
      for k1 = 1: NP
         C(k1,k) = sum(SC(:,k).*SC(:,k1)./Var);
      end
   end

%% ----- Calculate "D"
   for k = 1:NP
      D(k) = sum(SC(:,k).*Resid./Var);
   end

%% ----- Calculate the "P" matrix from the "C" matrix coefficients
   PINV = C;

   if NP == 1
      P(1,1) = 1./PINV;
   else
      P = inv(PINV);        % invert C matrix
   end

   DeltaB = [0 0];
   for k = 1:NP
      for j = 1:NP
         DeltaB(k) = DeltaB(k) + (P(j,k)*D(j));
      end
   end

   for k = 1:NP
      B(k) = BS(k) + DeltaB(k)/2;
   end

%     if B(1) <= 0
%        B(1) = 0.000001;
%     end
   if B(2)<=0
      B(2) = 0.000001;
   end

   for k = 1:NP
      CI(k) = sqrt(abs(P(k,k)))*1.96;     % 95% confidence interval
   end

% ********** End of Sequential Gauss Estimation Scheme ********** %
% ************************************************************************** %

%%% Check the parameter estimates for w and Rc against the criteria for a
%%% converged solution (ratio <= 0.0001).  Update "change" accordingly.

   change = 0;

   for j = 1:NP
      Ratio = abs((B(j) - BS(j))./BS(j));
      if Ratio <= 0.0001
         change = change +1;
      end
   end
```

```
%%% Check to see that both paramters have converged.  If not, check to see if
%%% the maximum number of iterations have been used.  If not, then program
%%% runs through Gaussian estimation loop again using the updated
%%% parameter estimates as the initial guesses.

      outputs(1,control) = B(1);
      outputs(2,control) = B(2);
      outputs(3,control) = SSy;
      outputs';

      if change == NP
         control = MaxIt + 1;
         fprintf(fid,'%10.5f %28.5f %26.5f \n\n',outputs);
         fprintf(fid,'Final Perfusion Estimate (mL/mL/s) = %6.5f \n', B(1));
         fprintf(fid,'Final Contact Resistance Estimate (m^2-K/W) = %6.5f \n', B(2));
         fprintf(fid,'Sum of Squares for Final Estimates = %6.5f \n', SSy);
%           fprintf(fid,'Sum of Residual Squares for Final Estimates = %6.5f \n', RSSy);
         fclose(fid);
         figure(1)
         plot(time,Y, time,Qpredicted,'--r');
         xlabel('Time (sec)');  ylabel('Heat Flux (W/m^2)')
         legend('Experimental','Predicted')
         title('Heat flux data for the Flow =    cc/min');
         grid on;
      else
         BS = B;
         control = control+1;
      end

      if control == MaxIt
         fprintf(fid,'%13.5f %28.5f %26.5f \n\n',outputs);
         fprintf('Maximum number of iterations reached.');
         fclose(fid);
      end

   end     % end "if" statement
end     % end "while" statement


FinalP=B(1);
FinalCr=B(2);
FinalSS=SSy;
%open Estimates.txt
h=figure(1);
z='C:\MATLAB701\work\NewDAQ\FinalCode\FinalResults\Fig';
q=[z,d];
filepath=q;
suffix='.fig';
fullout=strcat(filepath,suffix);
saveas(h,fullout);
 close all;

  % t - total run time for program
```

C.3 Phantom_ExpDataFormatting.m

```
function [time,FD_tstp,initial_guesses,temperatures,variance,SmoothAirTemp,...
  heat_flux,const5]   = Phantom_ExpDataFormatting(filename1,R_Temp,Art_Temp,Top_Temp,Skin_Temp,Rs,MFP,MFS,MFT,d)

format short e;
 global N NP
global start stop
% My Modification dated 16th Sept 2005
%    filename1 = input('Enter name of experimental heat flux and Temperature data file:  ');
   y=load(filename1, '%f');
  %y=load('test4_UNC.txt', '%f');
  [maxv ind1] = max(y(1:end,2));
%starting point of the heat flux data
start= ind1;%input('Enter starting point of thermal event: ');

% ending point from heat flux data
stop= length(y(1:end,2));%input('Enter stopping point of thermal event:  ');

%Option for Phantom tissue tests and Rat tests
% NTherm = input('Enter 1 for Rat/Forearm tests or 2 for Phantom test:    ');

% initial guesses for perfusion (1) and contact resistance (2)
initial_guesses(1)=0.0001;
initial_guesses(2)=0.0001;

% if NTherm == 2
   RefT = R_Temp; %input('Enter the Reference Temperature:  ');            %Required to convert the voltage into Temp CJC
   InletTemp= Art_Temp; %input('Enter the Arterial Temperature:   ');       %z(:,4); % Channel 4 reading from DAQ
   TissueTemp= Skin_Temp; %input('Enter the Skin Temperature:    ');        %z(:,3); % Channel 3 reading from the DAQ
   TopTemp = Top_Temp; %input('Enter the Top Thermocouple Temperature:    '); %Temperature measured from Doric

   TempTime = y(:,1)*MFT;          % With Old DAQ %Actual time is used with new DAQ
   dt = TempTime(2)- TempTime(1);              % time step for temperature measurement
   Tstart = (TempTime(start)); % Rounding off the starting point
   Tend = (TempTime(stop)); % Rounding off the ending point
   % Temperatures from the DAQ
   AirTemp= y(:,3)./40.6e-04 + RefT; % Experimental Air Temp. , Channel 3 reading from Old DAQ

   % Protocol Established by Ashvin, Caroline and Dr. Diller for Initial
   % Condition
   InitialTemp1 = InletTemp;     %mean(InletTemp(1:Tstart-1)) with new DAQ;
   InitialTemp2 = TopTemp;       %mean(TopTemp(1:Tstart-1)); with new DAQ
   AirT=AirTemp(start:stop-1);   % Truncated Air temperature during the thermal event
   temperatures(1) = mean(AirTemp(start:stop));       % air temp.
   temperatures(2) = InletTemp;                    % arterial temp.
   temperatures(3) = InitialTemp1;                  % Initial Temperatures for tissue and sensor are different
   temperatures(4) = InitialTemp2;                  % Finalized by Ashvin, Dr. Scott and Dr. Diller Dated 23rd Sept 2005
   temperatures(5) = TissueTemp;%mean(SensorTemp(1:Tstart-1));        % Sensor Initial Condition
  % Removing the zero offset in heat flux measurement from the Amplifier
   q = y(:,2).*MFS;%6561.68;       %Voltage converted into Heat flux;
   offset = mean(q(1:start-1)); %calculating the offset heat flux
   const3 = length(q);         %length of the Experimental heat flux
```

```
for i=1:const3
   Actual_heat_flux(i) = q(i)- offset; %Removing the offset in the measurement
end
%    figure(2)
%    plot(y(:,1),Actual_heat_flux);
%    xlabel('Time in Seconds');
%    ylabel('Heat Flux Data in W/m^2');
%    title('Raw Heat Flux Data');

  heat_flux = Actual_heat_flux(start:stop-1)*MFP; % Scaling factor taken in consideration because of the change in sensing area
  consthf = length(heat_flux);
     %Air temperature interpolated for 600 time steps to match the array size with FD model
   %AirTime = 0:dt:(Tend-Tstart);   %Time vector for Air temperature by offsetting starting from zero
   if MFT == 2
      time = 0:(Tend-Tstart)/(consthf-1):(Tend-Tstart);
      FD_Time = 0:time(2)/MFT:time(end);% Finite Difference time
      FD_tstp = FD_Time(2)-FD_Time(1);
      SmoothAirTemp = spline(time,AirT,FD_Time);
   elseif MFT == 1
      time = 0:(Tend-Tstart)/(consthf-1):(Tend-Tstart);
      FD_Time = 0:time(2)/MFT:time(end);% Finite Difference time
      FD_tstp = FD_Time(2)-FD_Time(1);
      SmoothAirTemp = AirT;
   end
   const5 = length(FD_Time);
% option for plotting smoothed air temperature
%     figure(3)
%     plot(FD_Time,SmoothAirTemp);
%     xlabel('Time');
%     ylabel('Temperature');
%     title('Smooth Air Temperature for FD model');

%Option for plotting the scaled heat flux data during the thermal event for
%big probe
%    figure(4)
%    plot(time, heat_flux,'r--');
%    xlabel('Time in seconds');
%    ylabel('q" in W/m^2');
%    title('Scaled Heat Flux');

% Variance for the heat flux data
   Var1 = var(heat_flux);

   % Weighing the residual by factor of 100000. The first 15 seconds of data
   % is dominated contact resistance. The region of interest is after 15
   % seconds where perfusion is dominant
   for i = 1:consthf
      if i <= 50
         variance(i) = Var1*100000;
      else
         variance(i) = Var1;
      end
   end

%************End of Formatting Experimental Data**************************
```

C.4 Phantom_Model.m

```
function  [TIME, SMOOTHQ] = Phantom_MODEL(BS, temperatures,NTSTP,Tair_smooth,FD_tstp, Rs, MFT)
% This code is being developed to replace the code written by Mitchener,
% Robinson, Cardinali and Comas. The code written by them was in
% non-dimensional form and the current code is in dimensional form. This
% code is written by Ashvinikumar Mudaliar on 17th of April 2006
format long e;

%Rs = 0.00427;%0.00427;%0.00953; %input('Radius of the Sensor'); % Radius of sensor
Rt = 2*Rs;
Tiss_t = 0.0127; %input(' Thickness of the Tissue'); % Sponge thickness
Sens_t = 0.00025; % input(' Thickness of the Sensor'); % Sensor thickness
Nodes_Radial = 15;
Nodes_Rs = Nodes_Radial+2; % number of nodes in radial direction on the Sensor
Nodes_Rt = 2*Nodes_Rs-2;%2*Nodes_Rs; % number of nodes in radial direction on Tissue
Nodes_Zs = 5; % number of nodes along the sensor thickness
Nodes_Zt = 51*Nodes_Zs; % number of nodes along thickness of the tissue

dr = Rs/(Nodes_Rs-2); %spacing between the nodes in radial direction

r = dr/2:dr:Rt; % Radius discretized

dz = (Sens_t)/(Nodes_Zs); % Node spacing in axial direction

z = dz/2:dz:(Sens_t+Tiss_t); % Thickness discretized


% Properties of the sensor

rho_s = 1250; % Density of sensor kg/m^3
sp_heat_s = 1340; % Specific heat of the sensor J/kg-K
k_s = 0.25;% Thermal condcutivity of the sensor W/m-K
alpha_s = k_s/(rho_s*sp_heat_s); % Thermal diffusivity of the sensor m^2/s

% Properties of the Tissue

rho_t = 998.2; %density of tissue in kg/m^3
sp_heat_t = 4182; %Specific heat of tissue J-kg/K
k_t = 0.5723;% Thermal conductivity of tissue W/m-K
alpha_t = k_t/(rho_t*sp_heat_t); %Thermal diffusivity of the tissue

dt1 = FD_tstp;%FD_tstp; %time step sec

%Initial Temperature and other required data
Tair = temperatures(1);
Tart = temperatures(2); %Arterial Temperature
TopT = temperatures(4);
Tinit_sen = temperatures(5); %Initial Temperature of sensor deg C
Tinf = Tair_smooth;
TempGrad = (TopT - Tart)/(Nodes_Zt-1);

Ta = Tart; % Just alloting Ta as Arterial Temperature
h = 1000; %Convective heat transfer coefficient W/m^2-K
```

```
Rc = BS(2); %Contact resistance m^2-K
w =  BS(1); %blood perfusion in ml/ml/s

%Initial Condition for the Sensor and Tissue
for i = 1:Nodes_Zs
   for j = 1:Nodes_Rs
      T(i,j) = Tinit_sen; % Initial Temp condition for the sensor
   end
end

for i = Nodes_Zs+2:(Nodes_Zs+Nodes_Zt)
   for j = 1: Nodes_Rt
      T(Nodes_Zs,Nodes_Rs:Nodes_Rt) = TopT; %Initial Temp for ghost cells for open tissue portion
      T(Nodes_Zs+1,j) = TopT; % Initial Temp condition as Temp gradient
      T(i,j) = T(i-1,j)+ TempGrad;
    end
end

 %Defining constants for Sensor
 As = -alpha_s*dt1/(2*dz^2);
 Bs = 1 + alpha_s*dt1/(dz^2);
 Ds = 1 - alpha_s*dt1/(dr^2);

 for j = 2: Nodes_Rs-1
    Cs(j-1) = alpha_s*dt1/(2*dr)*(1/dr-1/(2*r(j-1)));
    Es(j-1) = alpha_s*dt1/(2*dr)*(1/dr+1/(2*r(j-1)));
 end

%Defining constants for Tissue
   A1t = -alpha_t*dt1/(2*dz^2);
   B1t = 1 + alpha_t*dt1/dz^2 + w*dt1/2;
   B2t = 1 + alpha_t*dt1/dr^2 + w*dt1/2;
   D1t = 1 - alpha_t*dt1/dr^2 ;
   D2t = 1 - alpha_t*dt1/dz^2 ;

   for j = 2:Nodes_Rt-1
      C1t(j-1) = alpha_t*dt1/(2*dr)*(1/dr-1/(2*r(j-1)));
      E1t(j-1) = alpha_t*dt1/(2*dr)*(1/dr+1/(2*r(j-1)));
   end

 %Matrix elements for axial sweep in sensor
 C1 = k_s/dz;
 C2 = (1/h + dz/(2*k_s));
 C3 = (dz/(2*k_s) + Rc + dz/(2*k_t));
 for j = 2:Nodes_Rs-1
    A(1,j) = 0;
    B(1,j) = 1+ C1*C2;
    C(1,j) = -C1*C2;

    A(Nodes_Zs,j)= -C1*C3;
    B(Nodes_Zs,j) = 1 + C1*C3;
    C(Nodes_Zs,j) = 0;
 end

 for j = 2:Nodes_Rs-1
```

```
   for i = 2:Nodes_Zs-1
      A(i,j) = As;
      B(i,j) = Bs;
      C(i,j) = As;
   end
end

% Matrix elements for Radial sweep in Sensor
for i = 1:Nodes_Zs
   D(i,1) = 0;
   E(i,1) = 1;
   F(i,1) = -1;

   D(i,Nodes_Rs) = -1;
   E(i,Nodes_Rs) = 1;
   F(i,Nodes_Rs) = 0;
end

for i = 1:Nodes_Zs
   for j = 2:Nodes_Rs-1
      D(i,j) = -Cs(j-1);
      E(i,j) = 2-Ds;
      F(i,j) = -Es(j-1);
   end
end

% Matrix elements for Axial sweep in Tissue
   C4 = k_t/dz;
   C5 = rho_t*sp_heat_t*w*dz;
   C6 = rho_t*sp_heat_t*w*dr;
for j = 2:Nodes_Rs-1
   A(Nodes_Zs+1,j) = 0;
   B(Nodes_Zs+1,j) = 1 + C3*C4 + C3*C5;
   C(Nodes_Zs+1,j) = -C3*C4;

   A(Nodes_Zs + Nodes_Zt,j) = 0;
   B(Nodes_Zs + Nodes_Zt,j) = 1;
   C(Nodes_Zs + Nodes_Zt,j) = 0;
end

for j = Nodes_Rs:Nodes_Rt-1
   A(Nodes_Zs,j) = 0;
   B(Nodes_Zs,j) = 1 ;
   C(Nodes_Zs,j) = -1;

   A(Nodes_Zs + Nodes_Zt,j) = 0;
   B(Nodes_Zs + Nodes_Zt,j) = 1;
   C(Nodes_Zs + Nodes_Zt,j) = 0;
end

for j = 2:Nodes_Rt-1
   for i = Nodes_Zs+2:Nodes_Zs + Nodes_Zt-1
      A(i,j) = A1t;
      B(i,j) = B1t;
      C(i,j) = A1t;
```

```
   end
end
for j = Nodes_Rs:Nodes_Rt-1
   for i = Nodes_Zs+1
      A(i,j)= A1t;
      B(i,j)= B1t;
      C(i,j)= A1t;
   end
end
% Matrix elements for Radial sweep in Tissue
for i = Nodes_Zs+1:Nodes_Zs + Nodes_Zt
   D(i,1) = 0;
   E(i,1) = 1;
   F(i,1) = -1;

   D(i,Nodes_Rt) = -1;
   E(i,Nodes_Rt) = 1;
   F(i,Nodes_Rt) = 0;
end

for i = Nodes_Zs+1:Nodes_Zs + Nodes_Zt
   for j = 2:Nodes_Rt-1
      D(i,j) = -C1t(j-1);
      E(i,j) =  B2t;
      F(i,j) = -E1t(j-1);
   end
end
 %**************************************************************************



for t = 1:NTSTP %time counter
%*****************************Axial Sweep for Sensor starts**************

%Top boundary condition
     for i = 1
      for j = 2:Nodes_Rs-1
         RHS1(i,j) = Tinf(t);
      end
     end
%Top boundary condition

%Bottom boundary condition
     for i = Nodes_Zs
      for j = 2:Nodes_Rs-1
            RHS1(i,j)= T(i+1,j);
      end
     end
 %Bottom boundary condition

%Middle Columns of the Sensor
    for i = 2:Nodes_Zs-1
       for j = 2
          RHS1(i,j)=  Cs(j-1)*T(i,j-1)+Ds*T(i,j)+Es(j-1)*T(i,j+1);
       end
```

```
      for j = Nodes_Rs-1
          RHS1(i,j) = Cs(j-1)*T(i,j-1)+Ds*T(i,j)+Es(j-1)*T(i,j+1);
      end
    end

     for  i = 2:Nodes_Zs-1
        for j = 3:Nodes_Rs-2
          RHS1(i,j) = Cs(j-1)*T(i,j-1) + Ds*T(i,j) + Es(j-1)*T(i,j+1);
        end
     end
 %Middle Columns of the Sensor


 %Thomas Algorithm starts
  for j = 2:Nodes_Rs-1
     PS1(1,j) = B(1,j);
     QS1(1,j) = RHS1(1,j)/PS1(1,j);

     for i = 2:Nodes_Zs
        PS1(i,j) = B(i,j)-A(i,j)*C(i-1,j)/PS1(i-1,j);
        QS1(i,j) = (RHS1(i,j)-A(i,j)*QS1(i-1,j))/PS1(i,j);
     end
        T(Nodes_Zs,j) = QS1(Nodes_Zs,j);

        %Backward substitution

        for k = Nodes_Zs-1:-1:1
           T(k,j) = QS1(k,j) - C(k,j)*T(k+1,j)/PS1(k,j);
        end
  end
  T(1:Nodes_Zs,1) = T(1:Nodes_Zs,2);
  T(1:Nodes_Zs,Nodes_Rs) = T(1:Nodes_Zs,Nodes_Rs-1);

   %Thomas Algorithm ends
 %**********************End of Axial Sweep for sensor*********************

 %***********************************Axial Sweep for% Tissue*************
%Top boundary condition
     for i = Nodes_Zs+1
      for j = 2:Nodes_Rs-1
           RHT1(i,j) = T(i-1,j)+ C3*C5*Ta;
      end
     end

     for i = Nodes_Zs
      for j = Nodes_Rs:Nodes_Rt-1
        RHT1(i,j) = 0;
      end
     end

 %Top boundary condition

 %Bottom boundary condition
     for i = Nodes_Zs+Nodes_Zt
      for j = 1:Nodes_Rt
```

```
        RHT1(i,j)= Ta;
       end
      end
 %Bottom boundary condition

%Middle Columns of the Tissue
       for  i = Nodes_Zs+2:Nodes_Zs + Nodes_Zt-1
          for j = 2:Nodes_Rs-1
            RHT1(i,j) = C1t(j-1)*T(i,j-1) + D1t*T(i,j) + E1t(j-1)*T(i,j+1)+ w*dt1/2*Ta;
          end
       end
       for  i = Nodes_Zs+1:Nodes_Zs + Nodes_Zt-1
          for j = Nodes_Rs:Nodes_Rt-1
            RHT1(i,j) = C1t(j-1)*T(i,j-1) + D1t*T(i,j) + E1t(j-1)*T(i,j+1)+ w*dt1/2*Ta;
          end
       end
%Middle Columns of the Tissue


  %Thomas Algorithm starts
   for j = 2:Nodes_Rs-1
      PT1(Nodes_Zs+1,j) = B(Nodes_Zs+1,j);
      QT1(Nodes_Zs+1,j) = RHT1(Nodes_Zs+1,j)/PT1(Nodes_Zs+1,j);

      for i = Nodes_Zs+2:Nodes_Zs + Nodes_Zt
         PT1(i,j) = B(i,j)-A(i,j)*C(i-1,j)/PT1(i-1,j);
         QT1(i,j) = (RHT1(i,j)-A(i,j)*QT1(i-1,j))/PT1(i,j);
      end
         T(Nodes_Zs + Nodes_Zt,j) = QT1(Nodes_Zs + Nodes_Zt,j);

         %Backward substitution

         for k = Nodes_Zs+Nodes_Zt-1:-1:Nodes_Zs+1
            T(k,j) = QT1(k,j) - C(k,j)*T(k+1,j)/PT1(k,j);
         end
   end
%     Thomas Algorithm ends

%      Thomas Algorithm starts
   for j = Nodes_Rs:Nodes_Rt-1
      PT1(Nodes_Zs,j) = B(Nodes_Zs,j);
      QT1(Nodes_Zs,j) = RHT1(Nodes_Zs,j)/PT1(Nodes_Zs,j);

      for i = Nodes_Zs+1:Nodes_Zs + Nodes_Zt
         PT1(i,j) = B(i,j)-A(i,j)*C(i-1,j)/PT1(i-1,j);
         QT1(i,j) = (RHT1(i,j)-A(i,j)*QT1(i-1,j))/PT1(i,j);
      end
         T(Nodes_Zs + Nodes_Zt,j) = QT1(Nodes_Zs + Nodes_Zt,j);

         %Backward substitution

         for k = Nodes_Zs+Nodes_Zt-1:-1:Nodes_Zs+1
            T(k,j) = QT1(k,j) - C(k,j)*T(k+1,j)/PT1(k,j);
         end
   end
```

```
  %Thomas Algorithm ends

 %Temperature updated to satisfy boundary condition
 T(Nodes_Zs+1:Nodes_Zs+Nodes_Zt,1) = T(Nodes_Zs+1:Nodes_Zs+Nodes_Zt,2);
 T(Nodes_Zs+1:Nodes_Zs+Nodes_Zt,Nodes_Rt) = T(Nodes_Zs+1:Nodes_Zs+Nodes_Zt,Nodes_Rt-1);
 T(Nodes_Zs, Nodes_Rs:Nodes_Rt-1) = T(Nodes_Zs+1, Nodes_Rs:Nodes_Rt-1);
 %*****************************Axial Sweep for Tissue ends************

% %*********************Start of Radial Sweep for  % Sensor**************
   %LHS boundary condition
    for j = 1
     for i = 1:Nodes_Zs
       RHS2(i,j) = 0;
     end
    end
   %LHS boundary condition

  %RHS boundary condition
    for j = Nodes_Rs
     for i = 1:Nodes_Zs
      RHS2(i,j)= 0;
     end
    end
  %RHS boundary condition


%Middle Columns of the Sensor
     for  j = 2:Nodes_Rs-1
        for i = 2:Nodes_Zs-1
          RHS2(i,j) = -As*T(i-1,j) + (2-Bs)*T(i,j) -As*T(i+1,j);
        end
     end
 %Middle Columns of the Sensor


 %Thomas Algorithm starts
 for i = 2:Nodes_Zs-1
    PS2(i,1) = E(i,1);
    QS2(i,1) = RHS2(i,1)/PS2(i,1);

    for j = 2:Nodes_Rs
       PS2(i,j) = E(i,j)-D(i,j)*F(i,j-1)/PS2(i,j-1);
       QS2(i,j) = (RHS2(i,j)-D(i,j)*QS2(i,j-1))/PS2(i,j);
    end
       T(i,Nodes_Rs) = QS2(i,Nodes_Rs);

       %Backward substitution

       for k = Nodes_Rs-1:-1:1
          T(i,k) = QS2(i,k) - F(i,k)*T(i,k+1)/PS2(i,k);
       end
 end
  %Thomas Algorithm ends
%
 %Temperature updated to satisfy boundary condition
```

```
T(1,2:Nodes_Rs-1) = (Tinf(t) + T(2,2:Nodes_Rs-1)*C1*C2)/(1+ C1*C2);
T(Nodes_Zs,2:Nodes_Rs-1) = (T(Nodes_Zs-1,2:Nodes_Rs-1)*C1*C3+ T(Nodes_Zs+1,2:Nodes_Rs-1))/(1 + C1*C3);
% % **************************End of Sensor Radial Sweep*********************

% %************************Radial Sweep of Tissue begins*******************
    %LHS boundary condition
   for j = 1
      for i = Nodes_Zs+1:Nodes_Zs+Nodes_Zt
         RHT2(i,j) = 0;
      end
   end
%LHS boundary condition

%RHS boundary condition
  for j = Nodes_Rt
   for i = Nodes_Zs+1:Nodes_Zs+Nodes_Zt
      RHT2(i,j)= 0;
   end
  end
%RHS boundary condition

%Middle Columns of the Tissue
    for  j = 2:Nodes_Rs-1
       for i = Nodes_Zs+2:Nodes_Zs+Nodes_Zt-1
         RHT2(i,j) = -A1t*T(i-1,j) + D2t*T(i,j) -A1t*T(i+1,j)+ w*dt1/2*Ta;
       end
    end
    for  j = Nodes_Rs:Nodes_Rt-1
       for i = Nodes_Zs+1:Nodes_Zs+Nodes_Zt-1
         RHT2(i,j) = -A1t*T(i-1,j) + D2t*T(i,j) -A1t*T(i+1,j)+ w*dt1/2*Ta;
       end
    end
%Middle Columns of the Tissue


 %Thomas Algorithm starts for the region below the sensor
 for i = Nodes_Zs+2:Nodes_Zs+Nodes_Zt-1
    PT2(i,1) = E(i,1);
    QT2(i,1) = RHT2(i,1)/PT2(i,1);

    for j = 2:Nodes_Rt
       PT2(i,j) = E(i,j)-D(i,j)*F(i,j-1)/PT2(i,j-1);
       QT2(i,j) = (RHT2(i,j)-D(i,j)*QT2(i,j-1))/PT2(i,j);
    end
       T(i,Nodes_Rt) = QT2(i,Nodes_Rt);

       %Backward substitution

       for k = Nodes_Rt-1:-1:1
          T(i,k) = QT2(i,k) - F(i,k)*T(i,k+1)/PT2(i,k);
       end
 end
 %Thomas Algorithm ends for the region below the sensor
```

```
   %Temperature updated to satisfy boundary condition
      T(Nodes_Zs+1,2:Nodes_Rs-1) = (T(Nodes_Zs+2,2:Nodes_Rs-1)*C3*C4 + T(Nodes_Zs,2:Nodes_Rs-1)+ C3*C5*Ta)/(1 + C3*C4+
C3*C5);
      for j = Nodes_Rs:Nodes_Rt-1
         for i = Nodes_Zs+1
         T(i,j) = (C4*(T(i,j-1)+T(i,j+1)) + C6*Ta)/(2*C4 + C6);
         end
      end
      T(Nodes_Zs,Nodes_Rs:Nodes_Rt-1)= T(Nodes_Zs+1, Nodes_Rs:Nodes_Rt-1);
      T(Nodes_Zs + Nodes_Zt,2:Nodes_Rt-1) = Ta;
 %************************Radial Sweep of Tissue ends********************
%      Final Calculations
      r1 = r(1:Nodes_Rs-2);
%
       for i = 2:Nodes_Rs-1
            q(i-1)= k_s/(z(Nodes_Zs)-z(1))*(T(Nodes_Zs,i)- T(1,i));
            Twa(i-1) = T(1,i);
            Tws(i-1) = T(Nodes_Zs,i);
            Twt(i-1) = T(Nodes_Zs+1,i);
        end
         qcond(t) = sum(q*r1')/sum(r1);
         qconv(t)= ((sum(Twa*r1')/sum(r1))-Tinf(t))/C2;
         qres(t) = ((sum(Twt*r1')/sum(r1)) - (sum(Tws*r1')/sum(r1)))/C3;
         qcenter(t) = k_s/(z(Nodes_Zs)-z(1))*(T(Nodes_Zs,2)-T(1,2));
         qcenter1(t)= k_s/(z(Nodes_Zs-1)-z(1))*(T(Nodes_Zs-1,2) - T(1,2));
         qcenter2(t)= k_s/dz*(T(2,2) - T(1,2));
         MP = qcond';
         length(MP);
         SMOOTHQ = MP(1:MFT:end);
         length(SMOOTHQ);
         TIME(t) = t*dt1;

 end

%  plot(time, qcenter,'--k');
%  box off;
%  plot(time, qcond,'--k',time,qconv,'-r',time,qres,'-.b');
%  box off;
%  xlabel('Time');
%  ylabel('Heat flux (W/m^2)');
%  title('Conduction, Convection and Resistive Heat fluxes');
%  legend('qcond','qconv','qres');
% plotting contours
% for j = 1:Nodes_Zs+Nodes_Zt
% TEMP3(j,1:Nodes_Rt) = T(Nodes_Zs+Nodes_Zt+1-j,1:Nodes_Rt);
% end
% contourf(r,z,TEMP3);
```

C.5 Phantom_SensitivityCoefficient.m

```
function SC = Phantom_SensitivityCoefficients(BS, temperatures, SMOOTHPQ,NTSTP,Tair_smooth, FD_tstp, Rs, MFT)

% ************************************************************************** %
%% SENSITIVITY COEFFICIENTS
%%       by Ashvin Mudaliar
%%
%% This program calculates the sensitivity coefficients for heat flux
%% sensitivity to perfusion and contact resistance, which are used in the
%% parameter estimation routine.
%%
%%     Inputs: BS:  [perfusion, contact reistance]
%%             temperatures:  passes air, arterial and initial
%%                temperatures, which are used in MODEL.m
%%             SMOOTHPQ:  passes the calculated heat flux for the
%%                parameters, BS
%%
%%     Outputs:  SC:  Sensitivity coefficients
% ************************************************************************** %

global N

Beta1 = BS(1);
Beta2 = BS(2);

Factor = 1.01;
Beta1P = Beta1*Factor;
Beta2P = Beta2*Factor;

[TIME, SMOOTHPQ1] = Phantom_MODEL([Beta1P,Beta2], temperatures, NTSTP,Tair_smooth, FD_tstp, Rs, MFT);
[TIME, SMOOTHPQ2] = Phantom_MODEL([Beta1,Beta2P], temperatures, NTSTP,Tair_smooth, FD_tstp, Rs, MFT);


SC(:,1) = (SMOOTHPQ1 - SMOOTHPQ)./(Beta1P - Beta1);
SC(:,2) = (SMOOTHPQ2 - SMOOTHPQ)./(Beta2P - Beta2);
```

C.6 Phantom_BloodPerfusion.m

```
function Phantom_BloodPerfusion
format long e;
% ************************************************************************** %
%% MAIN PROGRAM
%%  by Ashvinikumar Mudaliar September 16th 2005
%% This Program is modified from Caroline which take the actual
%% air temperature for estimating the blood perfusion values.

%% This is the main file for running ParameterEstimation.m and Model.m.
%% First enter value for decision to run ParameterEstimation.m or
%% Model. M by entering (1) or (2) (see below).  Then, enter the required
%% values when prompted.  When the program is done running a new m-file window
%% opens in MatLab containing the output data (if running the parameter
%% estimation routine, a convergence plot also appears).  The text file
%% that is opened, as well as the plot can be saved to any directory.
% ************************************************************************** %
   BS(1) = input('Enter value for blood perfusion (ml/ml/s):  ');
   BS(2) = input('Enter value for contact resistance (m^2-K/W):  ');
   temperatures(1) = input('Enter air temperature (C):  ');
   temperatures(2) = input('Enter arterial temperatures (C): ');
   temperatures(3) = input('Enter initial skin temperaure (C):  ');
   temperatures(4) = temperatures(3);
   temperatures(5) = temperatures(3);
   FD_tstp = 0.1;
   NTSTP = 600; %input('Enter the number of time steps (600 = 60 sec):  ');
   Tair_smooth = temperatures(1)*ones(1,600);
   [TIME, SMOOTHQ] = Phantom_MODEL1a(BS, temperatures,NTSTP,Tair_smooth,FD_tstp);
   for i = 1:length(TIME)
      ModelOutputs(1,i) = TIME(i);
      ModelOutputs(2,i) = SMOOTHQ(i);
   end
   filepath='C:\MATLAB701\work\NewDAQ\FinalCode\ModelResults'; % Make sure you have the correct
   suffix='.txt';                          % directory name for MatLab on
   fulloutputname=strcat(filepath,suffix);    % the computer you are using.

   fid=fopen(fulloutputname,'w');
   fprintf(fid,'***PROBE/TISSUE BIOHEAT TRANSFER MODEL*** \n\n');
   fprintf(fid,'Date & Time: %4.0f/%02.0f/%02.0f, %02.0f:%02.0f:%02.0f\n\n', clock);
   fprintf(fid,'T_arterial = %4.2f \n',temperatures(1));
   fprintf(fid,'T_air = %4.2f \n',temperatures(2));
   fprintf(fid,'T_initial = %4.2f \n\n',temperatures(3));
   fprintf(fid,' Time (sec) \t\t Heat Flux (W/m^2) \n');
   fprintf(fid,'-------------- \t ------------------- \n');
   fprintf(fid,' %8.5f %20.5f \n', ModelOutputs);
   fclose(fid);

   open ModelResults.txt

   figure(1)
   plot(TIME, SMOOTHQ);
   xlabel('Time (sec)');  ylabel ('Heat Flux (W/m^2)');
   title('Heat flux data for the Finite Difference Model');
```

C.7 Phantom_Model1a.m

```
function  [TIME, SMOOTHQ] = Phantom_MODEL(BS, temperatures,NTSTP,Tair_smooth,FD_tstp, Rs, MFT)
% This code is being developed to replace the code written by Mitchener,
% Robinson, Cardinali and Comas. The code written by them was in
% non-dimensional form and the current code is in dimensional form. This
% code is written by Ashvinikumar Mudaliar on 17th of April 2006
format long e;

%Rs = 0.00427;%0.00427;%0.00953; %input('Radius of the Sensor'); % Radius of sensor
Rt = 2*Rs;
Tiss_t = 0.0127; %input(' Thickness of the Tissue'); % Sponge thickness
Sens_t = 0.00025; % input(' Thickness of the Sensor'); % Sensor thickness
Nodes_Radial = 15;
Nodes_Rs = Nodes_Radial+2; % number of nodes in radial direction on the Sensor
Nodes_Rt = 2*Nodes_Rs-2;%2*Nodes_Rs; % number of nodes in radial direction on Tissue
Nodes_Zs = 5; % number of nodes along the sensor thickness
Nodes_Zt = 51*Nodes_Zs; % number of nodes along thickness of the tissue

dr = Rs/(Nodes_Rs-2); %spacing between the nodes in radial direction

r = dr/2:dr:Rt; % Radius discretized

dz = (Sens_t)/(Nodes_Zs); % Node spacing in axial direction

z = dz/2:dz:(Sens_t+Tiss_t); % Thickness discretized


% Properties of the sensor

rho_s = 1250; % Density of sensor kg/m^3
sp_heat_s = 1340; % Specific heat of the sensor J/kg-K
k_s = 0.25;% Thermal condcutivity of the sensor W/m-K
alpha_s = k_s/(rho_s*sp_heat_s); % Thermal diffusivity of the sensor m^2/s

% Properties of the Tissue

rho_t = 998.2; %density of tissue in kg/m^3
sp_heat_t = 4182; %Specific heat of tissue J-kg/K
k_t = 0.5723;% Thermal conductivity of tissue W/m-K
alpha_t = k_t/(rho_t*sp_heat_t); %Thermal diffusivity of the tissue

dt1 = FD_tstp;%FD_tstp; %time step sec

%Initial Temperature and other required data
Tair = temperatures(1);
Tart = temperatures(2); %Arterial Temperature
TopT = temperatures(4);
Tinit_sen = temperatures(5); %Initial Temperature of sensor deg C
Tinf = Tair_smooth;
TempGrad = (TopT - Tart)/(Nodes_Zt-1);

Ta = Tart; % Just alloting Ta as Arterial Temperature
h = 100000; %Convective heat transfer coefficient W/m^2-K
```

```
Rc = BS(2); %Contact resistance m^2-K
w =  BS(1); %blood perfusion in ml/ml/s

%Initial Condition for the Sensor and Tissue
for i = 1:Nodes_Zs
   for j = 1:Nodes_Rs
      T(i,j) = Tinit_sen; % Initial Temp condition for the sensor
   end
end

for i = Nodes_Zs+2:(Nodes_Zs+Nodes_Zt)
   for j = 1: Nodes_Rt
      T(Nodes_Zs,Nodes_Rs:Nodes_Rt) = TopT; %Initial Temp for ghost cells for open tissue portion
      T(Nodes_Zs+1,j) = TopT; % Initial Temp condition as Temp gradient
      T(i,j) = T(i-1,j)+ TempGrad;
    end
end

 %Defining constants for Sensor
 As = -alpha_s*dt1/(2*dz^2);
 Bs = 1 + alpha_s*dt1/(dz^2);
 Ds = 1 - alpha_s*dt1/(dr^2);

 for j = 2: Nodes_Rs-1
    Cs(j-1) = alpha_s*dt1/(2*dr)*(1/dr-1/(2*r(j-1)));
    Es(j-1) = alpha_s*dt1/(2*dr)*(1/dr+1/(2*r(j-1)));
 end

%Defining constants for Tissue
   A1t = -alpha_t*dt1/(2*dz^2);
   B1t = 1 + alpha_t*dt1/dz^2 + w*dt1/2;
   B2t = 1 + alpha_t*dt1/dr^2 + w*dt1/2;
   D1t = 1 - alpha_t*dt1/dr^2 ;
   D2t = 1 - alpha_t*dt1/dz^2 ;

   for j = 2:Nodes_Rt-1
      C1t(j-1) = alpha_t*dt1/(2*dr)*(1/dr-1/(2*r(j-1)));
      E1t(j-1) = alpha_t*dt1/(2*dr)*(1/dr+1/(2*r(j-1)));
   end

 %Matrix elements for axial sweep in sensor
 C1 = k_s/dz;
 C2 = (1/h + dz/(2*k_s));
 C3 = (dz/(2*k_s) + Rc + dz/(2*k_t));
 for j = 2:Nodes_Rs-1
    A(1,j) = 0;
    B(1,j) = 1+ C1*C2;
    C(1,j) = -C1*C2;

    A(Nodes_Zs,j)= -C1*C3;
    B(Nodes_Zs,j) = 1 + C1*C3;
    C(Nodes_Zs,j) = 0;
 end

 for j = 2:Nodes_Rs-1
```

```
    for i = 2:Nodes_Zs-1
        A(i,j) = As;
        B(i,j) = Bs;
        C(i,j) = As;
    end
end

% Matrix elements for Radial sweep in Sensor
for i = 1:Nodes_Zs
    D(i,1) = 0;
    E(i,1) = 1;
    F(i,1) = -1;

    D(i,Nodes_Rs) = -1;
    E(i,Nodes_Rs) = 1;
    F(i,Nodes_Rs) = 0;
end

for i = 1:Nodes_Zs
    for j = 2:Nodes_Rs-1
        D(i,j) = -Cs(j-1);
        E(i,j) = 2-Ds;
        F(i,j) = -Es(j-1);
    end
end

% Matrix elements for Axial sweep in Tissue
    C4 = k_t/dz;
    C5 = rho_t*sp_heat_t*w*dz;
    C6 = rho_t*sp_heat_t*w*dr;
for j = 2:Nodes_Rs-1
    A(Nodes_Zs+1,j) = 0;
    B(Nodes_Zs+1,j) = 1 + C3*C4 + C3*C5;
    C(Nodes_Zs+1,j) = -C3*C4;

    A(Nodes_Zs + Nodes_Zt,j) = 0;
    B(Nodes_Zs + Nodes_Zt,j) = 1;
    C(Nodes_Zs + Nodes_Zt,j) = 0;
end

for j = Nodes_Rs:Nodes_Rt-1
    A(Nodes_Zs,j) = 0;
    B(Nodes_Zs,j) = 1 ;
    C(Nodes_Zs,j) = -1;

    A(Nodes_Zs + Nodes_Zt,j) = 0;
    B(Nodes_Zs + Nodes_Zt,j) = 1;
    C(Nodes_Zs + Nodes_Zt,j) = 0;
end

for j = 2:Nodes_Rt-1
    for i = Nodes_Zs+2:Nodes_Zs + Nodes_Zt-1
        A(i,j) = A1t;
        B(i,j) = B1t;
        C(i,j) = A1t;
```

```
    end
end
for j = Nodes_Rs:Nodes_Rt-1
    for i = Nodes_Zs+1
        A(i,j)= A1t;
        B(i,j)= B1t;
        C(i,j)= A1t;
    end
end
% Matrix elements for Radial sweep in Tissue
for i = Nodes_Zs+1:Nodes_Zs + Nodes_Zt
    D(i,1) = 0;
    E(i,1) = 1;
    F(i,1) = -1;

    D(i,Nodes_Rt) = -1;
    E(i,Nodes_Rt) = 1;
    F(i,Nodes_Rt) = 0;
end

for i = Nodes_Zs+1:Nodes_Zs + Nodes_Zt
    for j = 2:Nodes_Rt-1
        D(i,j) = -C1t(j-1);
        E(i,j) =  B2t;
        F(i,j) = -E1t(j-1);
    end
end
  %**************************************************************************



for t = 1:NTSTP %time counter
%*****************************Axial Sweep for Sensor starts**************

%Top boundary condition
      for i = 1
       for j = 2:Nodes_Rs-1
          RHS1(i,j) = Tinf(t);
       end
      end
 %Top boundary condition

 %Bottom boundary condition
      for i = Nodes_Zs
       for j = 2:Nodes_Rs-1
            RHS1(i,j)= T(i+1,j);
       end
      end
  %Bottom boundary condition

%Middle Columns of the Sensor
      for i = 2:Nodes_Zs-1
         for j = 2
            RHS1(i,j)=  Cs(j-1)*T(i,j-1)+Ds*T(i,j)+Es(j-1)*T(i,j+1);
         end
```

```
      for j = Nodes_Rs-1
          RHS1(i,j) = Cs(j-1)*T(i,j-1)+Ds*T(i,j)+Es(j-1)*T(i,j+1);
      end
    end

     for  i = 2:Nodes_Zs-1
        for j = 3:Nodes_Rs-2
          RHS1(i,j) = Cs(j-1)*T(i,j-1) + Ds*T(i,j) + Es(j-1)*T(i,j+1);
        end
     end
 %Middle Columns of the Sensor


 %Thomas Algorithm starts
  for j = 2:Nodes_Rs-1
     PS1(1,j) = B(1,j);
     QS1(1,j) = RHS1(1,j)/PS1(1,j);

     for i = 2:Nodes_Zs
        PS1(i,j) = B(i,j)-A(i,j)*C(i-1,j)/PS1(i-1,j);
        QS1(i,j) = (RHS1(i,j)-A(i,j)*QS1(i-1,j))/PS1(i,j);
     end
        T(Nodes_Zs,j) = QS1(Nodes_Zs,j);

        %Backward substitution

        for k = Nodes_Zs-1:-1:1
           T(k,j) = QS1(k,j) - C(k,j)*T(k+1,j)/PS1(k,j);
        end
  end
  T(1:Nodes_Zs,1) = T(1:Nodes_Zs,2);
  T(1:Nodes_Zs,Nodes_Rs) = T(1:Nodes_Zs,Nodes_Rs-1);

   %Thomas Algorithm ends
 %**********************End of Axial Sweep for sensor*********************

 %***********************************Axial Sweep for% Tissue*************
%Top boundary condition
     for i = Nodes_Zs+1
      for j = 2:Nodes_Rs-1
           RHT1(i,j) = T(i-1,j)+ C3*C5*Ta;
      end
     end

     for i = Nodes_Zs
      for j = Nodes_Rs:Nodes_Rt-1
         RHT1(i,j) = 0;
      end
     end

 %Top boundary condition

 %Bottom boundary condition
     for i = Nodes_Zs+Nodes_Zt
      for j = 1:Nodes_Rt
```

```
        RHT1(i,j)= Ta;
       end
      end
  %Bottom boundary condition

%Middle Columns of the Tissue
       for  i = Nodes_Zs+2:Nodes_Zs + Nodes_Zt-1
          for j = 2:Nodes_Rs-1
            RHT1(i,j) = C1t(j-1)*T(i,j-1) + D1t*T(i,j) + E1t(j-1)*T(i,j+1)+ w*dt1/2*Ta;
          end
       end
       for  i = Nodes_Zs+1:Nodes_Zs + Nodes_Zt-1
          for j = Nodes_Rs:Nodes_Rt-1
            RHT1(i,j) = C1t(j-1)*T(i,j-1) + D1t*T(i,j) + E1t(j-1)*T(i,j+1)+ w*dt1/2*Ta;
          end
       end
%Middle Columns of the Tissue


   %Thomas Algorithm starts
    for j = 2:Nodes_Rs-1
       PT1(Nodes_Zs+1,j) = B(Nodes_Zs+1,j);
       QT1(Nodes_Zs+1,j) = RHT1(Nodes_Zs+1,j)/PT1(Nodes_Zs+1,j);

       for i = Nodes_Zs+2:Nodes_Zs + Nodes_Zt
          PT1(i,j) = B(i,j)-A(i,j)*C(i-1,j)/PT1(i-1,j);
          QT1(i,j) = (RHT1(i,j)-A(i,j)*QT1(i-1,j))/PT1(i,j);
       end
          T(Nodes_Zs + Nodes_Zt,j) = QT1(Nodes_Zs + Nodes_Zt,j);

          %Backward substitution

          for k = Nodes_Zs+Nodes_Zt-1:-1:Nodes_Zs+1
             T(k,j) = QT1(k,j) - C(k,j)*T(k+1,j)/PT1(k,j);
          end
    end
%      Thomas Algorithm ends

%       Thomas Algorithm starts
    for j = Nodes_Rs:Nodes_Rt-1
       PT1(Nodes_Zs,j) = B(Nodes_Zs,j);
       QT1(Nodes_Zs,j) = RHT1(Nodes_Zs,j)/PT1(Nodes_Zs,j);

       for i = Nodes_Zs+1:Nodes_Zs + Nodes_Zt
          PT1(i,j) = B(i,j)-A(i,j)*C(i-1,j)/PT1(i-1,j);
          QT1(i,j) = (RHT1(i,j)-A(i,j)*QT1(i-1,j))/PT1(i,j);
       end
          T(Nodes_Zs + Nodes_Zt,j) = QT1(Nodes_Zs + Nodes_Zt,j);

          %Backward substitution

          for k = Nodes_Zs+Nodes_Zt-1:-1:Nodes_Zs+1
             T(k,j) = QT1(k,j) - C(k,j)*T(k+1,j)/PT1(k,j);
          end
    end
```

```
   %Thomas Algorithm ends

  %Temperature updated to satisfy boundary condition
  T(Nodes_Zs+1:Nodes_Zs+Nodes_Zt,1) = T(Nodes_Zs+1:Nodes_Zs+Nodes_Zt,2);
  T(Nodes_Zs+1:Nodes_Zs+Nodes_Zt,Nodes_Rt) = T(Nodes_Zs+1:Nodes_Zs+Nodes_Zt,Nodes_Rt-1);
  T(Nodes_Zs, Nodes_Rs:Nodes_Rt-1) = T(Nodes_Zs+1, Nodes_Rs:Nodes_Rt-1);
  %*****************************Axial Sweep for Tissue ends************

 % %*********************Start of Radial Sweep for  % Sensor**************
    %LHS boundary condition
     for j = 1
      for i = 1:Nodes_Zs
        RHS2(i,j) = 0;
      end
     end
    %LHS boundary condition

   %RHS boundary condition
    for j = Nodes_Rs
     for i = 1:Nodes_Zs
      RHS2(i,j)= 0;
     end
    end
   %RHS boundary condition


 %Middle Columns of the Sensor
       for  j = 2:Nodes_Rs-1
          for i = 2:Nodes_Zs-1
            RHS2(i,j) = -As*T(i-1,j) + (2-Bs)*T(i,j) -As*T(i+1,j);
          end
       end
  %Middle Columns of the Sensor


  %Thomas Algorithm starts
   for i = 2:Nodes_Zs-1
      PS2(i,1) = E(i,1);
      QS2(i,1) = RHS2(i,1)/PS2(i,1);

      for j = 2:Nodes_Rs
         PS2(i,j) = E(i,j)-D(i,j)*F(i,j-1)/PS2(i,j-1);
         QS2(i,j) = (RHS2(i,j)-D(i,j)*QS2(i,j-1))/PS2(i,j);
      end
         T(i,Nodes_Rs) = QS2(i,Nodes_Rs);

         %Backward substitution

         for k = Nodes_Rs-1:-1:1
            T(i,k) = QS2(i,k) - F(i,k)*T(i,k+1)/PS2(i,k);
         end
   end
    %Thomas Algorithm ends
%
 %Temperature updated to satisfy boundary condition
```

```
T(1,2:Nodes_Rs-1) = (Tinf(t) + T(2,2:Nodes_Rs-1)*C1*C2)/(1+ C1*C2);
T(Nodes_Zs,2:Nodes_Rs-1) = (T(Nodes_Zs-1,2:Nodes_Rs-1)*C1*C3+ T(Nodes_Zs+1,2:Nodes_Rs-1))/(1 + C1*C3);
% % **************************End of Sensor Radial Sweep*********************

% %************************Radial Sweep of Tissue begins*******************
    %LHS boundary condition
   for j = 1
      for i = Nodes_Zs+1:Nodes_Zs+Nodes_Zt
         RHT2(i,j) = 0;
      end
   end
%LHS boundary condition

%RHS boundary condition
  for j = Nodes_Rt
   for i = Nodes_Zs+1:Nodes_Zs+Nodes_Zt
      RHT2(i,j)= 0;
   end
  end
%RHS boundary condition

%Middle Columns of the Tissue
    for  j = 2:Nodes_Rs-1
      for i = Nodes_Zs+2:Nodes_Zs+Nodes_Zt-1
         RHT2(i,j) = -A1t*T(i-1,j) + D2t*T(i,j) -A1t*T(i+1,j)+ w*dt1/2*Ta;
      end
    end
    for  j = Nodes_Rs:Nodes_Rt-1
      for i = Nodes_Zs+1:Nodes_Zs+Nodes_Zt-1
         RHT2(i,j) = -A1t*T(i-1,j) + D2t*T(i,j) -A1t*T(i+1,j)+ w*dt1/2*Ta;
      end
    end
%Middle Columns of the Tissue


%Thomas Algorithm starts for the region below the sensor
 for i = Nodes_Zs+2:Nodes_Zs+Nodes_Zt-1
   PT2(i,1) = E(i,1);
   QT2(i,1) = RHT2(i,1)/PT2(i,1);

   for j = 2:Nodes_Rt
      PT2(i,j) = E(i,j)-D(i,j)*F(i,j-1)/PT2(i,j-1);
      QT2(i,j) = (RHT2(i,j)-D(i,j)*QT2(i,j-1))/PT2(i,j);
   end
      T(i,Nodes_Rt) = QT2(i,Nodes_Rt);

      %Backward substitution

      for k = Nodes_Rt-1:-1:1
         T(i,k) = QT2(i,k) - F(i,k)*T(i,k+1)/PT2(i,k);
      end
 end
 %Thomas Algorithm ends for the region below the sensor
```

```
   %Temperature updated to satisfy boundary condition
      T(Nodes_Zs+1,2:Nodes_Rs-1) = (T(Nodes_Zs+2,2:Nodes_Rs-1)*C3*C4 + T(Nodes_Zs,2:Nodes_Rs-1)+ C3*C5*Ta)/(1 + C3*C4+
C3*C5);
      for j = Nodes_Rs:Nodes_Rt-1
         for i = Nodes_Zs+1
         T(i,j) = (C4*(T(i,j-1)+T(i,j+1)) + C6*Ta)/(2*C4 + C6);
         end
      end
      T(Nodes_Zs,Nodes_Rs:Nodes_Rt-1)= T(Nodes_Zs+1, Nodes_Rs:Nodes_Rt-1);
      T(Nodes_Zs + Nodes_Zt,2:Nodes_Rt-1) = Ta;
 %************************Radial Sweep of Tissue ends*******************
%       Final Calculations
      r1 = r(1:Nodes_Rs-2);
%
       for i = 2:Nodes_Rs-1
            q(i-1)= k_s/(z(Nodes_Zs)-z(1))*(T(Nodes_Zs,i)- T(1,i));
            Twa(i-1) = T(1,i);
            Tws(i-1) = T(Nodes_Zs,i);
            Twt(i-1) = T(Nodes_Zs+1,i);
        end
         qcond(t) = sum(q*r1')/sum(r1);
         qconv(t)= ((sum(Twa*r1')/sum(r1))-Tinf(t))/C2;
         qres(t) = ((sum(Twt*r1')/sum(r1)) - (sum(Tws*r1')/sum(r1)))/C3;
         qcenter(t) = k_s/(z(Nodes_Zs)-z(1))*(T(Nodes_Zs,2)-T(1,2));
         qcenter1(t)= k_s/(z(Nodes_Zs-1)-z(1))*(T(Nodes_Zs-1,2) - T(1,2));
         qcenter2(t)= k_s/dz*(T(2,2) - T(1,2));
         MP = qcond';
         length(MP);
         SMOOTHQ = MP(1:MFT:end);
         length(SMOOTHQ);
         TIME(t) = t*dt1;

 end

%  plot(time, qcenter,'--k');
%  box off;
%  plot(time, qcond,'--k',time,qconv,'-r',time,qres,'-.b');
%  box off;
%  xlabel('Time');
%  ylabel('Heat flux (W/m^2)');
%  title('Conduction, Convection and Resistive Heat fluxes');
%  legend('qcond','qconv','qres');
% plotting contours
% for j = 1:Nodes_Zs+Nodes_Zt
% TEMP3(j,1:Nodes_Rt) = T(Nodes_Zs+Nodes_Zt+1-j,1:Nodes_Rt);
% end
% contourf(r,z,TEMP3);
```

Appendix D

User Manual for BPP_DriverProgram.m

1. Before starting the program make sure that the file path are correctly specified in *BPP_DriverProgram, Phantom_ParameterEstimation,*and *Phantom_BloodPerfusion* Matlab files.
2. Make sure to create a folder for saving all the output files and also specify the corresponding file path in the *Phantom_ParameterEstimation* file and *BPP_DriverProgram* file.
3. Open Matlab and change the current directory from C:\MATLAB701\work to the directory where all the files are stored. Type BPP_DriverProgram into the Matlab work space. You will be prompted to enter 1 or 2 to run the parameter estimation, or to run the bioheat transfer model, respectively.

Running the Model only (decision = 2):

1. Enter the value of blood perfusion (ml/ml/s) for the bioheat transfer model when prompted.
2. Enter the value of contact resistance for the bioheat transfer model (m^2-K/W) when prompted.
3. Enter the value of air temperature (°C or K, be consistent with units) when prompted.
4. Enter the value of arterial temperature (°C or K) when prompted.
5. Enter the value of initial tissue temperature (°C or K) when prompted.
6. The output text file will open in a new m-file window. The output file contains the input parameters that were used as well as the time and heat flux data that were calculated.
7. This file should be saved by renaming, failing to do will overwrite the old data. A plot of average heat flux across the heat flux gage as a function of time will also pop up. This plot can also be saved into the same folder.

Running the Parameter Estimation Routine (decision = 1):

1. Enter 1 to run big probe experimental data and 2 to run small probe experimental data.
2. Enter the multiplication factor for converting the voltage signal into heat flux data. The multiplication factor is the reciprocal of the sensitivity coefficient of the heat flux gage in SI units ($V/W/m^2$) divided this by a factor of 100 to account for gain if amplifier is used.

3. Enter 1 if the 16 bit DAQ is used, which acquires the sample at 10 Hz/channel or 2 if the old traditional 24 bit DAQ is used, which acquires at 10 Hz/2 channel.
4. Enter 1 if you want to enter one set of data or 2 for multiple set of data.

4.1 For running single set of data (decision = 1):

1. Enter the value of the reference temperature (°C or K) when prompted.
2. Enter the value of the arterial temperature (°C or K) when prompted.
3. Enter the value of initial tissue temperature (°C or K) when prompted.
4. Enter 1 for phantom tissue test and 2 for animal model test when prompted. If you enter 1, it will prompt you to enter the top thermocouple temperature.
5. Enter the name of the file containing the heat flux and air temperature data in volts. Make sure you save the data files names in numeric only. For example if you want to enter the first data of the five tests conducted at 10 cc/min flow rate, save that file as 101.txt. The last digit on the file name represents the nth test conducted at the flow rate (cc/min), represented by the remaining digits.
6. The parameter estimation will run and will save the corresponding text file namely 101.txt containing perfusion, contact resistance and sum of the squares for all the iterations till it converges in the folder that has been created before. To read this file, open it in MS Excel only. A Matlab figure file named 101.fig will also be saved in the same folder
7. If the parameter estimation does not converge it will prompt a message in Matlab work space that maximum iterations have been reached.

4.2 For running multiple set of data (decision = 2):

1. For running multiple set of data in one shot you need to create another text file have all the information about heat flux data and temperatures for each test case. Make sure all your data files are stored in the same folder as the parameter estimation code is saved.
2. An example of the text file created is shown below. Make sure that all the data columns are in same sequence as shown. The first column is the file name; the second column represents reference temperature. Arterial, top thermocouple and tissue temperature are represented by third, fourth and fifth column respectively. The headers shown below in the example should be removed before running the data in parameter estimation program. The file name 53 belongs to the third test conducted at 5 cc/min in phantom tissue

experiments, and the temperatures required to run the bioheat model are shown in the shown in the corresponding row.

File name	Reference	Arterial	Top	Tissue
1	25.8	35.6	34.1	33.9
2	25.8	35.5	34.1	33.8
3	25.8	35.4	34.2	33.7
51	25.8	35.5	34.1	34
52	25.8	35.4	34.2	33.9
53	25.8	35.3	34.1	33.9
101	25.7	35.4	34.7	34.4
102	25.7	35.3	34.5	34.2
103	25.8	35.4	34.4	34.2
151	25.7	35.2	34.6	34.4
152	25.7	35.1	34.7	34.4
153	25.7	35.1	34.6	34.3

3. Enter the text file name that you have created, when prompted.

4. Enter the number of experiments files when prompted. The parameter estimation program will run for all these test cases and save the resulting perfusion estimates and the convergence plots in the specified folder for each case with *.txt and *.fig extensions and a final consolidates estimated file which will have converged values for perfusion, contact resistances and sum of the squares for individual tests.

Appendix E

Phantom Tissue Test Stand Development

Two phantom tissue test stand designs were explored. The main difference between the two is the way in which the flow was imparted onto the phantom tissue in order to produce a uniform, non-directional flow. The first test stand had a side-entrance flow pattern and the second test stand had a bottom entrance flow pattern. The design of the two test stands is described in further detail in the following sections.

E.1 Side-Entrance Phantom Tissue Test Stand

In the side-entrance phantom tissue test stand, perfusion through the material was accomplished by forcing water through two 10 mm^2 square inlets on opposing sides of the porous media, and allowing the water to exit through the two remaining sides. The dimensions of the porous media were 100 mm $\times$100 mm$\times$12.7 mm. The porous media was sandwiched between a plexiglass plate on the bottom and a Latex layer on the top to keep the flow from escaping through the top or bottom of the material. The Latex layer also served to simulate an epidermal surface. To collect data, the blood perfusion probe was placed on top of the Latex layer, and centered on the porous media. A schematic of the test section is shown in Figure 44. The arrows designate the direction of water flow.

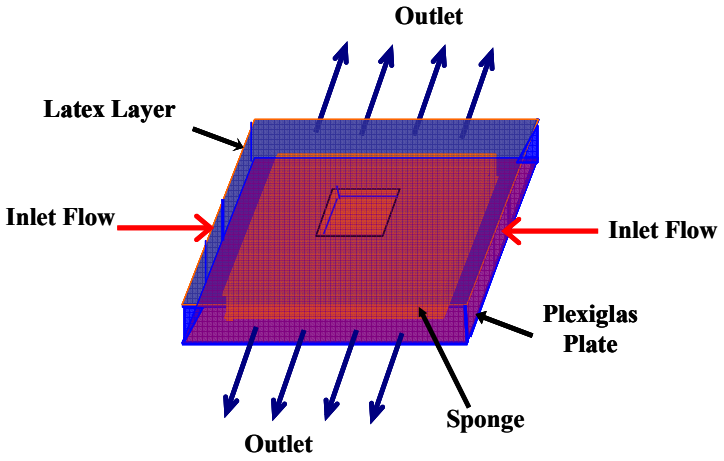

Figure 44: Schematic of side-entrance phantom tissue test stand

The test section sat within a larger plexiglass box which acted as a water bath. A cartridge heater with an automatic temperature controller was used to maintain the water bath at a constant temperature since the water was used to simulate blood, which is held at the core body temperature. The water bath also served as a storage reservoir, to ensure that the inlet flow rate into the porous material remained constant. The flow into the test section was provided by a centrifugal pump that pumped water from the water bath into two small headers that were affixed at the inlets on both sides of the porous media. The water supplied into each header was metered and controlled at the desired flow rate. The water flowed out of the headers and into the porous media, and exited through the two outlets, into the water bath. Figure 45 is a picture of the fully constructed side-entrance phantom tissue test stand

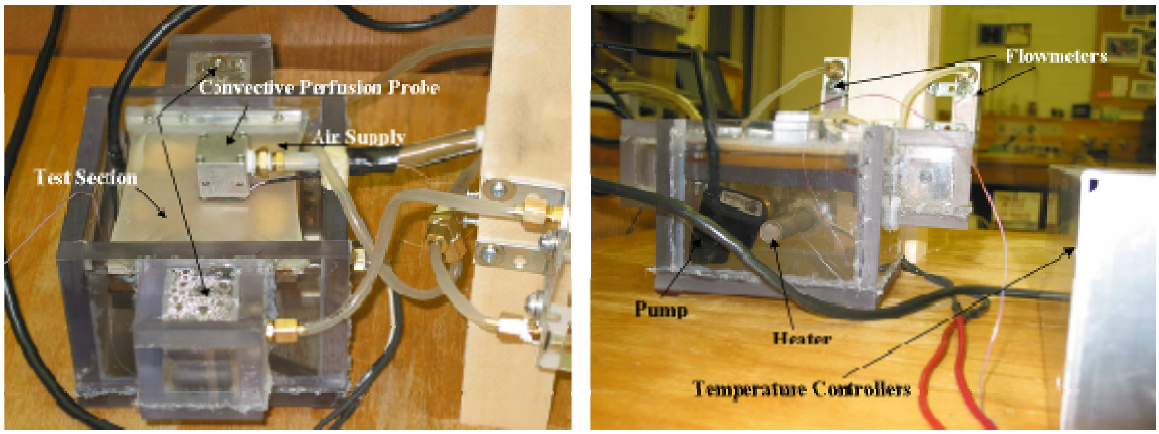

Figure 45: Picture of side-entrance phantom tissue test stand with controls

The side-entrance phantom tissue test stand was the first test stand that was designed and built. The probe used for this test is the one used by Comas. The probe was tested on this test stand following the experimental procedures as discussed in chapter 3, for an inlet flow rate range of 0 to 100 cc/min, at 20 cc/min intervals. For each flow rate there were 3 experimental runs. The results for the perfusion estimates that were obtained are shown in Figure 46. The resulting heat flux data was input to the parameter estimation code written by Robinson.

Figure 46 shows the lack of trend between perfusion and inlet flow rate into the porous media. One explanation for this lack of trend is that the entire volume of the porous media was not actually being supplied with the inlet flow rate that the flowmeter was set to. It was found that boundary layers formed at the top and bottom of the porous media due to the geometry of the inlets and the heat transfer was dominant in the boundary layer. For this reason the flow of water was not reaching the center of the porous media over which the heat flux was measured by the heat flux gage.

Consequently, the estimates of perfusion that were found for the experimental data did not correlate to the inlet flow rate.

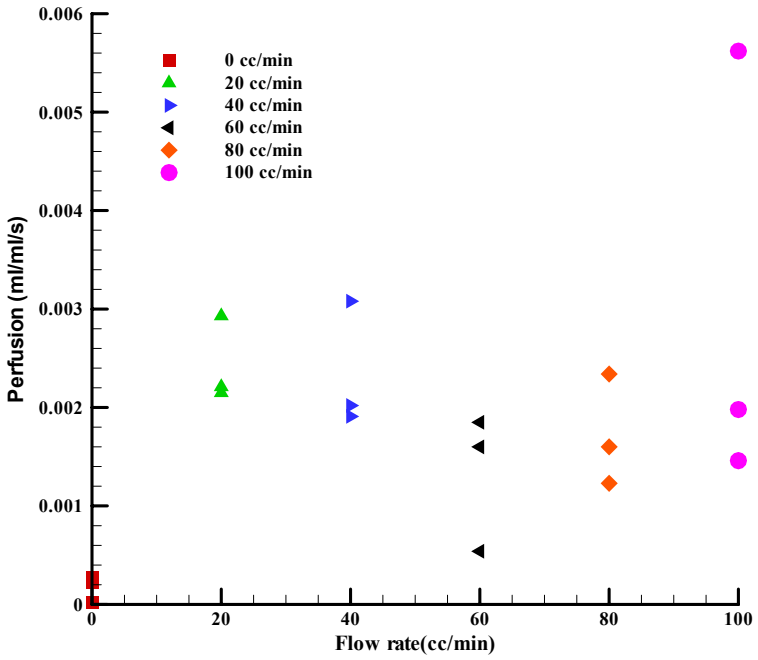

Figure 46: Perfusion estimated for side-entrance phantom tissue test

E.2 Bottom-Entrance phantom tissue test stand

The new bottom-entrance test stand was constructed to address the problems encountered in side-entrance test stand by changing the location of the inlet to the bottom, rather than the sides of the porous material. The bottom-entrance flow pattern was modeled using computational fluid dynamics software (Fluent). It was found that the bottom-entrance flow pattern exhibited uniform and non-directional flow through out the porous media, and boundary layers did not form at the inlet. Another change that was made to the test stand was a reduction in the size of the porous matrix from 100 mm x 100 mm x 12.7 mm to 40 mm x 40 mm x 12.7 mm. This reduction in the top surface area of the porous media over which the probe was measuring (25.4 mm x 25.4 mm) did not have any effect in the heat flux measured was concluded from the CFD results.

In the bottom entrance test stand, the porous matrix is sandwiched between the plexiglass at the bottom and plastic layer on the top to keep the flow from escaping from top and bottom of the porous matrix. All the other sides of the porous matrix served as the outlet for the flow. Perfusion through the porous material was accomplished by pumping the water through a 6.35 mm diameter, circular inlet in the bottom of the plexiglass plate. To collect the heat flux data the probe was directly placed over the top plastic layer centered, so that the center of the probe coincides with that of the center of the inlet at the bottom of the plexiglass plate. The schematic of the bottom-entrance test stand is shown in the Figure 47.

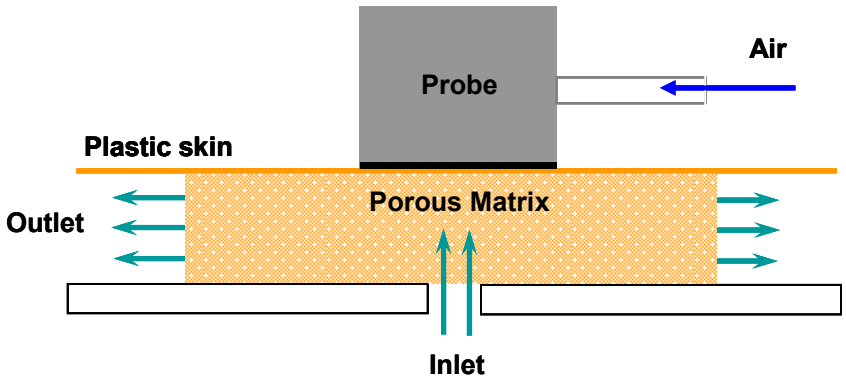

Figure 47: Schematic of bottom-entrance phantom tissue test section.

The test section of the bottom entrance test stand sits within a larger plexiglass box, which contains a water bath maintained at constant temperature of 37°C, i.e. core temperature of human body. The water bath also serves as storage reservoir to ensure that the flow rate into the porous material remained constant. The flow into the test section was provided by a centrifugal pump that pumped water from the water bath directly into the inlet of the test section. The water then flowed into the porous media, and exited through the four sides of the porous matrix, and into the water bath. The inlet flow was controlled by a Dwyer Instruments Inc. Visi-Float ®, model VFB-82-BV (0-30 cc/min flow range). A photograph of bottom-entrance phantom tissue test stand and controls used are shown in Figure 48.

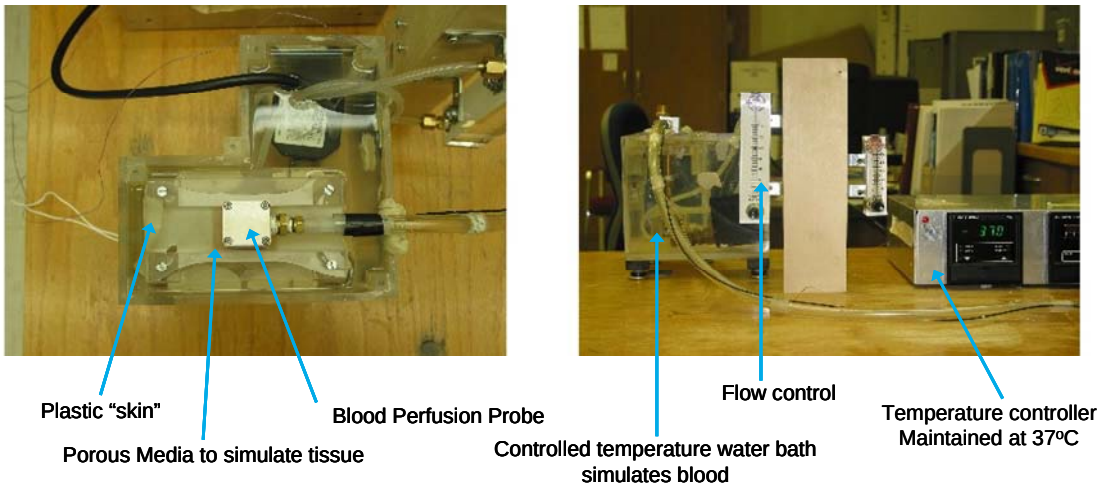

Figure 48: Bottom-Entrance phantom tissue test stand setup with the controls

A new probe smaller in size similar to the big probe was developed so that it can be used for testing on animal models. Figure 49 shows the measurement repeatability for the big and small perfusion probe used for 0 – 30 cc/min. The parameter estimation was carried out using program written by Comas. The perfusion estimates for the given test with the above phantom tissue test stand is shown in the Figure 50. It is evident that perfusion is function of the inlet flow rate. Also the perfusion estimated is compared with that of the CFD model (Fluent). The CFD model development is discussed in the next appendix. They are in good agreement till 15 cc/min after that there is a bigger variation in the perfusion estimated. There might be a heat loss through the probe housing, which was made of aluminum and the other source of loss was due to the tubes coming out of the test section to connect it to flowmeter. To eliminate all such experimental uncertainty a new compact test stand was designed which is discussed in the Chapter 3 in detail. The probe housing material was changed to Lexan to address the issue of heat loss from the metal housing. The research was further concentrated only for small probe, since it has an easy access to carry out experiments on rats and other animal models.

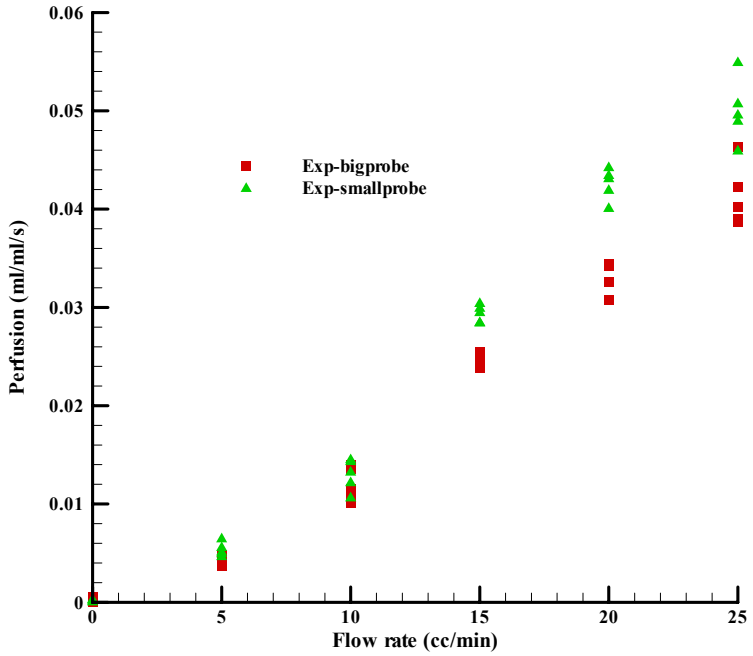

Figure 49: Repeatability test using the bottom entrance test stand for both big and small perfusion probe

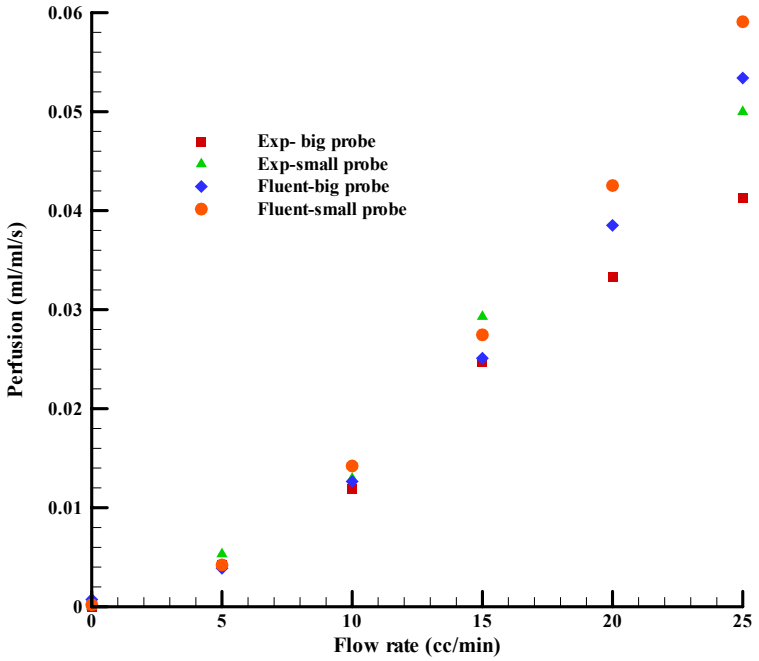

Figure 50: Comparison of experimental and CFD model perfusion estimates

Appendix F
CFD Model Development

In order to evaluate the phantom tissue test stand a computational fluid dynamics model of the test section was developed using Fluent. The domain of the model was set to 4 cm x 4 cm x 1.27 cm to match the experimental test section. The sponge in the experimental setup was modeled as porous media in Fluent. In Fluent the porous media is modeled by addition of a momentum term to the standard fluid flow equations. The source term is composed of two parts: a viscous term (Darcy), and an inertial loss term. This momentum sink contributes to the pressure gradient in the porous cell, creating a pressure drop that is proportional to the fluid velocity (or velocity squared) in the cell.

For porous media model two additional inputs are required by the Fluent, the inertial and viscous resistances. The inertial resistance for the present study is assumed to be negligible because we are dealing with low flow rates. The viscous resistance [50] is a function of the permeability, which in turn is a function of the porosity and the fiber diameter. The permeability of the porous matrix can be calculated using the equation shown below:

$$K = \varepsilon^2 D^2 / 150 (1- \varepsilon)^2 \quad [50] \qquad (F.1)$$

$$\text{Viscous Resistance} = 1/K \qquad (F.2)$$

where K is permeability, (m^2) ε is the porosity and D is the fiber diameter (m).

F.1 Initial Fluent Model without Heat Flux Gage

Figure 51 shows the very basic model initially constructed to mimic the non-directional flow of blood near the surface where heat flux was measured. The inlet of the model is the same as in the experimental test stand i.e. 6.35 mm (1/4") diameter at the bottom face of the sponge. The four sides of the sponge are modeled as constant pressure outlet boundary with gage pressure equal to zero. At the top of the sponge instead of the heat flux gage a convective boundary of equivalent area that of the sensor was imposed. Since the gage was 0.25 mm in thickness, there will be conduction through this thickness. Thermal conduction across the thickness of the heat flux gage was assumed to be 1-D in this model. To incorporate this, thermal resistance based on the thickness of the gage and the thermal conductivity was calculated and applied in the model instead of the gage itself. The bottom face of the tissue was modeled as insulated. The temperature gradient at the bottom face of the sponge is zero since the sponge is immersed in water which is maintained at constant temperature. The top face of the

sponge other then the convective boundary was modeled as insulated. The heat flux measured at ambient condition in the experimental setup without the thermal event is small and is removed as offset in the parameter estimation. Therefore, the assumption stands good and is also validation is discussed in Appendix H. The Reynolds number for the maximum flow rate of 30 cc/min is 100. Therefore, it takes only six diameters to get a fully developed flow at the inlet of the test section. Hence, a fully developed velocity profile was used in the Fluent model at the inlet.

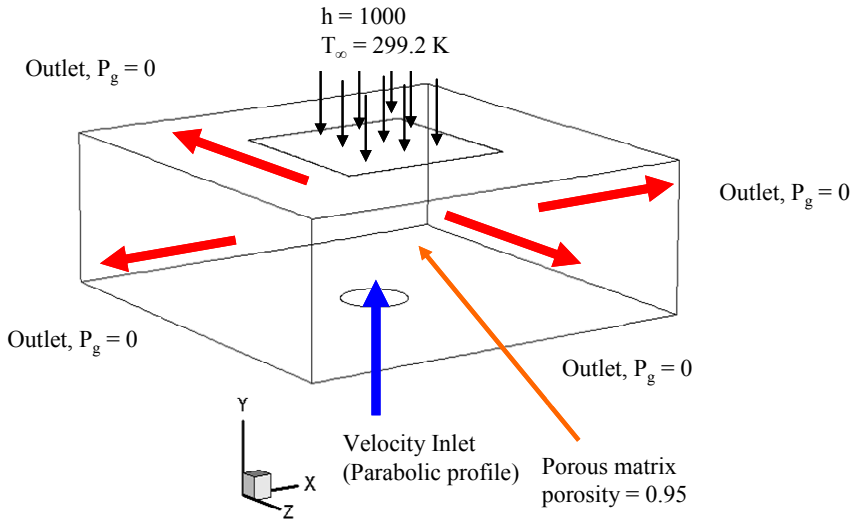

Figure 51: Initial Fluent model of phantom tissue test section

The heat flux data from the computational model, when the flow is induced in the porous matrix gives a direct comparison with the heat flux data resulting from the experiments. The perfusion for both heat flux results was estimated using parameter estimation routine developed. All the simulations were carried out for big probe with convective area of 285 mm^2. The experimental results are obtained from the bottom entrance test stand discussed in Appendix E. A good agreement between these three results will get the right value of absolute perfusion. By inducing flow inside the porous matrix, perfusion is introduced. Simulations were carried out for flow rates of 0-25 cc/min. The heat flux for the computational model corresponding to the velocity is shown in Figure 52. The heat flux response shows that it is sensitive to the flow. The heat flux comparison of CFD model and experimental results is shown in Figure 53 for 25 cc/min. The relative error with respect to experimental heat flux in the computational model is between 4- 8% for flow rates between 0 – 25 cc/min. The heat flux of the CFD model is in good comparison for first 15 seconds but after the slope

changes and is lower than the experimental results for the corresponding flow. The experimental data becomes flatter even before the CFD model at a higher magnitude, thus concluding the CFD model is underestimating the perfusion. Comparison of the experimental and CFD perfusion estimates is shown in the Figure 54. The experimental perfusion is the average of five sets of data for each flow rate. The CFD perfusion estimate closely follows the experimental data till 5 cc/min flow rate. For flow rate of 10 cc/min and up the differences in the perfusion between the experimental and CFD model keeps increasing. A better CFD model was built to address this issue, which is discussed in the next section.

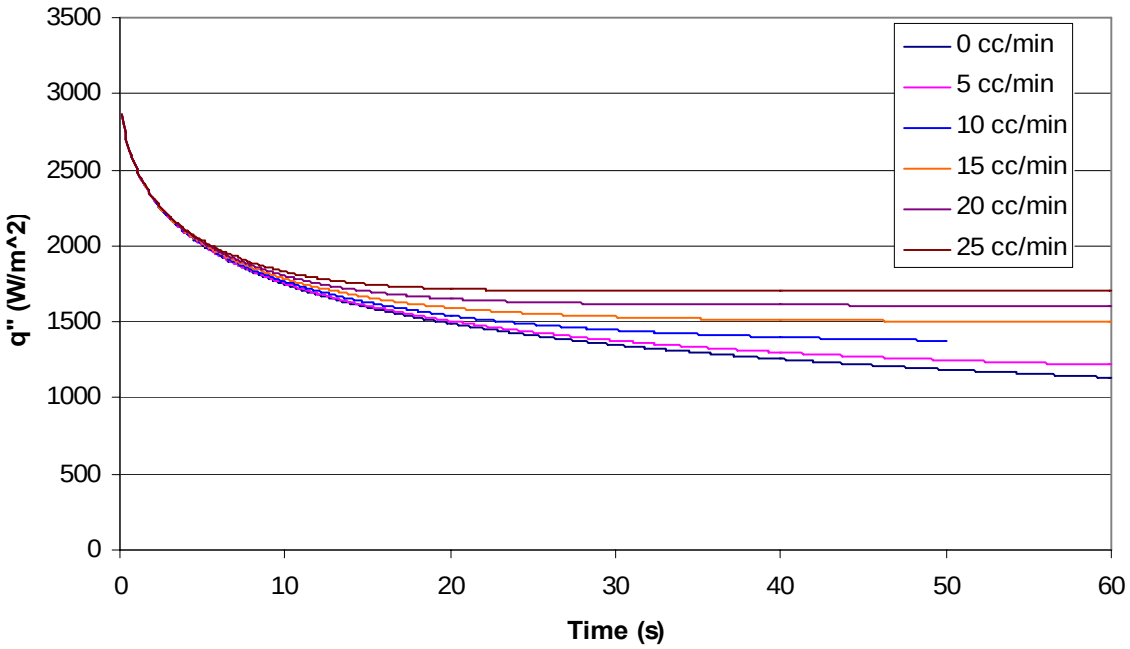

Figure 52: Computational heat flux curves for flow rate 0-25 cc/min

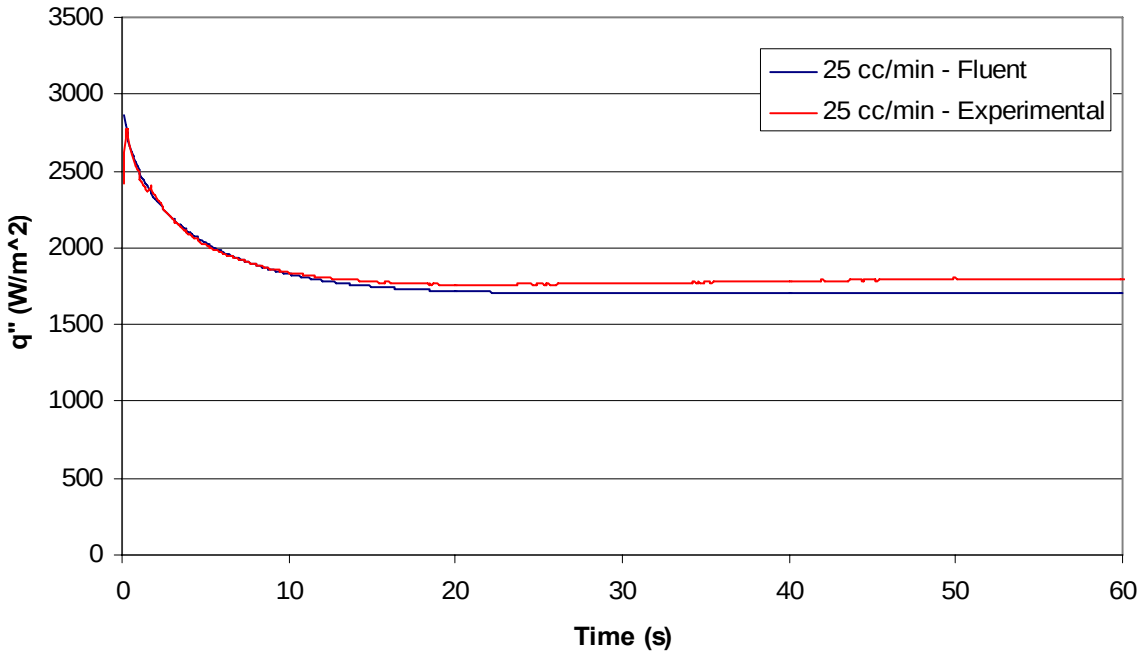

Figure 53: Experimental and computational heat flux comparison for 25 cc/min flow rate

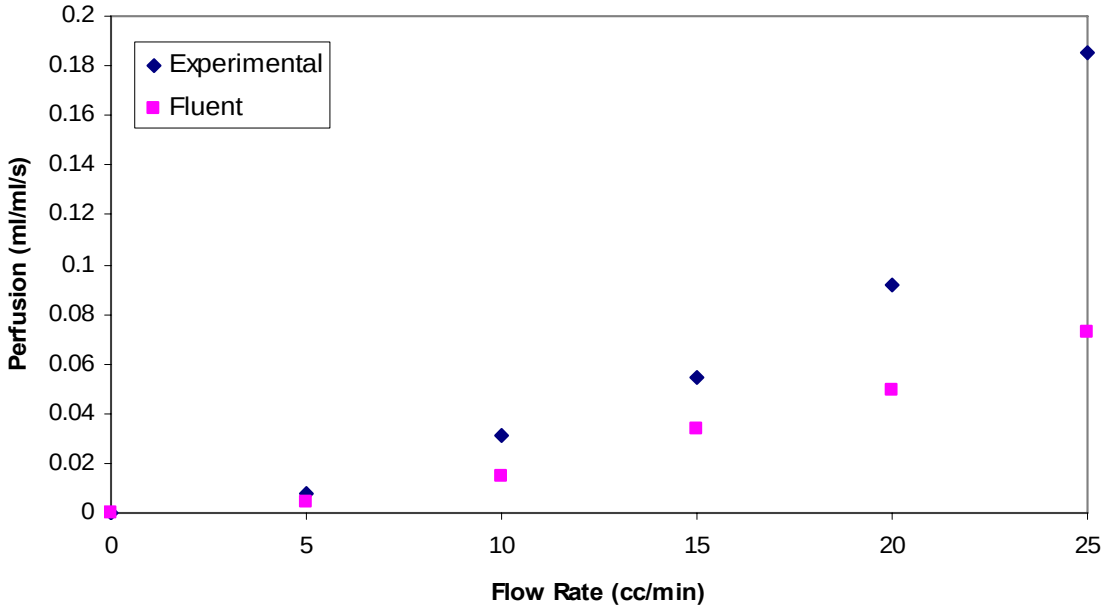

Figure 54: Comparison of experimental and computational perfusion estimates

F.2 Symmetric Model in Cartesian coordinate

The previous CFD model took about 12 hours on a dual processor workstation (3.06 GHz) with 4 GB of memory. The objective of the new model was to reduce the computational time and also to get good agreement between the experimental and computational results. A new computational model was built utilizing the advantage of the symmetric boundary condition. The computational domain was reduced to one quarter of the previous model thereby reducing the computational time drastically. Another modification included was incorporating the heat flux gage in the CFD model. The main reason for including the heat flux gage was because the way the actual gage measures heat flux. The gage is a thermopile and measures the heat flux based on the temperature difference between its two faces. The sensor is modeled as a solid with the thermal properties listed in Appendix A. The tissue was modeled as porous matrix similar to the previous model. The model was simulated for different flows from 0 – 25 cc/min with interval of 5 cc/min. This model took approximately 6 hours to solve the simulations at each flow rate. Figure 55 shows the symmetric model with stream traces at a typical flow of 15 cc/min. The properties of the tissue used are shown in the Table 7.

Table 7: Properties of tissue used in Fluent Model

Property	**Values**
Density	998.2 kg/ m^3
Specific Heat	4182 J/kg-K
Conductivity	0.5723 W/m-K
Viscosity	0.001 kg/m-s

The simulations were conducted using sensing area for both big and small sensor. Parameter estimation code was used predict the perfusion in both the experimental and CFD model. The results of this model are compared with experimental results and are shown in Figure 56. Both the experimental and CFD model results follows the same trend of increase in perfusion with the increase in flow rate. Also it is seen that the big probe predicts higher perfusion as compared to the small probe. Therefore, it can be concluded that with increase in the sensing area the perfusion increases. This gave confidence in the CFD model. The difference in perfusion between CFD model and experimental increases for flow

rates higher than 15 cc/min. To address this issue a new parameter estimation code was developed and is discussed in Appendix B.

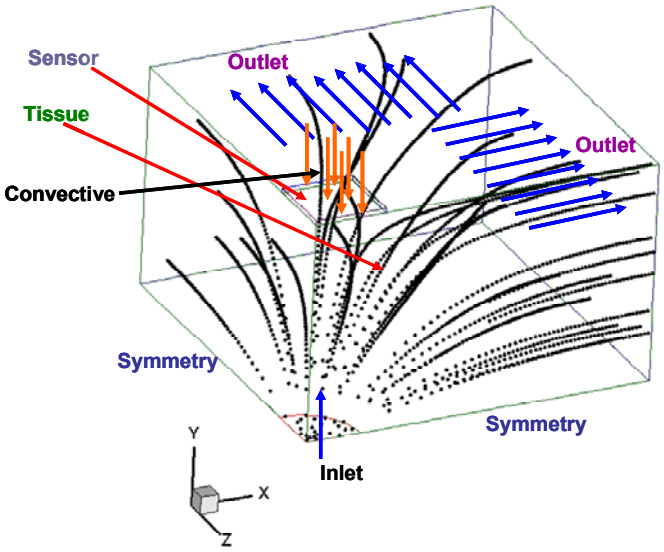

Figure 55: Fluent 3D model using symmetric boundaries

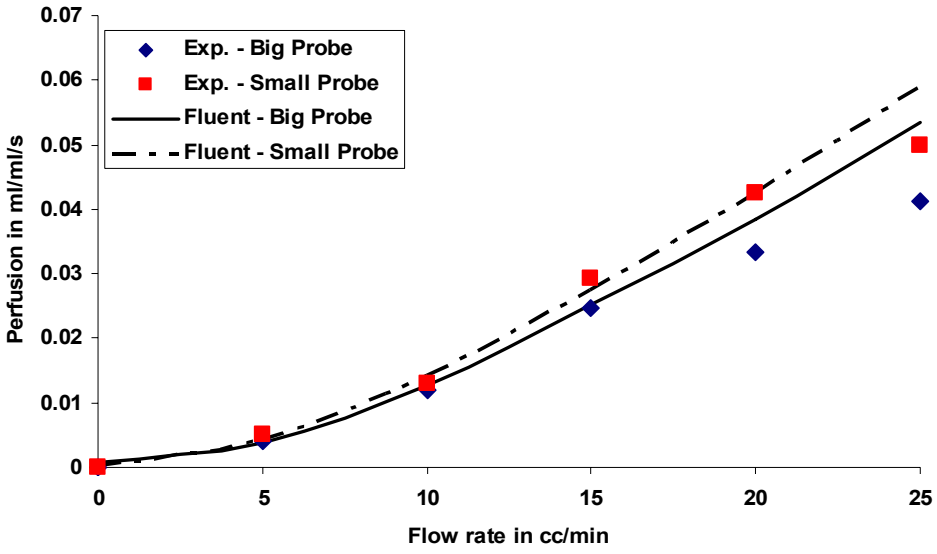

Figure 56: Comparison of symmetric CFD model with experimental results

F.3 Axis-symmetric Model

The finite-difference code in the new parameter estimation program takes approximately 2 to 3 minutes to process the data. So, a CFD model was developed exactly like the finite difference model with same number of cells (260 x 30). The new 2D axis-symmetric model reduced the computational time to just 10 minutes as compared to 6 hours for 3D model with same accuracy in estimating perfusion. This detail of model is discussed in chapter 3. The results of this model were in excellent agreement with that of the results from symmetric 3D model.

F.4 Symmetric Model in Cylindrical Coordinate

A 3D model in cylindrical model with sensing area only shown in Figure 57 was simulated to see if there is any difference in the Cartesian 3D model and cylindrical 3D model. This model was tested at 30 cc/min flow rate. Comparison of the perfusion estimated for 2D axis-symmetric, 3D Cartesian coordinate model and 3D cylindrical model is shown in Figure 58. There is very small difference in perfusion estimated for these three models and hence it is concluded that all these models yield same perfusion for the same convective area of the sensor

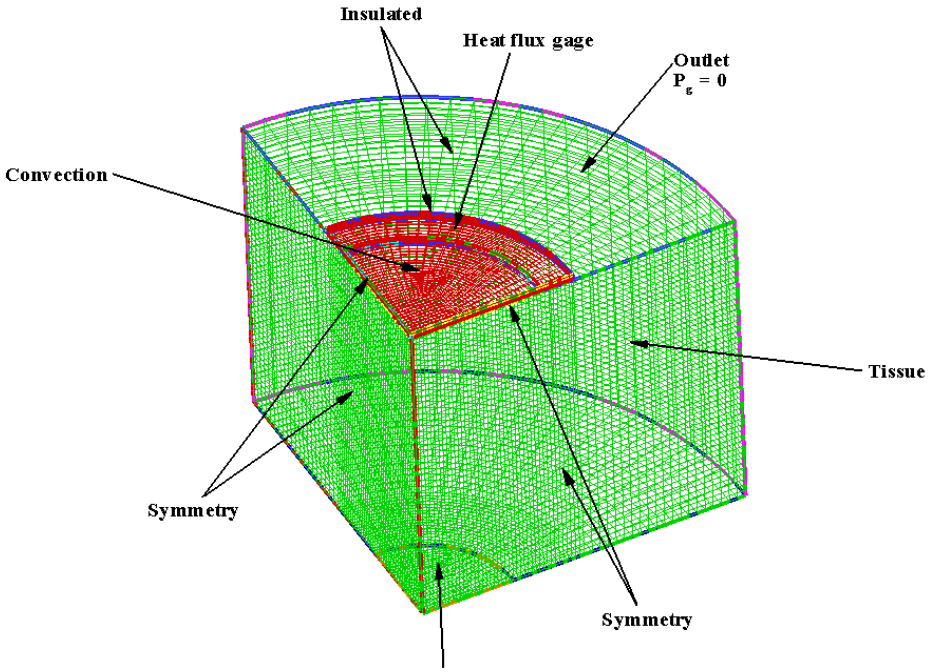

Figure 57: 3D model of tissue and sensor in cylindrical coordinate

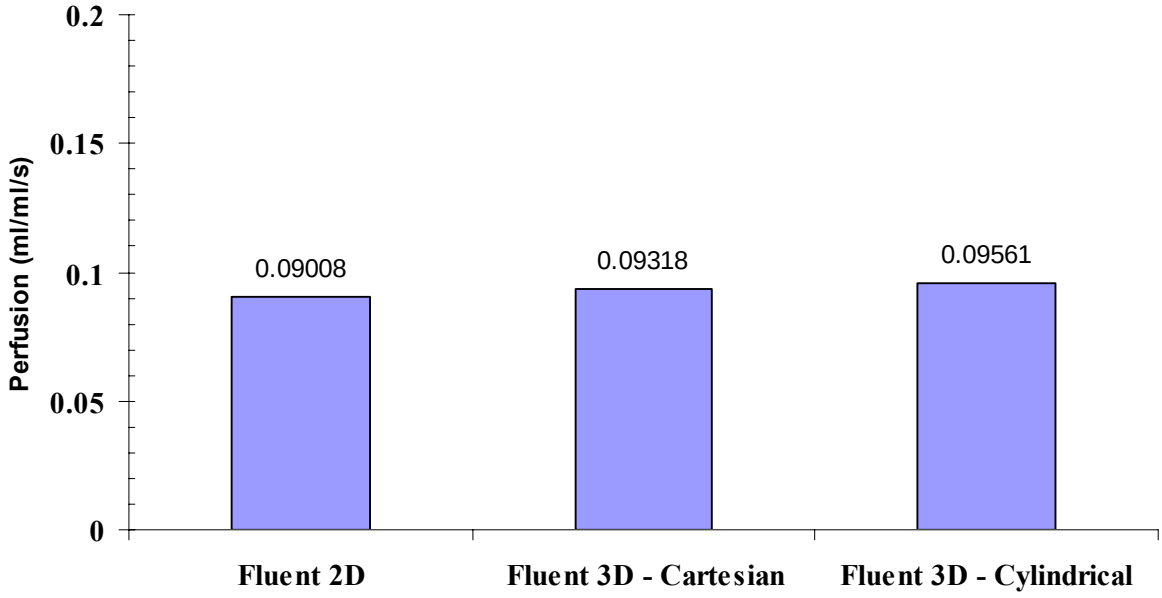

Figure 58: Comparison of perfusion estimated for Fluent 2D axis-symmetric, 3D Cartesian and 3D cylindrical model

F.5 Effect of Convective Area on Perfusion Estimates

The actual heat flux gage size is 10 mm × 10 mm and in the CFD model only the sensing area of the gage is modeled since it is only the thermopile area (57.4 mm^2) which measures the heat flux. To check the effects of the total gage area in the model, simulations were conducted both for 2D axis-symmetric and 3D models. In the actual probe, only the thermopile is exposed to the convection and the remaining area, which is just pc board material, is covered by the probe housing and there is no convection over that region. The heat flux from the model was measured over the sensing area of the gage only. The results of the perfusion with the gage area for both 2D and 3D model are shown in Figure 59. The perfusion estimates follow the same trend as with the model discussed with sensing area only, except that the estimated perfusion is higher when gage area is also modeled. This is also seen from the results of big probe and small probe perfusion estimates discussed in F.2. The 2D and 3D results are in good agreement, but the perfusion estimates are higher as compared to model when convection is only over the sensing area. Therefore, it can be concluded that an increase in the convection area will increase the perfusion estimate.

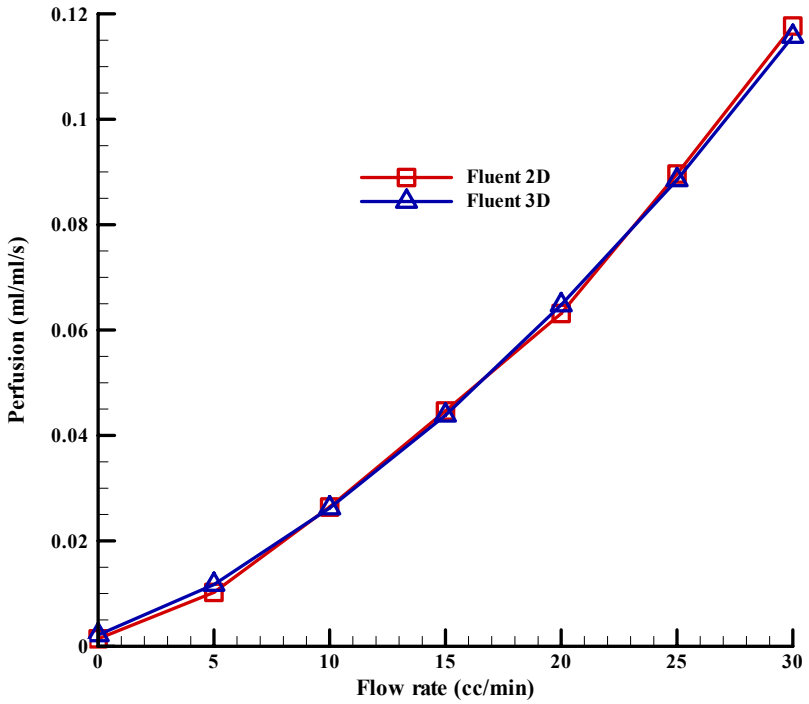

Figure 59: Perfusion estimates with convection over the whole gage area

F.6 Effect of Natural Convection on Heat Flux Response

The effect of natural convection in the model was also explored. Simulations were carried out at 0 cc/min, 5cc/min and 25 cc/min flow rate with two different porosities of 0% and 95% at steady state. The viscous resistance was calculated based on the equation F.1 and inertial resistance was set to zero. The Reynolds number for the maximum flow rate is 100, so the inertial effects are negligible that why the inertial resistance was set to zero. The effect of natural convection was suppressed due the presence of porous media. When this porosity was set to zero in the simulation the effect of natural convection was found to be dominant. Table 8 and Table 9 shows heat flux measured by the heat flux gage in the simulation for flow rates 0 cc/min, 5 cc/min and 25 cc/min.

Table 8: Effect of natural convection for porosity = 0%

Flow Rate cc/min	Heat flux (W/m^2) with natural convection	Heat flux (W/m^2) without natural convection
0	2046.7	656.8
5	2115.96	1146.2
25	2527.27	2519.4

Table 9: Effect of natural convection for porosity = 95%

Flow Rate cc/min	Heat flux (W/m^2) with natural convection	Heat flux (W/m^2) without natural convection
0	683.5	635.8
5	1121.6	1121.14
25	2525	2525

Appendix G
Sensitivity and Statistical Analysis

G.1: Sensitivity Analysis

In order to assess how a given input will affect the calculated perfusion from the bioheat transfer model, a sensitivity analysis of the parameters was performed. It is important to understand how sensitive the model is to the input parameters to determine which parameters most critically affect the output variables. To determine this sensitivity, a dimensionless sensitivity coefficient, X_i^+, was defined as:

$$X_i^+ = \frac{\delta \omega_i^+}{\delta \beta_i^+} = \frac{\Delta \omega_i^+}{\Delta \beta_i^+} \tag{G.1}$$

where $\Delta\omega_i^+$ is the dimensionless parameter of the difference of the perfusion for a nominal value and a perturbed value of the parameter, β. The difference of the nominal and perturbed parameter values are represented by $\Delta\beta_i^+$ and are calculated from equation G.2.

$$\Delta\beta_{Pi}^+ = \left|\frac{\Delta\beta_{Pi}}{\beta_{Ni}}\right| = \left|\frac{\beta_{Pi} - \beta_{Ni}}{\beta_{Ni}}\right| \tag{G.2}$$

In equatiom G.2 β_{Pi} and β_{Ni} represent the perturbed and nominal values of the parameter, β. For a 5% variation in the nominal parameter value, the above equation can be reduced as shown in equation G.3.

$$\Delta\beta_{Pi}^+ = \left|\frac{\beta_{Pi} - \beta_{Ni}}{\beta_{Ni}}\right| = \left|\frac{(\beta_{Ni} + 0.05\beta_{Ni}) - \beta_{Ni}}{\beta_{Ni}}\right| = \left|\frac{0.05\beta_{Ni}}{\beta_{Ni}}\right| = 0.05 \tag{G.3}$$

Equation G.3 states that $\Delta\beta_i^+$ respresents a variation of 5% in the nominal parameter value. The dimensionless perfusion, $\Delta\omega_i^+$ can be calculated as:

$$\Delta\omega_i^+ = \left| \frac{\omega_{Pi} - \omega_{Ni}}{\omega_{Ni}} \right| \qquad \text{(G.4)}$$

where ω''_{Pi} and ω''_{Ni} are the perfusion values for the perturbed and nominal parameter values, respectively. For this analysis, the heat flux curve was generated using $\omega = 0.085$ ml/ml/s and $R_c'' = 0.001$ m^2-K/W and other parameters with their nominal values are shown in Table 10. Table 10 shows the parameters that were studied and their corresponding nominal and perturbed values, for a 5% perturbation. Also shown are the corresponding perfusion estimated by the bioheat transfer model and the sensitivity coefficient defined in equation G.1. Figure 60 shows the dimensionless sensitivity coefficient for each of the parameters listed in the table. Specifically, the arterial and air temperatures were found to be the most sensitive parameters. The other dominant parameters are sensitive are then heat flux and the thermal conductivity of the tissue. Figure 61 shows the relative percentage change in perfusion with respect to the nominal perfusion values used for this analysis. As expected the arterial temperature and the air temperature which have the high sensitivity coefficient will have maximum change in the perfusion measure due to perturbation of 5% from the nominal values. The maximum change in the perfusion is 3.96% for the arterial temperature followed by air temperature with 3.35% change in the estimated perfusion. The other parameters show a small change in perfusion due to the perturbation caused.

Table 10: Summary of the sensitivity analysis

Parameters	Nominal Value	Perturbed Value (5%)	Sensitivity Coefficient
T_{air} (°C)	23.96	25.158	0.670588235
T_{art} (°C)	35.2	36.96	0.792941176
T_{init} (°C)	34.5	36.225	0.002352941
q'' (W/m^2)	1	1.05	0.272941176
h (W/m^2 -K)	1000	1050	0.021176471
C_{pt} (J/kg-K)	4182	4391.1	0.009411765
k_t (W/m-K)	0.5723	0.600915	0.254117647
C_{ps} (J/kg-K)	1340	1407	0.023529412
k_s (W/m-K)	0.25	0.2625	0.016470588
R_c (m^2-K / W)	0.001	0.00105	0.002352941

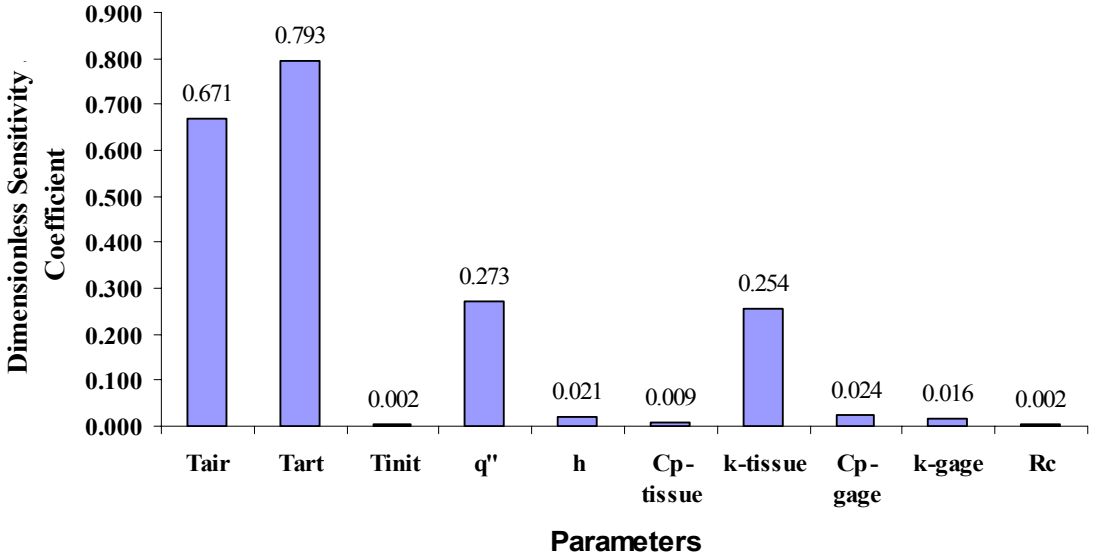

Figure 60: Dimensionless sensitivity coefficient for various parameters of the bioheat transfer model

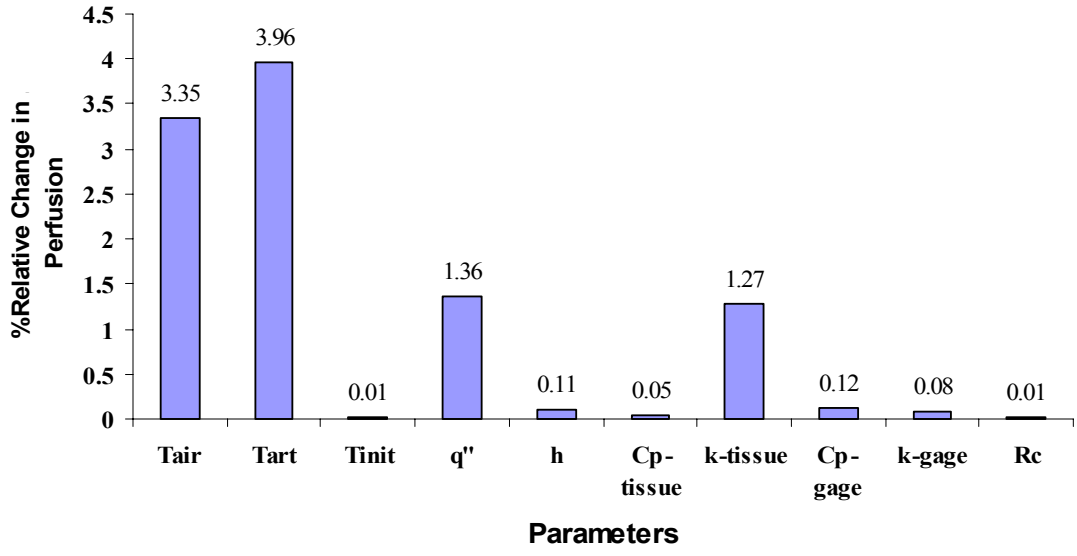

Figure 61: Percentage relative change in perfusion estimated due to perturbations with respect to the nominal perfusion value

G.2 Statistical Analysis

The *t* test is probably the simplest commonly used statistical procedure. To compare the mean of a continuous variable in two different populations, the difference between the two means divided by its standard deviation has a special distribution, known in this case as the "*t* distribution". This relationship also allows construction of confidence intervals for the difference in means, and these provide information about the mean difference and its variability. When the difference between the two means (the between groups variability) is large relative to its standard deviation (the random variability) the *t* test will be statistically significant. If there is a difference in means among three or more groups, Analysis of variance (ANOVA), generalizes the *t* test to several groups. Since there are more than two groups being compared, we have to look at more than just mean differences. The method for testing whether the mean level in all of the groups is the same follows a general pattern similar to that for the *t* test. The variance between groups summarizes the part of the total variability in the measures that can be explained by the assumption that the measurements come from different populations. The general test in the ANOVA model tests the null hypothesis that all of the group means are equal. Rejecting this hypothesis means that we believe that at least one difference of two means is not zero.

For the phantom tissue test the analysis of variance was carried out for perfusion and contact resistance to validate whether these estimates are statistically significant. Figure 62 shows results of ANOVA carried out on perfusion estimates. The statistical mean of perfusion estimate with 95% confidence intervals is plotted against the corresponding flow rate. The statistical mean for zero with confidence intervals is shown with vertical dashed lines. It is clear from the Figure that the statistical mean of all other flow rates are different from each other. Thus, the null hypothesis can be rejected. Therefore, the perfusion estimates are statistically significant and they are a function of flow rate. Similar analysis was carried out for the contact resistances shown in Figure 63. The vertical dashed lines indicate the 95% confidence intervals for the statistical mean of the contact resistance for a flow rate of 15 cc/min. Only one mean for the flow rate of 30 cc/min is statistically different from the rest of the flow rates. Therefore, the null hypothesis can be accepted as the mean are statistically same. This implies that the differences in contact resistance are statistically insignificant and therefore contact resistances are independent of the flow rates.

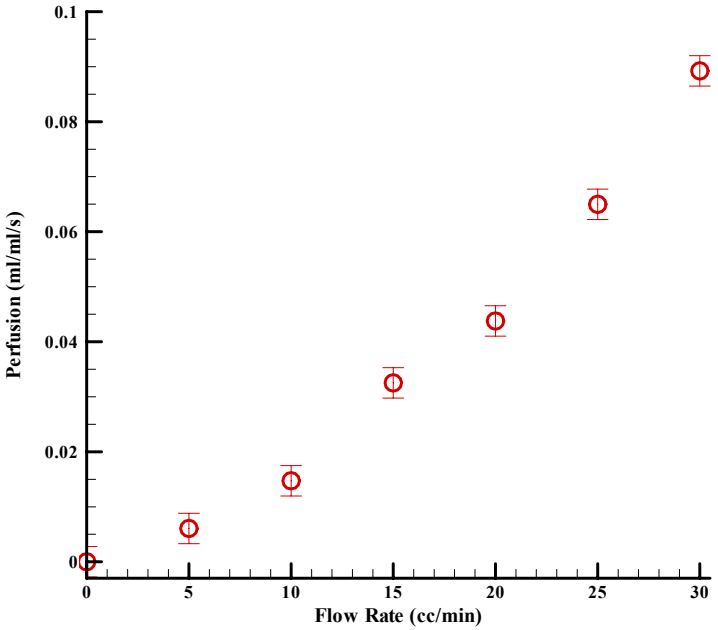

Figure 62: Statistical mean of estimated perfusion, ω, with 95% confidence intervals for different flowrates

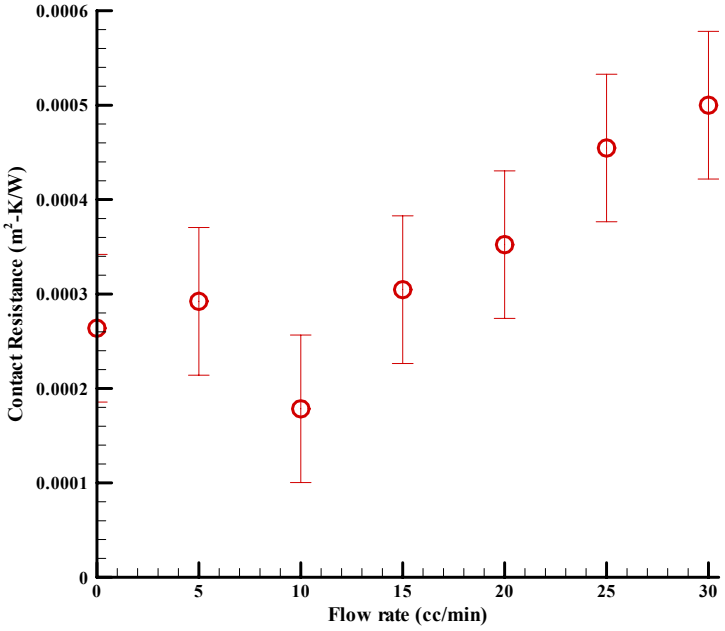

Figure 63: Statistical mean of estimated contact resistance, R_c", with 95% confidence intervals for different flow rates

Appendix H
Effects of Heat Transfer Coefficient

H.1 Effect of Heat Transfer Coefficient on Heat Flux Gage

The effect of the heat transfer coefficient is important because the heat flux response from the tissue is based on the thermal event imposed which is dependent on the heat transfer coefficient. The heat transfer coefficient was calculated from the calibration of the heat flux gage with the housing with microsensor. In the finite-difference model the top face of the sensor is modeled as convective boundary. To see how the parameter estimation model behaves for different values of convection coefficient, the 2D axis-symmetric model simulation was conducted at 15 cc/min for the convection coefficient values of 10^3, 10^4, 10^5, 10^6 and 10^{10} W/m^2-K respectively. The heat flux response measured by the gage in Fluent is shown in Figure 64. The heat flux for convection coefficient of 10^3 W/m^2-K is lower than for the other convection coefficient values. Also it can be seen that the heat flux for coefficient equal to or more than 10^4 W/m^2-K are identical. Therefore it can be concluded that the heat flux response is independent for convection coefficient more than 10^4 W/m^2-K. These heat fluxes were used in the parameter estimation program to estimate the perfusion values. Figure 65 shows the perfusion estimate for different values of the convection coefficient. The maximum difference in the perfusion is about 2.7% relative to the values obtained for 10^3 W/m^2-K. The perfusion estimate becomes almost constant after 10^4 W/m^2-K. This concludes that the parameter estimation program is robust and is independent of the magnitude of the heat flux. The parameter estimation is highly sensitive to the shape of the heat flux curve rather than the magnitude.

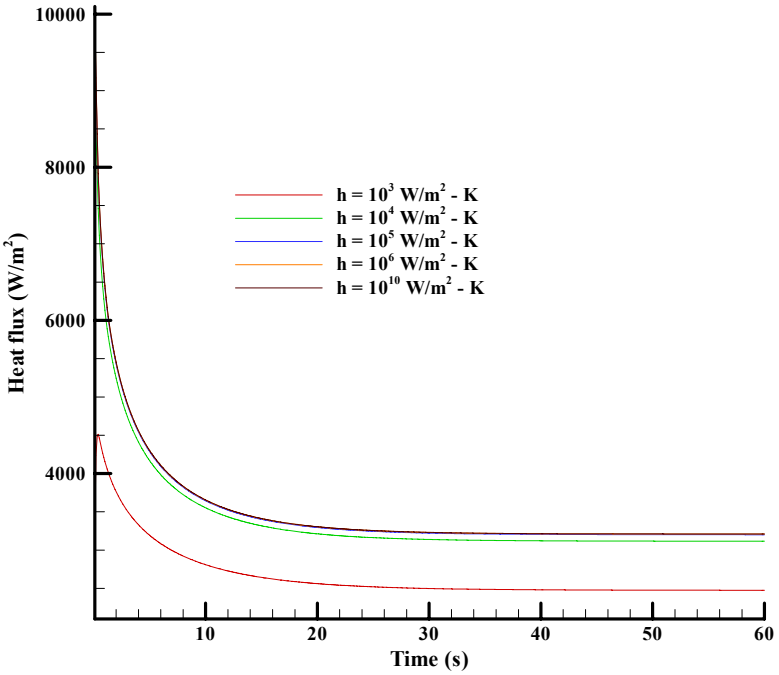

Figure 64: Heat flux response from 2D axis-symmetric flow model for different values of convection coefficient at 15 cc/min

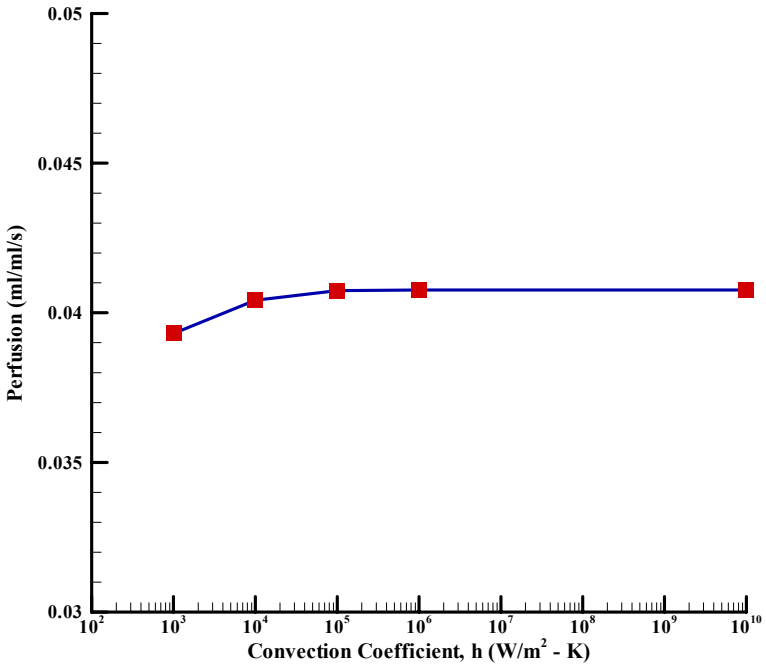

Figure 65: Perfusion estimates for different values of convection coefficient

H.2 Effect of Heat Transfer Coefficient of Tissue

The finite-difference model used in the parameter estimation routine assumes the top of the tissue which is exposed to ambient condition is an insulated boundary. To verify this assumption the top surface of the tissue, which is exposed to atmosphere, was modeled as convective boundary in the Fluent 2D axis-symmetric model with convection coefficient 10 W/m^2-K and ambient temperature 27 °C. The model was simulated for flow of 15 cc/min. The heat flux measured was compared with the case when the top tissue surface modeled as insulated boundary. The heat comparison of the heat flux is shown in the Figure 66. It is evident from the figure that the heat flux is not affected by change in the boundary and therefore implies that the assumption of insulated boundary at the top tissue surface stands good.

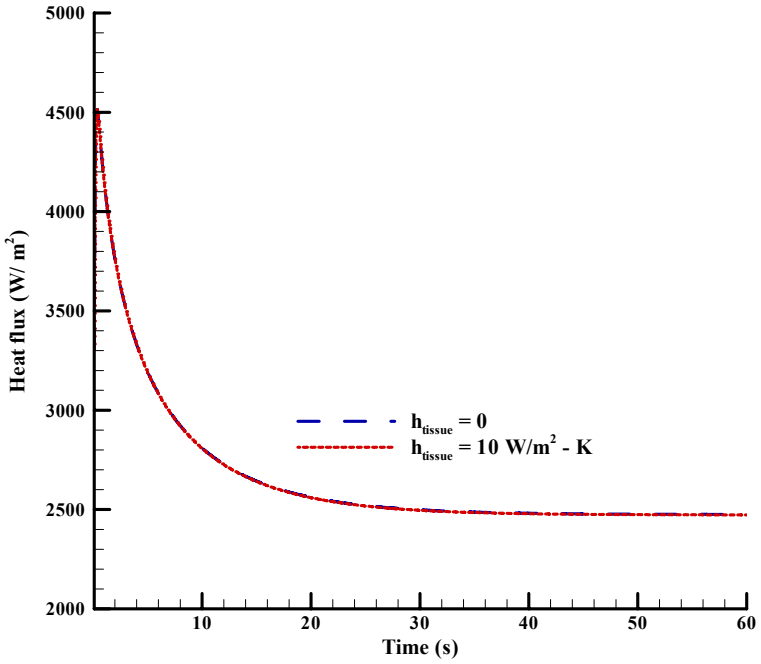

Figure 66: Effect of change in boundary condition on the top surface of the tissue exposed to ambient condition

Appendix I

Porosity and Viscous Resistance Calculation

The porous matrix in Fluent was assumed to be 95% porous. The porosity of the sponge was estimated approximately on the wet and dry weight of the sponge. Porosity is defined as the ratio of volume of void to the total volume. In order to estimates the porosity of the test specimen (sponge), the volume of the void is needs to be measured. First the dry weight of the sponge is measured and recorded (W_d).To calculate the volume of the void, the sponge is saturated with water so that the void gets filled with water and we can measure the volume of the water retained in the sponge. The water retained in the sponge is measured by squeezing out the water from the sponge (V_{wo}). Still some of the water is retained in the sponge as moisture; to calculate this moist weight (W_m) of the sponge is recorded. The volume of the water absorbed in sponge (V_m) as moisture is calculated by dividing the difference between the moist and dry weight of the sponge by the density of the water. Therefore the total volume of water absorbed is sum of the V_{wo} and V_m. The total volume (V_t) of the sponge can be calculated by knowing the sponge dimensions. The porosity can be estimated as the ratio of the total volume of water to the total volume of the sponge. The procedure for porosity estimation calculation is shown below

Total volume of the sponge = V_t

Dry weight of the sponge = W_d

Volume of the water squeezed out = V_{wo}

Moist weight of the sponge = W_m

Volume of water in sponge after squeezing out = $(W_m - W_d)$/Density of water = V_m

Porosity = $(V_{wo} + V_m)/ V_t$

The porous media in Fluent is modeled by addition of a momentum term to the standard fluid flow equations. The momentum source term is composed of two parts, a viscous loss term (Darcy), and an inertial term. This momentum sink contributes to the pressure gradient in the porous cell term, creating a pressure drop that is proportional to the fluid velocity (or velocity squared) in the cell. The

inertial and viscous resistances are required to run the Fluent model correctly. Since the maximum Reynolds number is 100 for the current work the inertial resistance can be assumed to be negligible.

To calculate the viscous resistance static pressure at the center inlet was measured using a U-tube manometer shown in the Figure 67. The viscous resistance initially used in the model (1.75×10^9 m^{-2}) was calculated from equation F.2 and it was adjusted from there to get the static pressure at the center equal to that of the experimental data. The static pressure is linearly proportional with $R^2 = 0.9962$ to the inlet flow rate. The new viscous resistance for which Fluent gave the static pressure at the center of the inlet equal to that of the experimental values was found out to be 1.18×10^9 m^{-2}. The static pressure from the Fluent model for flow rate of 5 cc/min and 25 cc/min are in good agreement with the correlation obtained from the experimental results. The static pressure distribution across the thickness of the sponge is shown in Figure 68. This ensures that the pressure distribution in the Fluent model is same as that of experimental setup.

Since the viscous resistance was changed by 48.3% simulation was carried out to check its effects on the heat flux measured. Figure 69 shows the comparison of heat flux curve at 5 cc/min flow rate with both old and new viscous resistances values. The heat flux for both the viscous resistances is in excellent agreement with each other. The heat flux measured is independent of the change in viscous resistances, and it only changes the pressure distribution in the tissue.

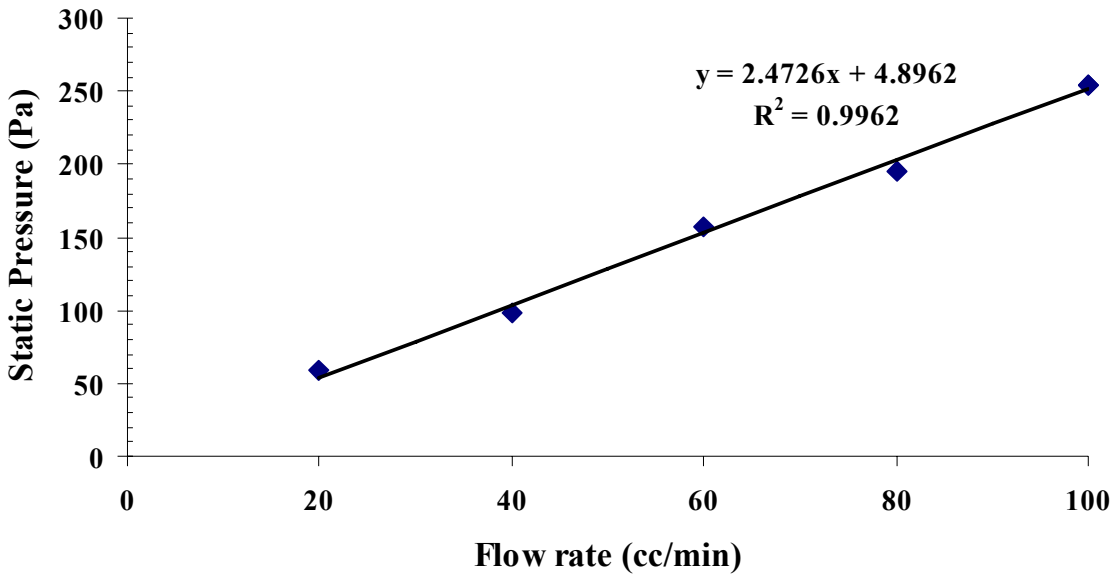

Figure 67: Experimental static pressure measurement for different flow rates

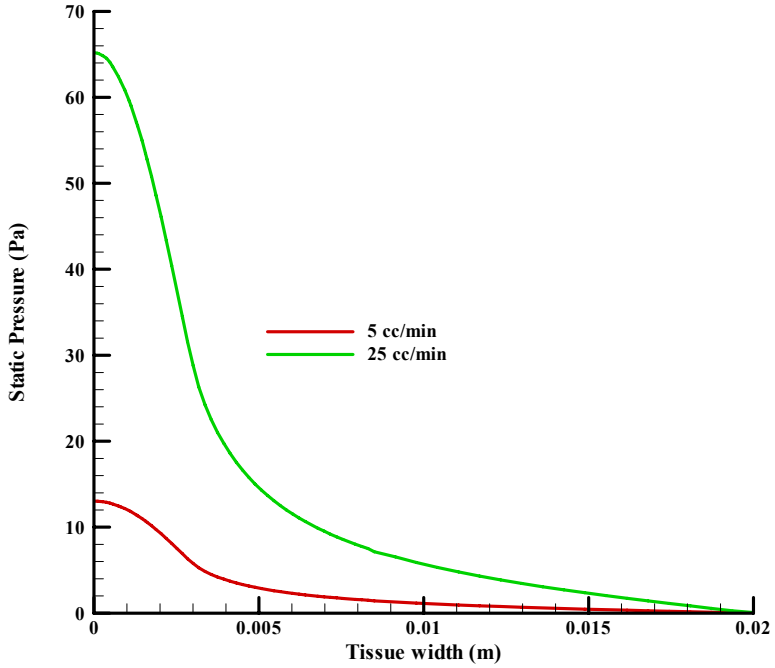

Figure 68: Static pressure distribution for the new viscous resistance calculated for 5 cc/min and 25 cc/min flow rate

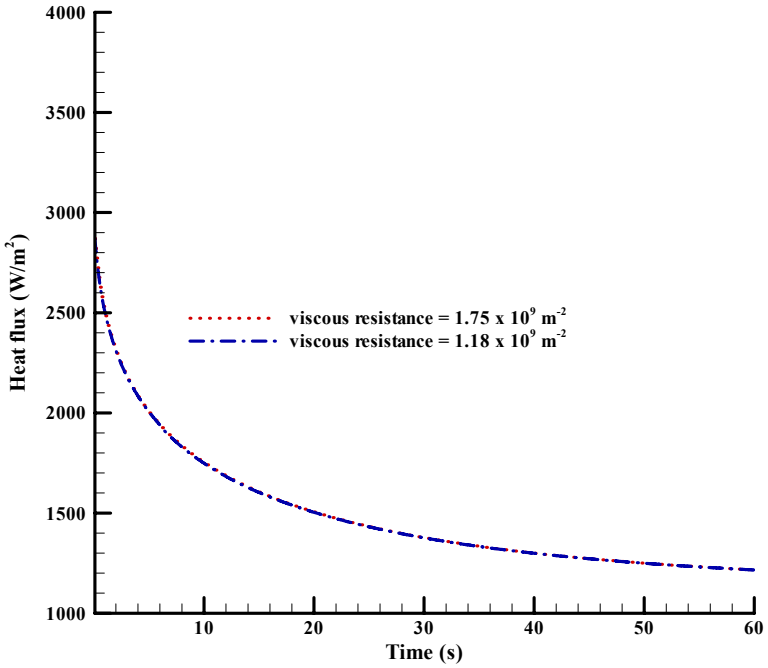

Figure 69: Comparison of heat flux for change in viscous resistance

Appendix J

Laser Doppler Flowmetry Tests

Laser Doppler Flowmetry was used to validate the performance of the convective perfusion probe. A Vasamedics BPM^2 blood perfusion monitor was used to measure noninvasively the blood perfusion on the epidermal surface of the rat in real time using advanced laser and fiber optics technology is shown in Figure 70. A low power beam of laser light is delivered to the sample tissue being monitored via a fiber optic capable, which illuminates a volume of tissue in which there are both moving red blood cells as well as stationary tissue cells. Light energy, in the form of photons, is randomly scattered by both cell types. Photons scattered by the moving red blood cells are Doppler shifted in frequency while photons scattered by non-moving cells are not. A portion of the entire scattered laser light is collected by receiving optical fibers and returned to the photodetector located within the BPM^2. The photodetector converts this light into an electronic signal which the BPM^2 processes using digital technology to determine blood flow, volume and velocity.

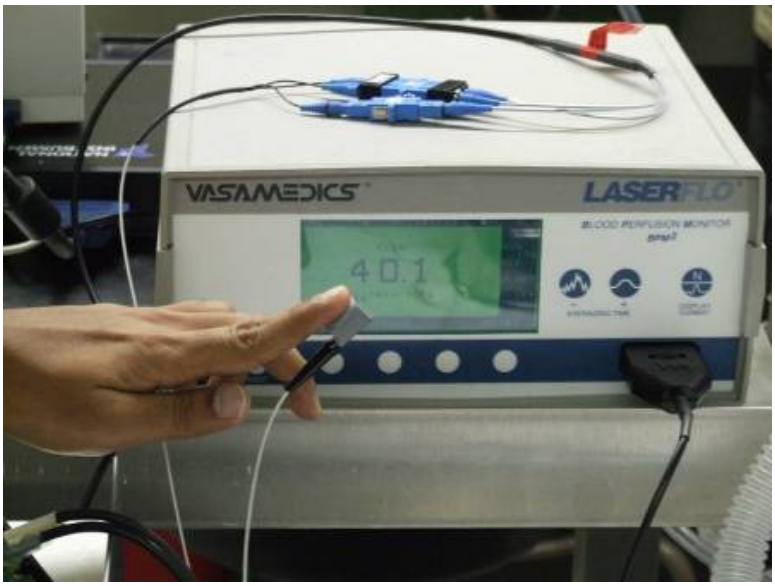

Figure 70: BPM^2 LDF blood perfusion monitor in operation

Tests were carried out for two different probe positions setup. In the first setup the two probes i.e. the LDF probe and the convective perfusion probe, were placed on the chest and on the stomach

respectively. The LDF probe was placed on the skin near the chest region and the convective perfusion probe was placed over the tummy and nine tests were carried out. In the second setup both the probes were place adjacent to each other over the abdomen and six tests were carried out. The picture of the second setup is shown in the Figure 71.

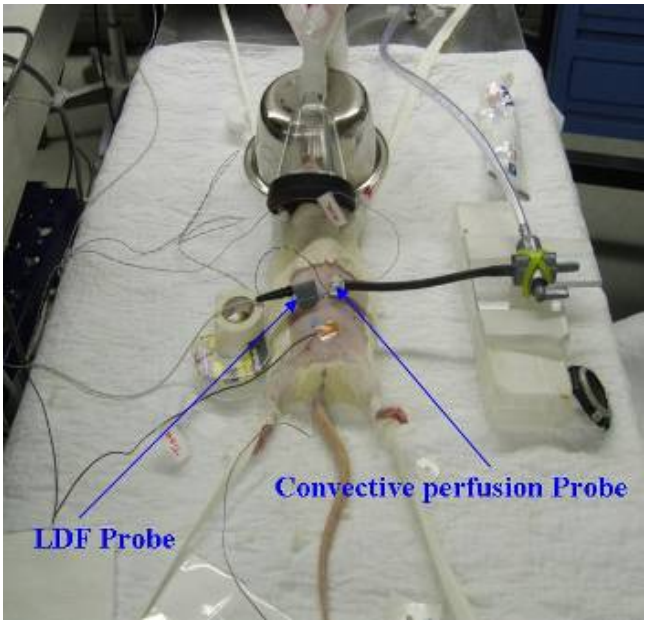

Figure 71: Convective perfusion probe and LDF probe test setup on the epidermal surface of the rat

Figure 72 shows comparison between the LDF and convective perfusion probe results. The probe estimates and the LDF measurements do not correlate with each other. Since the LDF measures red blood cell flux and not perfusion it is difficult to correlate with estimates from the probe. Also the perfusion was measured at different location hence nothing can be concluded from the results obtained for the first setup. To address the problems of correlating the performance of the first setup, experiments were carried out for the second setup as explained before. The results of the second setup are shown in Figure 73. The perfusion estimated from the convective probe shows similar trend to that of the LDF measurements. These results are inconclusive as the LDF measurements are relative as compared to absolute measurements from the convective perfusion probes.

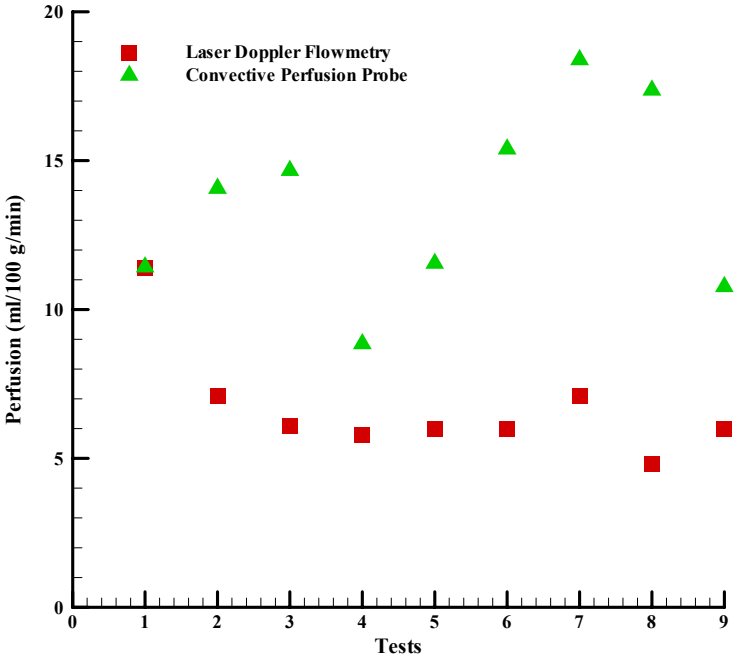

Figure 72: Comparison of LDF and convective probe perfusion estimates when both the probes are placed apart

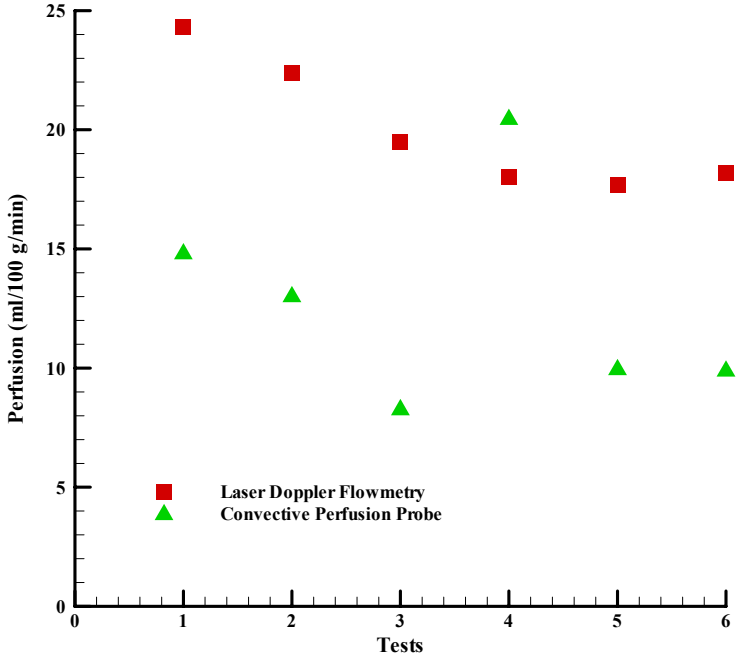

Figure 73: Comparison of LDF and convective probe perfusion estimates when both the probes are placed adjacent to each other

Appendix K

Results from Phantom Tissue, Animal model and Fluent simulations

Table 11: Results of Day 1 Perfusion estimates and Temperatures

Flow rate	Perfusion	CR	Ssy	Tref	Ta	Ttop	Tskin
cc/min	ml/ml/s	m^2-K/W		°C	°C	°C	°C
0	9E-05	0.00071	0.22865	25	35	34	33.9
0	0.00048	0.00077	0.27226	25	34.9	33.9	33.8
0	1E-04	0.00081	0.10398	25	35.1	34	33.9
0	0.00017	0.00078	0.12594	25	35.1	34.1	34
0	-0.00085	0.0008	0.1237	25	34.9	33.9	33.4
5	0.00848	0.00063	0.05888	24.9	35	34.3	34
5	0.00717	0.00075	0.0419	24.9	35.4	34.4	34.1
5	0.00767	0.00065	0.08954	24.9	35	34.2	34
5	0.00741	0.00074	0.07562	24.9	35.2	34.3	34
5	0.00817	0.00074	0.05161	24.9	35.3	34.3	34
10	0.01605	0.00045	0.10623	25	35.3	34.7	34.2
10	0.01423	0.00058	0.2005	25	35.4	34.7	34.2
10	0.01617	0.00057	0.16423	25	35.3	34.6	34.2
10	0.01572	0.00047	0.11528	25	35.5	35.1	34.7
10	0.01597	0.00056	0.0913	25	35.4	34.7	34.2
15	0.03026	0.00064	0.19586	24.8	35.4	34.9	34.5
15	0.03003	0.00066	0.25626	24.9	35.5	34.9	34.5
15	0.03103	0.00069	0.1955	24.9	35.4	34.8	34.4
15	0.03182	0.00066	0.11672	24.9	35.4	34.8	34.4
15	0.03137	0.00072	0.22435	24.9	35.4	34.7	34.3
20	0.04179	0.0007	0.35887	24.8	35.2	34.8	34.5
20	0.04201	0.00072	0.27648	24.8	35.3	34.8	34.5
20	0.04104	0.0007	0.22317	24.9	35.3	34.8	34.5
20	0.0416	0.00069	0.36718	24.9	35.3	34.7	34.4
20	0.04393	0.00078	0.43	24.9	35.3	34.7	34.4
25	0.06113	0.00082	0.15655	24.8	35.3	34.8	34.4
25	0.06027	0.00083	0.19632	24.8	35.3	34.7	34.4
25	0.06477	0.00084	0.26667	24.8	35.2	34.7	34.4
25	0.06182	0.00077	0.23347	24.8	35.1	34.7	34.4
25	0.05932	0.00078	0.21747	24.8	35.2	34.7	34.4
30	0.08079	0.0007	1.78326	24.9	35.3	35	34.7
30	0.08405	0.00078	0.29617	24.9	35.2	34.9	34.6
30	0.07967	0.00075	0.32856	24.9	35.2	34.9	34.6
30	0.07615	0.00073	0.83335	24.9	35.2	34.8	34.5
30	0.08831	0.00085	0.76038	24.9	35.2	34.8	34.5

Table 12: Results of Day 2 Perfusion estimates and Temperatures

Flow rate	Perfusion	CR	Ssy	Tref	Ta	Ttop	Tskin
cc/min	ml/ml/s	m^2-K/W		°C	°C	°C	°C
0	-0.00013	0.00025	0.22554	26.6	35.1	34.6	34.3
0	1E-05	0.00028	0.33822	26.7	35.2	34.6	34.3
0	0.00012	0.00031	0.19009	26.7	35.2	34.6	34.3
5	0.00742	0.00026	0.3234	26.6	35.4	34.6	34.3
5	0.00407	0.00022	1.59376	26.6	35.4	34.6	34.3
5	0.007	0.0003	0.23572	26.6	35.4	34.5	34.3
10	0.01643	0.00019	0.33919	26.6	35.4	34.8	34.6
10	0.01721	0.00026	0.43095	26.6	35.3	34.7	34.5
10	0.01569	0.00023	0.28548	26.6	35.4	34.7	34.5
15	0.03286	0.00036	0.63963	26.6	35.4	34.9	34.6
15	0.03326	0.00039	0.42709	26.6	35.4	34.8	34.5
15	0.03148	0.00032	0.48787	26.6	35.3	34.8	34.6
20	0.03964	0.00034	0.65965	26.5	35.3	34.8	34.6
20	0.04644	0.00047	0.6873	26.5	35.3	34.8	34.5
20	0.04103	0.00037	0.47938	26.5	35.3	34.9	34.6
25	0.06447	0.00052	0.96602	26.5	35.2	34.7	34.5
25	0.06143	0.00045	1.16472	26.5	35.2	34.7	34.5
25	0.06322	0.0005	0.59478	26.5	35.2	34.8	34.6
30	0.08014	0.00051	1.59902	26.4	35	34.6	34.4
30	0.08655	0.00064	0.78477	26.4	35.1	34.7	34.4
30	0.09007	0.00055	1.29347	26.5	35.1	34.7	34.5

Table 13: Results of Day 2 Perfusion estimates and Temperatures

Flow rate	Perfusion	CR	Ssy	Tref	Ta	Ttop	Tskin
cc/min	ml/ml/s	m^2-K/W		°C	°C	°C	°C
0	-0.00108	0.00027	0.83141	26.7	35.4	34.5	34.6
0	3E-05	0.00025	0.29198	26.8	35.3	34.6	34.7
0	0.00032	0.00031	0.34742	26.8	35.2	34.5	34.6
0	0.00115	0.00027	0.16955	26.7	35.2	34.6	34.7
0	-0.0004	0.00031	0.20292	26.8	35.2	34.5	34.6
5	0.00611	0.0003	0.34698	26.7	35.6	34.5	34.7
5	0.00455	0.00042	0.73444	26.7	35.6	34.4	34.7
5	0.00222	0.0004	0.31762	26.7	35.6	34.5	34.8
5	0.00529	0.00026	0.55304	26.7	35.6	34.5	34.8
5	0.00329	0.00027	0.45605	26.7	35.5	34.5	34.8
10	0.0137	0.00009	0.65784	26.7	35.5	34.5	34.9
10	0.01259	0.00008	0.50768	26.7	35.5	34.6	35
10	0.01371	0.00013	0.32502	26.7	35.5	34.5	34.9
10	0.01231	0.00009	1.34566	26.7	35.5	34.6	34.9
10	0.01173	0.00011	1.11598	26.7	35.5	34.6	35
15	0.03106	0.00008	1.36644	26.7	35.5	34.6	35
15	0.03734	0.00019	0.25646	26.7	35.5	34.6	35
15	0.03554	0.00017	1.0578	26.7	35.5	34.6	35
15	0.03464	0.00018	0.61734	26.7	35.5	34.7	35
15	0.03219	0.00017	1.11801	26.7	35.5	34.7	35
20	0.05015	0.00026	1.38073	26.6	35.4	34.7	35.1
20	0.04155	0.00007	1.36197	26.6	35.4	34.7	35.1
20	0.05677	0.00023	8.85487	26.6	35.4	34.7	35.1
20	0.04045	0.00011	4.30407	26.7	35.4	34.8	35.2
20	0.04268	0.00015	1.13584	26.7	35.4	34.7	35
25	0.07763	0.00033	1.86294	26.7	35.5	35	35.3
25	0.06985	0.00029	1.08353	26.7	35.5	34.9	35.3
25	0.07307	0.00032	1.95205	26.6	35.5	34.8	35.1
25	0.05949	0.00011	1.32355	26.6	35.5	34.8	35.1
25	0.06831	0.00021	1.25771	26.6	35.5	34.8	35.1
30	0.10084	0.00025	11.252	26.6	35.4	34.7	35
30	0.10613	0.00035	4.35579	26.7	35.4	34.7	35
30	0.09215	0.00025	11.55938	26.6	35.4	34.8	35.1
30	0.09884	0.00034	1.12851	26.6	35.4	34.8	35.1
30	0.09646	0.00029	1.74487	26.7	35.5	34.8	35.1

Table 14: Isolated Tests Perfusion Estimates and Temperatures

Flow rate	Perfusion	CR	Ssy	Tref	Ta	Tskin
cc/min	ml/ml/s	m^2-K/W		°C	°C	°C
0	-0.00023	0.00164	0.76368	22.4	37.9	35.5
0	0.00024	0.00219	0.12747	22.4	37.9	34.4
5	0.00524	0.00125	0.20677	22.3	37.9	37.2
5	0.00429	0.00155	0.03574	22.3	37.9	37.1
5	0.00497	0.00142	0.06667	22.4	37.9	36.9
10	0.01175	0.00082	0.49153	22.3	37.9	37.6
10	0.0114	0.00082	0.22955	22.2	37.9	37.5
15	0.02074	0.00052	0.88203	22.2	37.9	36.5
15	0.02209	0.00064	0.22139	22.2	37.9	37.4
15	0.02002	0.00036	0.11139	22.2	37.9	37.4
15	0.01541	0.00055	0.20933	22.2	37.9	37.4
20	0.02164	0.00061	0.21519	22.4	37.9	37.1
20	0.0243	0.00066	0.16437	22.3	37.9	37.1
20	0.02138	0.00059	1.41836	22.3	37.9	37.3

Table 15: Exposed Kidney Tests Perfusion Estimates and Temperatures

Test	Perfusion	CR	Ssy	Tref	Ta	Tskin
Nos	ml/ml/s	m^2-K/W		°C	°C	°C
1	0.00784	0.00011	402.5102	23.8	34.9	35.1
2	0.00825	0.00042	311.7182	23.7	34.7	34.8
3	0.00882	0	329.1466	24	34.7	34.7
4	0.00198	0.00007	422.8492	24	34.7	34.7
5	0.01274	0.00004	313.3717	24	34.7	34.4
6	1E-05	0.00054	291.6142	24	34.7	34.3
7	0.01203	0.00031	350.3824	24	34.6	33.7
8	-0.00199	0.00115	370.3823	24.1	34.2	33.4
9	0.01478	0.00016	390.2858	24.1	34.1	32.8

Table 16: Fluent 2D Axis-Symmetric Flow Model Perfusion Estimates and Temperatures

Flow rate	Perfusion	CR	Ssy	Tair	Ta	Ttop	Tskin
cc/min	ml/ml/s	m^2-K/W		°C	°C	°C	°C
0	0.00043	0.00069	0.05372	23.96	34.9	34.9	34.9
5	0.00567	0.00074	0.0878	23.96	34.9	34.9	34.9
10	0.01849	0.00081	0.73458	23.96	34.9	34.9	34.9
15	0.03475	0.00087	1.17368	23.96	34.9	34.9	34.9
20	0.05238	0.0009	1.16862	23.96	34.9	34.9	34.9
25	0.07094	0.00092	0.97147	23.96	34.9	34.9	34.9
30	0.09008	0.00093	0.75208	23.96	34.9	34.9	34.9

Table 17: Fluent 3D Flow model Perfusion Estimates and Temperatures

Flow rate	Perfusion	CR	Ssy	Tair	Ta	Ttop	Tskin
cc/min	ml/ml/s	m^2-K/W		°C	°C	°C	°C
0	0.00031	0.00082	0.25988	23	35	34.5	34.5
5	0.00502	0.00079	0.3418	23	35	34.5	34.5
10	0.01727	0.00096	0.50222	23	35	34.5	34.5
15	0.03357	0.00111	2.61503	23	35	34.5	34.5
20	0.05104	0.00115	3.12056	23	35	34.5	34.5
25	0.07121	0.00118	2.95719	23	35	34.5	34.5
30	0.09318	0.0012	2.69945	23	35	34.5	34.5

Table 18: Fluent 2D Axis-Symmetric Pennes Model Perfusion Estimates and Temperatures

Perfusion in	Perfusion out	CR	Ssy	Tair	Ta	Ttop	Tskin
ml/ml/s	ml/ml/s	m^2-K/W		°C	°C	°C	°C
0.00043	0.00079	0.00069	0.0538	23.96	34.9	34.9	34.9
0.00567	0.00533	0.0007	0.04327	23.96	34.9	34.9	34.9
0.01849	0.01864	0.00052	0.1177	23.96	34.9	34.9	34.9
0.03475	0.03328	0.00058	0.07308	23.96	34.9	34.9	34.9
0.05238	0.04912	0.00062	0.04254	23.96	34.9	34.9	34.9
0.07094	0.06577	0.00065	0.02369	23.96	34.9	34.9	34.9
0.09008	0.08293	0.00067	0.01283	23.96	34.9	34.9	34.9

Appendix L

Steady State Analytical Solution for 1D Model of Phantom tissue

The analytical solution for steady-state Pennes bioheat equation was solved to get an idea of the thermal penetration when the heat flux response from the tissue reaches steady state after the thermal event. The temperature of the surface of the gage can be measured at steady state by adding the thermal resistance to the solution.

$k_t \nabla^2 T_t = (\rho C_p \omega)(T_t - T_a)$

Let $B^2 = (\rho C_p \omega)/ k_t$

For 1D model the above equation can be written as

$d^2T/dy^2 = B^2 (T_t - T_a)$

$d^2T/dy^2 - B^2 T_t = B^2 T_a$

The above equation is second order differential non-homogeneous equation with constant coefficients

The characteristic solution is

$T_C (y) = C_1 e^{By} + C_2 e^{-By}$

And the particular solution is

$T_p (y) = T_1 (y) V_1 + T_2 (y) V_2$

$C_1 \rightarrow 0$ and $C_2 = h(T_\infty - T_a)/(h + k_t B)$

$V_1 = T_a/2 * e^{-By}$ and $V_2 = T_a/2\, e^{By}$

Variation of parameter method was used to solve for the particular solution for the above differential equation

Solving the above equation for the semi-infinite wall with convective boundary condition, the following solution for the heat flux is obtained

$$\mathbf{T_t (y) = h(T_\infty - T_a)/(h + k_t B) * e^{-B y} + T_a}$$

Appendix M
Recovery Factor

The kinetic energy of a air in the probe housing moving at high velocity can be converted to sensible energy by reversibly and adiabatically bringing the flow to rest at a point. The temperature resulting from this is process is called the stagnation temperature. On the other hand, the static temperature of the gas is the temperature that would be measured by an instrument moving at the local fluid velocity. From a molecular point of view, the static temperature measures the magnitude of the random kinetic energy of the molecules that comprise the gas, while the stagnation temperature includes both the directed and random components of kinetic energy. The deceleration of the flow by the heat flux sensor in the probe converts some portion of the directed kinetic energy of the flow to thermal energy, and elevates the temperature above static temperature of the air. The fraction of kinetic energy recovered as thermal energy is called recovery factor defined as

$$\text{Recovery Factor} = (T_E - T_\infty) / (U^2/2\, C_p) \qquad \text{(M.1)}$$

where T_E represents the equilibrium temperature, T_∞ free stream temperature, U the velocity of the free stream and C_p specific heat of the air respectively.

The air temperature in the convective blood perfusion probe is measured by a thermocouple in the housing. The air temperature is measured before it forms a jet impinging on the heat flux gage. The velocity of the air jets is calculated based on the supply pressure of the air into the housing. The air supply pressure measured is around 58605 Pa (8.5 psi), and the velocity of the jet calculated at 290 K is 311.2 m/s. The air jet velocity is around 1 Ma, sonic flow, also, from the sensitivity analysis the perfusion estimates was found out to be highly sensitive air temperature measurements. Therefore it is important to check the effects of the recovery temperature.

The schematic of the experimental set up for calculating the recovery temperature is shown in the Figure 74. The Figure 75 shows the picture of HFM microsensor. The setup consists of HFM microsensor fixed at the center of aluminum plate through a slot provided in the plate and a thermocouple which is placed in such a way that the thermocouple bead just touched the surface of the plate. The experimental protocol used was same as that used for phantom tissue test. The air was bled into the atmosphere for a minute and for the next minute it was allowed to impinge on the heat flux

gage creating a measurable thermal event. The air temperature and the plate temperature were also recorded during this event. In all five tests were conducted to check the repeatability of the experimental results. The recovery temperature is calculated from the heat flux and the plate temperature measured. The difference between the recovery temperature and the air temperature was calculated to check the effect of the recovery factor. Figure 76 shows the difference between the recovery temperature and the air temperature. The difference is a small for tests 2-5, except for test 1. These differences might be due to the plate temperature measurement by thermocouple itself or due to the uncertainty in the heat flux and air temperature measurement. Hence we can conclude that there is no effect recover factor in the blood perfusion probe.

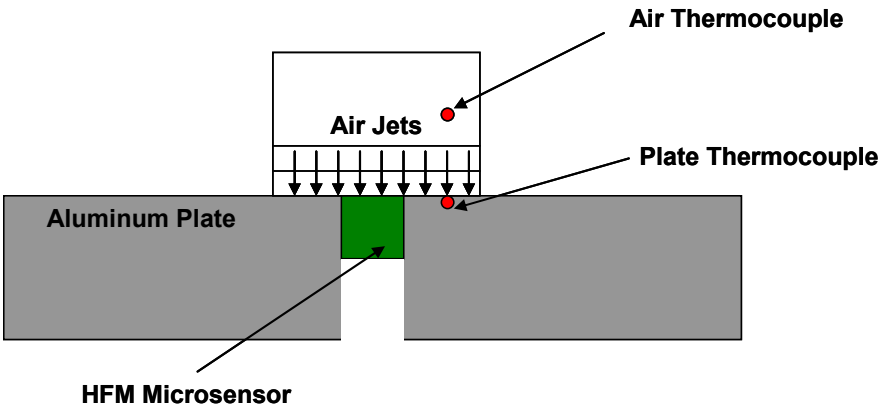

Figure 74: Experimental setup for calculating recovery temperature

Figure 75: HFM Microsensor

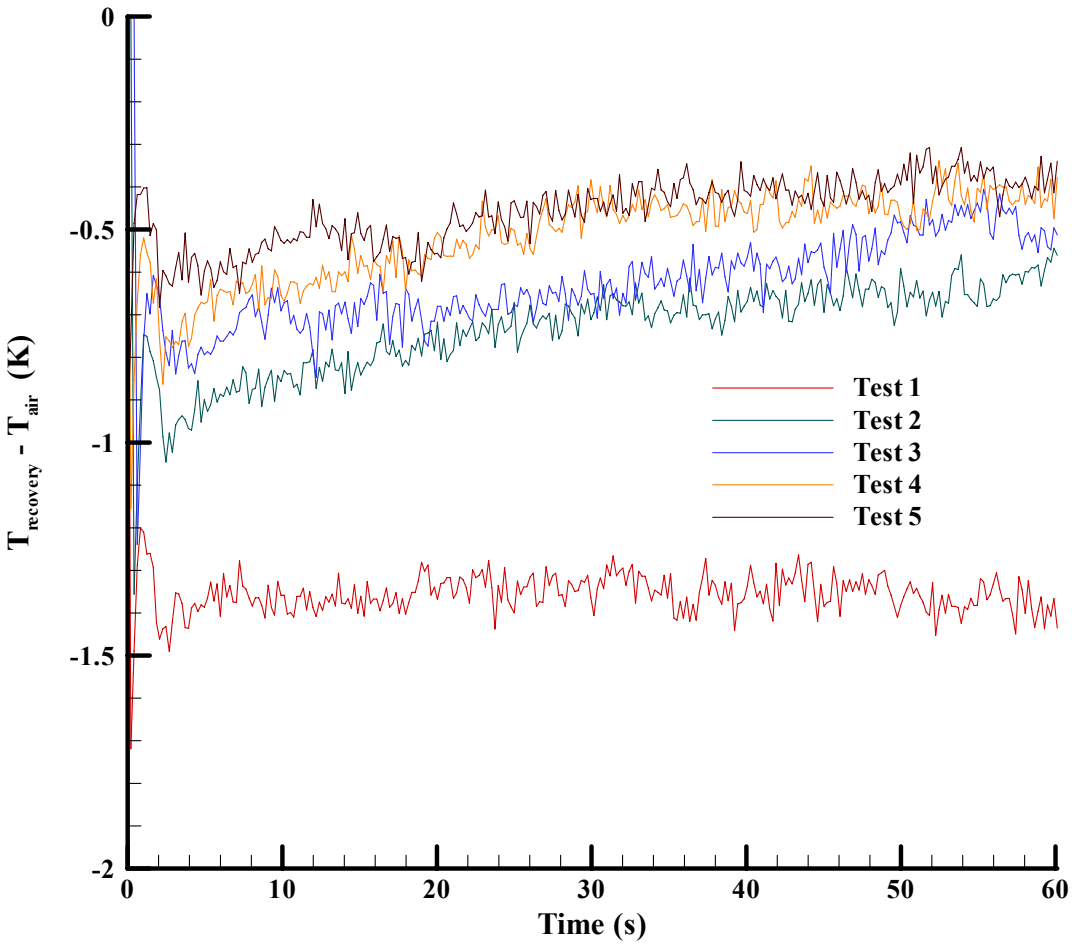

Figure 76: Difference between the calculated recovery temperature and measured air temperature

Appendix N

Heat flux, Air Temperature Data and Convergence Plots for all the tests

A DVD disc containing soft copy of dissertation, all MATLAB codes and all the data required to reproduce the results shown here is attached.

There is a folder named Data inside which there are eight different folders named:

1. Day1
2. Day2
3. Day3
4. Liver Tests
5. Kidney Tests
6. Fluent 2D
7. Fluent 3D
8. Fluent Pennes

Each of these folders has three subfolders named

1. Heat flux
2. Temperatures
3. Estimates and convergence plots

The other folders containing calibration and recovery factor calculation data are named as
Calibration
Recovery factor

All the respective folders have corresponding Fluent models and user defined function and other files required to reproduce the results discussed in this dissertation.

Bibliography

1. Anderson, G.T., and Burnside, G., 1990, "A Non-Invasive Technique to Measure Perfusion using a Focused Ultrasound Heating Source and a Tissue Surface Temperature Measurement", Advances in Measuring and Computing Temperatures in Biomedicine: Thermal Tomography Techniques, Bio-Heat Transfer Models, eds. R.G. Roemer et al., ASME, pp. 31-35.
2. Arkin, H., Chen M.M., Holmes, K.R., 1986, "Adaptive Thermal Modeling: A Concept for Measurement of Local Blood Perfusion in Heated Tissue", Journal of Biomechanical Engineering, Vol. 108, No. 4, pp. 306-311.
3. Arnaud, F., Delhomme, G., Dittmar, A., Girard, P., Netchiporouk, L., Martlet, C., Cespuglio, R., Newman, W.H., 1994, "A Micro Thermal Diffusion Sensor for Nan-Invasive Skin Characterization", Sensors and Actuators. A, Physical, 41-42, pp. 240-243.
4. Ballmer, A., Lanz, O., Scott, E.P., 2003a, "Perfusion Measurements using a Noninvasive Thermal Probe Phantom Test Stand", Proceedings of the ASME, IMECE'03, Paper No. IMECE2003-42014, Washington D.C., Nov 2003.
5. Ballmer, A., Lanz, O., Scott, E.P., Broadstone, R., 2003b, "Consistency of Perfusion Measurements using a Noninvasive Thermal Probe in Canine Tests", National Heat Transfer Conference, Paper No. NHC 2003-40447, Las Vegas, NV, July 2003.
6. Boellaard, R., P. Knaapen, A. Rijbroek, G. J. J. Lutersema, A. A. Lammertsma, 2005, "Evaluation of Basis Function and Linear Least Squares Methods for Generating Parametric Blood Flow Images Using ^{15}O-Water and Positron Emission Tomography" Molecular Imaging and Biology.
7. Bowman, H., 1985, "Estimation of Tissue Blood Flow", in : Heat Transfer in Medicine and Biology, eds. A. Shitzer and R. Eberhart, Vol. 1, Chap. 9, Plenum Press, pp. 192-203.
8. Burns, P.N., Powers, J.E., Hope- Simpson, D., Ulendorf , V., Fritzsc, T., 1994, " Power Doppler imaging combined with contrast enhancing harmonic Doppler: new method for small vessel imaging", (Abstr.) Radiology, Vol. 193 (P): 366.
9. Cardinali, A.V., 2002, "Validation of a Noninvasive Blood Perfusion Measurement Sensor", Master of Science in Mechanical Engineering, Virginia Polytechnic Institute and State University.

10. Castallena, F.S., Skalak, R., Cho, J.M., Case, R.B., 1983, “Steady State Analysis and Evaluation of New Thermal Sensor for Surface Measurement of Tissue Perfusion”, Annals of Biomedical Engineering, Vol. 11, pp. 101-115.
11. Charney, C.K., 1992, “Mathematical Model of Bio-heat Transfer”, in: Advances in Heat Transfer, ed. Y. Cho, Vol. 22, Academic Press Inc., Boston, pp. 19-155.
12. Comas, C.M., 2005, “Assessment of the Measurement Repeatability and Sensitivity of a Noninvasive Blood Perfusion Measuring Probe”, Master of Science in Mechanical Engineering, Virginia Polytechnic Institute and State University.
13. Eberhart, R., Shitzer, A., Hernandez, E., 1980, “Thermal Dilution Methods: Estimation of Tissue Blood Flow and Metabloism”, in Thermal Characteristics of Tissue: Applications in Detection and Treatment, Vol. 35, Annals of N.Y. Academy of Sciences, pp. 107-132.
14. Ellis, B.E., 2006, “Assessment of the Repeatability and Sensitivity of the Thermoelectric Perfusion Probe”, Master of Science in Mechanical Engineering, Virginia Polytechnic Institute and State University.
15. Eriksson, R., Persson, H.W., Dymling, S.O., Lindsröm, K., 1991, “Evaluation of Doppler Ultrasound for Blood Perfusion Measurements”, Ultrasound in Medicine & Biology, Vol. 17, No. 5, pp. 445-452.
16. Forrester, K., Shymkiw, R., Tulip, J., Sutherland, C., Hart, D., Bray, R., 2000, “Spatially resolved diffuse reflectance with Laser Doppler imaging for the simultaneous in-vivo measurement of tissue perfusion and metabolic state”, in Laser-Tissue Interaction XI: Photochemical, Photothermal, and Photomechanical, eds. D. Duncan, J. Hollinger and S. Jacques, Proceedings of SPIE Vol. 3914, pp. 324-32.
17. Fouqet, Y., Hager, J., Terrell, J., and Diller, T.E., 1993, “Blood Perfusion Estimation from Noninvasive Heat Flux Measurements”, Advances in Bioheat and Mass Transfer – 1993: Microscale Analysis of Thermal Injury Process, Instrumentation, Modeling, and Clinical Application, ed. R.Roemer, ASME, N.Y., pp. 53-60.
18. Frank, L.R., Haseler, L.J., Wong, E.C., Buxton, R., 1999, “Dynamic Imaging of Perfusion in Human Skeletal Muscle During Exercise with Arterial Spin Labeling”, Soc Magn Reson Med Proc, Vol. 6, pp. 1603.
19. Gregory, J. K., and J. Thirion., 2005 “Cardiovascular imaging to quantify the evolution of cardiac diseases in clinical development,” Biomarkers, Vol. 10, pp. S1-S9.
20. Heymann, M. A., B. D. Payne, J. I. Hoffman, A. M. Rudolph, 1977, “Blood flow measurements

with radionuclide-labeled particles," Prognoses of Cardiovascular Disease, Vol. 20, pp. 55-74.

21. Holti, G. and Mitchell, K.W., 1979, "Estimation of the Nutrient Skin Blood Flow using a Non-Invasive Segmented Thermal Clearance Probe", Non-Invasive Physiological Measurements, edited by E.P. rolfe, Vol. 1, Chap. 5, Academic Press, London, pp. 113-123.
22. Kinuya, K., K. Kakuda, K. Nobata, S. Sakai, K. Yamamoto, S. Itoh, M. Ohashi, S. Kinuya, 2004, "Role of brain perfusion single-photon emission tomography in traumatic head injury," Nuclear Medicine Communications, Vol. 25, No 4, pp 333-337.
23. Kress, R., Roemer, R., 1987, "A Comparative Analysis of Thermal Blood Perfusion Measurement Techniques", Journal of Biomechanical Engineering, Vol. 109, No. 3, pp. 218-225.
24. Liebert, A., Leahy, M., Maniewski, R., 1998, "Multichannel Laser Doppler probe for blood perfusion measurements with depth discrimination", in Medical and Biological Engineering and Computing, Vol. 36, pp. 740-747.
25. Liu, J., and Xu, L.X., 1999, "Estimation of Blood Perfusion Using Phase Shift in Temperature Response to Sinusoidal Heating at the Skin Surface", IEEE Transactions on Biomedical Engineering, Vol. 46, No. 9, pp. 1037-1043.
26. Machens, H., Pallua, N., Mailaender, P., Pasel, J., Frank, K., Reimer, R., Berger, A., 1996, "Measurements of Tissue Blood Flow by the Hydrogen Clearance Technique (HCT): A Comparative Study Including Laser Doppler Flowmetry (LDF) and the Erlangen Micro-Lightguide Spectrophotometer (EMPHO)", Microsurgery, Vol. 16, No. 12, pp. 808-817.
27. Madden, M., Scott, E.P., "An Agar and Saline Phantom for Perfused Tissue", in Proceedings of the ASME, IMECE, Paper No. IMECE2003-41415.
28. Marayuma, H., Matsutani, S., Ebara, M., Saisho, H., 1998, "Enhanced color flow findings in small hepatocellular carcinoma, Nippon Rinsho, Vol. 56(4): pp. 967-974.
29. Marxen, M., C. Paget, L. X. Yu, R. M. Henkelmann, 2006, "Estimating perfusion using microCT to locate microspheres," Physics in Medicine and Biology, Vol. 51. pp. N9-N16.
30. Mitchner, M., Hager, J.M., Terrell, J.P., Veit, H., Diller, T.E., 1991, "Noninvasive Blood Perfusion Measurement with Heat Flux Microsensor", Advances in Biological Heat and Mass Transfer, Vol. 18, pp. 9-14.

31. Montet, X., Ivancevic, M.K., Belenger, J. Jorge-Costa, M., Pochon, S., Pechér, A., Terrier, F., Vallé, J., 2003, "Noninvasive measurement of absolute renal perfusion by contrast medium enhanced magnetic resonance imaging", Investigative Radiology, Vol. 38, No.9, pp. 584-592.
32. Newman, W.H., and Lele, P.P., 1985, "A Transient Heating Technique for the Measurement of Thermal Properties of Perfused Biological Tissue", Journal of Biomechanical Engineering, Vol. 107: pp. 219-225.
33. Nuutilia, P. and K. Kalliokoski, 2000, "Use of positron emission tomography in the assessment of skeletal muscle and tendon metabolism and perfusion," Scandinavian Journal of medicine & Science in Sports Vol. 10, pp. 346-350.
34. O'Reilly, T., Gonzales, T., and Diller, T.E., 1996, " Development of Noninvasive Blood Perfusion Probe", in Advances in Biological Heat and Mass Transfer, eds. L. Hayes and S. Clegg, Vol. HTD 34, ASME, pp. 67-73.
35. Patankar, S.V., 1980, Numerical Heat Transfer and Fluid Flow, McGraw Hill, New York.
36. Patel, P.A., Valvano, J.W., Pearce, J.A., Prahl, S.A., Denham, C.R., 1987, "A Self-Heated Thermistor Technique to Measure Effective Thermal Properties from the Tissue Surface", Journal of Biomechancial Engineering, Vol. 109, pp. 330-335.
37. Peng, J., Xia, Y., Gao, T., Lei, X., Zhao, S., 2000, "A Surface Heat Disturbance Method for Measuring Local Tissue Blood Perfusion Rate", Asian Research, Vol. 29, No. 1, pp. 34-44.
38. Pennes, H.H., 1948, "Analysis of Tissue and Arteriole Blood Temperature in the Resting Forearm", Journal of Applied Physiology, Vol. 1, pp. 93-122.
39. Petersson, J. A. Sanchez-Crespo, M. Rohdin, S. Montmerle, S. Nyren, H. Jacobsson, S. S. Larsson, S. G. E. Lindahl, D. Linnarsson, R. W. Glenny, M. Mure, 2004, "Physiological evaluation of a new quantitative SPECT method measuring regional ventilation and perfusion," Journal of Applied Physiology, Vol. 96, pp. 1127-1136.
40. Porter, T.R., Xie, F., Kricsfeld, D., Armbruster, R.W., 1996, " Improved Myocardial Contrast with Second Harmonic Transient Ultrasound Response Imaging in Human using Intravenous Perfluorocarbon-Exposed Sonicated Dextrose Albumin", J. Am Coll Cardiol, Vol. 27: pp. 1497-1501.
41. Prinzen, F. W., and J. B. Bassingthwaighte, 2000, "Blood flow distributions by microsphere deposition methods," Cardiovascular Research, Vol. 45, pp. 13-21.

42. Richardson, R., Haseler, L.J., Nygren, A.T., Bluml, S., Frank, L.R., 2001, "Local Perfusion and Metabolic Demand During Exercise: A Noninvasive MRI Method of Assessment", Journal of Applied Physiology, Vol. 91, pp. 1845-153.
43. Riva, C.E., Ross, B., and Benedek, G.B., 1972, "Laser Doppler measurements of blood flow in capillary tubes and retinal arteries", Invest Opthalmol, Vol. 11: pp. 936-944.
44. Robinson, P.S., 1998, "Development of Methodologies for the Noninvasive Estimation of Blood Perfusion", Master of Science in Mechanical Engineering, Virginia Polytechnic Institute and State University.
45. Rumberger, J.A., 1990, "Non-Invasive Measurement of Blood Flow and Perfusion", Current Opinion in Radiology, Vol. 2, No. 4, pp. 567-574.
46. Schelbert, Heinrich R., 2000, "PET Contributions to Understanding Normal and Abnormal Cardiac Perfusion and Metabolism."Annals of Biomedical Engineering, Vol. 28, pp 922-929
47. Scott, E.P., Robinson, P.S., Diller, T.E., 1998, "Development of Methodologies for the Estimation of Blood Perfusion Using a Minimally Invasive Thermal Probe", Measurement Science and Technology, Vol. 9, pp. 888-897.
48. Shepherd, A.P., 1990, "History of Laser Doppler Blood Flowmetry", in : Laser Doppler Flowmetry, eds. A.P. Shepherd and P.A. Oberg, Chap. 1, Kluwer Academic Publishers, pp. 1-15.
49. Slomka, P. J., H. Nishina, D. S. Berman, X. Kang, C. Akincioglu, J. D. Friedman, S. W. Hayes, U. E. Aladl, G. Germano, 2004, "Motion-Frozen: Display and Quantification of Myocardial Perfusion," Journal of Nuclear Medicine, Vol. 45, pp. 1128-1134.
50. Stern, M.D., Lappe, D.L., Bowen, P.D., Chimosky, J.E., Holloway, Jr., G.A., Keiser, H.R., Bowman, R.L., 1977, "Continuous Measurement if Tissue Blood Flow by Laser-Doppler Spectroscopy", The American Journal of Physiology, Vol. 232, No. 4, H441-448.
51. Svedman, C., Cherry, G.W., Strigini, E., Ryan, T.J., 1998, "Laser Doppler Imaging of Skin Microcirculation", Acta Dermato-Venereologica, Vol. 78: pp. 114-118.
52. Vafai, K., 2005, Handbook of Porous Media, Taylor and Francis.
53. Vajkoczky, P., Roth, H., Horn, P., Lucke, T., Taumé, C., Hubner, U., Martin, G.T., Zappletal, C., Klar, E., Schilling, L., Schmiedek, P., 2000, "Continuous monitoring of Regional Blood Flow: Experimental and Clinical Validation of a Novel Thermal Diffusion Microprobe", Journal of Neurosurgery, Vol. 93: pp. 265-274.

54. Vallee, J.P., Lazeyras, F., Khan, H.G., et al., 2000, “Absolute blood flow quantification by dynamic MRI and Gd-DTPA”, European Radiology, Vol. 10, No. 8, pp. 1245-1252.
55. Valvano, J.W., Allen, J.T., Bowman, H.F., 1984, “The Simultaneous Measurement of Thermal conductivity, Thermal Diffusivity, and Perfusion in Small Volumes of Tissue”, Journal of Biomechanical Engineering, Vol. 106, pp. 192-197.
56. Walsh Jr., J.T., and Bowman, H.F., 1984, “A Non-Invasive Method for Quantifying Tissue Perfusion”, Advances in Bioengineering, pp. 5-6.
57. Wong, E.C., Buxton, R.B., Frank, L.R., 1997, “Implementation of Quantitative Perfusion Imaging Techniques for Function Brain Mapping Using Pulsed Arterial Spin Labeling”, Nucl Magn Reson Biomed, Vol. 10, pp. 237-249.
58. Woodcock, J.P., 1985, “Non-Invasive Blood Flow Measurement”, Critical Reviews in Biomedical Engineering, Vol. 12, No. 3, pp. 201-235.